5-2016

Investigating the Role of ADP-forming Acetyl-CoA Synthetase from the Protozoan Parasite Entamoeba histolytica

Cheryl Page Jones
Clemson University, cherylh@g.clemson.edu

INVESTIGATING THE ROLE OF ADP-FORMING ACETYL-COA SYNTHETASE FROM THE PROTOZOAN PARASITE *ENTAMOEBA HISTOLYTICA*

A Dissertation
Presented to
the Graduate School of
Clemson University

In Partial Fulfillment
of the Requirements for the Degree
Doctor of Philosophy
Biochemistry and Molecular Biology

---

by
Cheryl Page Jones
May 2016

Accepted by
Dr. Cheryl Ingram-Smith, Committee Chair
Dr. William Marcotte, Jr.
Dr. Julia Frugoli
Dr. Kimberly Paul

ABSTRACT

ADP-forming acetyl-CoA synthetase (ACD; EC 6.2.1.13) catalyzes the reversible conversion of acetyl-CoA to acetate coupled to the production of ATP. This enzyme is present only in certain acetate-producing archaea and a limited number of bacteria and eukaryotes. ACD belongs to the same NDP-forming acyl-CoA synthetase enzyme superfamily as succinyl-CoA synthetase (SCS; EC 6.2.1.4) from the citric acid cycle, and a similar three-step mechanism involving a phosphoenzyme intermediate was originally proposed for this enzyme.

ACD has been postulated to be a major acetate-producing enzyme in the protozoan parasite *Entamoeba histolytica* and may contribute to ATP production. Biochemical and kinetic characterization of recombinant *E. histolytica* ACD (EhACD) revealed that this enzyme may function in the direction of acetate production for generation of ATP and CoA during growth in the high glucose environment of the small intestine, and in acetate assimilation to acetyl-CoA in the high acetate environment of the lower intestine during colonization. *Eh*ACD utilizes multiple substrates including propionate and propionyl-CoA supporting an additional proposed role in amino acid degradation. EhACD activity is regulated by both ATP and PP_i, important energy molecules in *E. histolytica*.

The ACD mechanism has been controversial, as a required second phosphorylation step was proposed for the *Pyrococcus furiosus* enzyme. Investigation of the catalytic role of the two proposed phosphorylation sites in *Eh*ACD revealed that His252, the site of phosphorylation in the original three-step mechanism, is essential for

activity and His533, the proposed second phosphorylation site, is important but not essential. Likewise, Glu213, proposed to play a role in phosphorylation/ dephosphorylation of His252, is also required but Asp674 thought to stabilize the phosphohistidine is not. These results suggest that EhACD follows a three-step mechanism with a single phosphoenzyme intermediate.

Additional conserved active site residues were examined for their role in catalysis. Asp314 was shown to be essential for activity, possibly in both a catalytic role and a structural role. Alteration at this position resulted in complete loss of activity, and computational modeling based on the *Candidatus Korarchaeum cryptofilum* ACD-I structure suggests that this residue may be critical for dimerization. Future directions for understanding the complex mechanism of ACD and its physiological role are presented.

DEDICATION

I would like to dedicate this work to my late mother, Priscilla Ann Mills Howell. You always have and always will be my greatest inspiration in life. My dreams are your dreams. My accomplishments are because of you. To my uncle, Charles Mills – thank you for everything. My education would not have been possible without your kind soul and generous heart. To my father, Lewis Howell – thank you for gifting me with the stubbornness to succeed. And to the rest of my family who are too numerous to name. I love you all.

ACKNOWLEDGEMENTS

First, I'd like to acknowledge my advisor Dr. Cheryl Ingram-Smith. Thanks to fortuitous timing, I had the opportunity and pleasure of being your first graduate student. I've always felt that our pairing was meant to be, and I've learned a great deal about science, hard work, and life through this experience. You've played a tremendous role in my growth as a scientist and a professional. I can't wait to make you proud in the future.

I'd also like to acknowledge my committee members for the immeasurable support throughout this process. Thanks to Dr. Julia Frugoli for encouraging me to pursue the NSF fellowship. Aside from the financial support, the confidence the fellowship has given me was instrumental in my success. Thanks to Dr. Kimberly Paul for always having an open door and letting me hijack your classroom. Thanks to Dr. William Marcotte for letting me carve my own unconventional path at times. Thank you all for the extra support in pursuing my education certificate.

A special thanks goes to Dr. Kerry Smith and the Smith lab for constant support and collaboration. Without your advice (and many pieces of equipment), this project would not have been the same. Furthermore, all of the members of the Eukaryotic Pathogens Innovation Center have helped me in one way or another and made this journey truly enjoyable and entertaining.

I thank my fellow Ingram-Smith Lab graduate student, Thanh Dang, who has been a sounding board for all of my theories and ideas; Katie Glenn and Tonya Taylor for being excellent teachers and friends; and my fellow *Entamoeba* comrades, particularly Hollie Hendrick and Brenda Welter.

Two wonderful undergraduate students, Kirin Khan and Noah Smith, have directly contributed to this work. Thank you for the opportunity to be a mentor and the hard work you've invested in this project.

And finally, the National Science Foundation and the College of Agriculture, Forestry, and Life Sciences, that have provided me with three excellent fellowships during my tenure as a graduate student.

TABLE OF CONTENTS

PAGE

Table of Contents (Continued)

LIST OF TABLES

LIST OF FIGURES

List of Figures (Continued)

FIGURE PAGE

CHAPTER 1

LITERATURE REVIEW OF ACETATE METABOLISM, NDP-FORMING ACYL-COA SYNTHETASE ENZYMES, AND *ENTAMOEBA HISTOLYTICA*

I. INTRODUCTION

Acetate fermentation and assimilation are common processes in cellular metabolism spanning all three domains of life. Acetate can be excreted as an end product, utilized as a carbon source, and used for modification of proteins by acetylation. The conversion between acetyl-CoA and acetate is an important cellular process that can be catalyzed by multiple pathways. One such pathway utilizes a single enzyme, ADP-forming acetyl-CoA synthetase (ACD; EC 6.2.1.13; Eq. 1), to reversibly catalyze this reaction coupled to ATP hydrolysis or formation.

$$\text{acetyl-CoA} + \text{ADP} + P_i \leftrightarrow \text{acetate} + \text{ATP} + \text{CoA} \qquad \text{[Eq. 1]}$$

ACD is part of a superfamily of enzymes involved in the conversion of acyl-CoAs to their corresponding acids. Biochemical and structural characterization of this family of enzymes has focused on understanding the underlying mechanism. ACD is found in a subset of protozoan parasites, including the amitochondriate *Entamoeba histolytica* which causes amoebic dysentery and liver abscess. In this chapter, the common pathways of acetate metabolism are introduced along with a thorough background of the NDP-forming acyl-CoA synthetase family. Also, the metabolism of *E. histolytica* centered around central carbon metabolism and energy generation is discussed.

II. ACETATE METABOLISM

Acetate is a common anion in biology and is a major metabolic end product in a variety of organisms. When the incoming carbon flux surpasses the capacity of central metabolic pathways, excess acetyl-CoA will undergo fermentation and recycle CoA. An additional benefit of acetate fermentation is the generation of energy-containing compounds such as ATP. The production of acetate is therefore considered an "overflow" metabolism. Fermentation can also be a result of an incomplete or absent TCA cycle. Anaerobic fermentation pathways are then used for the primary flow of carbon (1).

Acetate assimilation as an alternative carbon source may occur under certain conditions such as when glucose is diminished (1). Acetate is typically activated to form acetyl-CoA, a central metabolic intermediate positioned at the junction of several pathways. The high-energy thioester bond between the acetyl group and CoA can be used to drive other reactions. Acetyl-CoA is also produced during the breakdown of carbohydrates through glycolysis or breakdown of fatty acids via beta-oxidation.

Acetylation is a common post-translational modification of proteins involved in regulating transcription and enzyme activity (2). Histone acetylation levels in the cell have also been implicated as a method for maintaining intracellular pH (3). Acetate in its protonated form (CH_3COOH) will traverse the plasma membrane freely and ionize in the neutral pH environment of the cell. Levels of free acetate within the cell must be controlled or pH changes could be toxic.

Acetate metabolism in archaea

Methane-producing archaea can be separated into CO_2-reducing species and the acetoclastic, or acetate-utilizing species. In the acetoclastic methanogens, consisting of the genera *Methanosaeta* and *Methanosarcina*, the methyl group of acetate is converted to methane and the carbonyl group to CO_2 (4). However, *Methanosarcina* and *Methanosaeta* use different strategies for acetate activation into acetyl-CoA. *Methanosarcina* is the only archaeal genus containing a two enzyme pathway typical of acetate-producing bacteria (5,6). Acetate is phosphorylated by ATP to form acetyl phosphate via acetate kinase (ACK; EC 2.7.2.1; Eq. 2), and then acetyl phosphate is converted to acetyl-CoA by phosphotransacetylase (PTA; EC 2.3.1.8; Eq. 3) (FIG 1.1A). This pathway functions in reverse to regenerate CoA and serves as a source of ATP. It is considered the 'low affinity' pathway that functions optimally when acetate concentrations are ≥ 30 mM (7).

$$\text{acetate} + \text{ATP} \leftrightarrow \text{acetyl phosphate} + \text{ADP} \qquad \text{[Eq. 2]}$$

$$\text{CoA} + \text{acetyl phosphate} \leftrightarrow \text{acetyl-CoA} + P_i \qquad \text{[Eq. 3]}$$

Methanosaeta is able to accomplish acetate activation by a single enzyme, AMP-forming acetyl-CoA synthetase (ACS; 6.2.1.1; Eq. 4) (8), which functions through a bi-uni-uni-bi ping pong mechanism (7). ACS first binds acetate and ATP and forms the enzyme-bound acetyladenylate (acetyl-AMP) intermediate and releases PP_i (FIG 1.1B) (9). Acetyl-AMP then reacts with CoA to form acetyl-CoA and release AMP. This pathway is considered the 'high affinity' pathway preferring acetate concentrations below 10 mM (7). Both strategies for acetate activation require ATP consumption, and consequently result in low energy output for the organism (4).

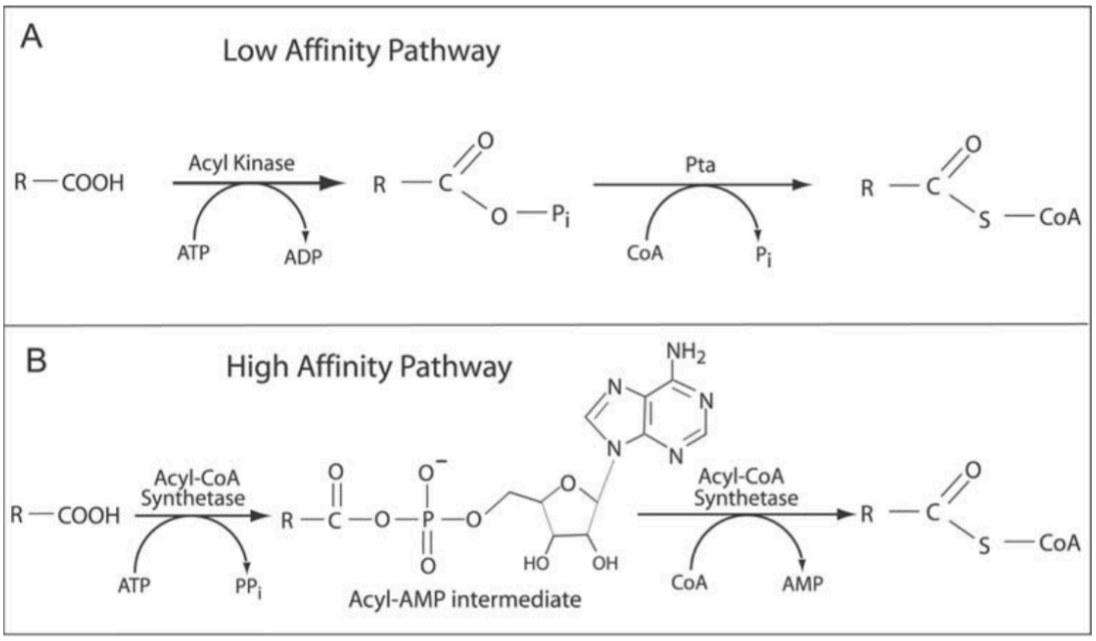

FIG 1.1 Pathways for conversion of acetate to acetyl-CoA. (A) Low affinity pathway involving acetate kinase and phosphotransacetylase, using an acetyl phosphate intermediate. (B) High affinity pathway involving acetyl-CoA synthetase (AMP-forming) which involves an enzyme-bound acyl-AMP intermediate. Obtained with permission from (7).

acetyl-CoA + AMP + PP_i → acetate + ATP + CoA [Eq. 4]

ACS is also found in several other archaeal organisms including *Ignicoccus hospitalis* (10), *Pyrobaculum aerophilum* (11), and multiple halophilic species (12,13). ACS serves as the primary acceptor in a novel CO_2 fixation pathway within the hyperthermophilic crenarchaeon *I. hospitalis* (10). Analysis of the *Ignicoccus* enzyme revealed an unusual subcellular localization associated with the outermost membrane. In contrast to the monomeric or dimeric forms in mesophilic species, ACS forms large octameric complexes in *Ignicoccus* and another hyperthermophilic crenarchaeon *P. aerophilum* (10,11). Most ACSs are limited to utilizing acetate as the acyl substrate, however biochemical characterization from a few archaeal species revealed an unexpected diversity in substrate utilization (11,14).

Investigation into acetate production and utilization in multiple halophilic species revealed that ACS is responsible for the utilization of acetate, while ACD is responsible for acetate formation when grown on glucose (12). Although the two enzymes both catalyze interconversion of acetate and acetyl-CoA, they use very different mechanisms and share no homology. ACS is widespread throughout the three domains of life; in contrast, occurrence of ACD is limited.

ACD has been thoroughly studied in the anaerobic hyperthermophile *Pyrococcus furiosus* (15-18). *P. furiosus* derives energy by carbohydrate and peptide fermentation and contains several enzymes specialized to this type of metabolism (19). Pyruvate, the end product of glycolysis, is converted to acetyl-CoA via the ferredoxin-dependent enzyme pyruvate:ferredoxin oxidoreductase (PFOR; EC 1.2.7.1; Eq. 5).

pyruvate + CoA + $ferredoxin^{ox}$ → acetyl-CoA + CO_2 + $ferredoxin^{red}$ [Eq. 5]

Additional ferredoxin-dependent enzymes convert the peptide catabolism end products (branched chain 2-keto acids, aromatic 2-keto acids, and 2-ketoglutarate) to their corresponding CoA esters (19). ACD then utilizes these products to produce ATP. *P. furiosus* contains two distinct ACD enzymes, classified as ACDI and ACDII, that vary in their substrate specificity allowing this organism to utilize acetyl-CoA as well as the branched chain acyl-CoAs and aryl-CoAs produced from peptide fermentation (19). Upon further characterization, purified ACD from *P. furiosus* demonstrated reversible activity, however there was no evidence for acetate utilization (17). ACDs from other archaeal genera have also been investigated including *Archaeoglobus* (20,21), *Thermococcus* (22), *Haloarcula* (23,24), *Pyrobaculum* (23), and *Methanococcus* (21).

Acetate metabolism in bacteria

Acetate production and utilization have been well studied in bacteria. *Escherichia coli* produces acetate anaerobically via mixed-acid fermentation or aerobically during rapid growth on glucose which causes inhibition of respiration. In contrast to the acetate utilization pathway in *Methanosarcina,* the ACK-PTA pathway commonly functions in acetate production in bacteria (FIG 1.2). The ACK-PTA pathway is also important for maintaining correct concentrations of intracellular acetyl phosphate, which is an important signaling molecule in many bacteria (25).

In *Bifidobacteria* and lactic acid bacteria, ACK partners with xylulose-5-phosphate/ fructose-6-phosphate phosphoketolase (XFP; EC 4.1.2.9 [Eq. 6] and 4.1.2.22 [Eq. 7]) to produce acetate as part of a modified pentose phosphate pathway (26).

xylulose 5-phosphate + P_i →

acetyl phosphate + glyceraldehyde 3-phosphate + H_2O [Eq. 6]

fructose-6-phosphate + P_i →

acetyl phosphate + erythrose 4-phosphate + H_2O [Eq. 7]

Acetate can also be produced directly from pyruvate via a pyruvate oxidase, POXB (EC 1.2.5.1; Eq. 8). Oxidative decarboxylation of pyruvate coupled to the reduction of ubiquinone produces acetate and CO_2 (FIG 1.2). This reaction is postulated to provide energy and acetyl groups under microaerophilic environments between the stationary and growth phases (1,27).

pyruvate + ubiquinone + H_2O → acetate + ubiquinol + CO_2 [Eq. 8]

Bacteria can rapidly grow and excrete acetate, however when carbon resources deplete, cells undergo a process called the “acetate switch” (1). Cells transition to a phase of slower growth accompanied by uptake and utilization of acetate as an essential carbon source. Recapture of acetate depends on activation of acetate by ACS (FIG 1.2). This reaction is driven by the removal of pyrophosphate (PP_i) by pyrophosphatase (PPase; EC 3.6.1.1; Eq. 9).

$PP_i + H_2O \rightarrow 2\ P_i$ [Eq. 9]

Activity of ACS is post-translationally regulated by acetylation on a critical lysine residue within the active site (28). Acetylation by a protein acetyltransferase inactivates ACS (29), whereas activation takes place by deacetylation by the sirtuin CobB (30). This regulation functions as a feedback system in which the activation of acetate is regulated by energy (acetyl-CoA) and reducing equivalents (NAD^+) (31). *Salmonella enterica*

grown on low levels of acetate resulted in depletion of ATP and growth arrest when regulation of ACS was disrupted (31). Consequently, tight regulation of ACS is necessary for proper energy balance within the cell.

The sole bacterial ACD characterized to date comes from the photoheterotrophic bacterium *Chloroflexus aurantiacus* (32), which lacks the PTA-ACK pathway to produce acetate. ACD was induced over 10-fold in *C. aurantiacus* during growth on glucose, suggesting it partners with glycolysis. Additional putative ACD homologs have been identified in other bacterial genomes, particularly from acetate-forming syntrophic bacteria lacking genes for PTA and ACK, suggesting ACD may serve as an alternative for acetate production (33,34).

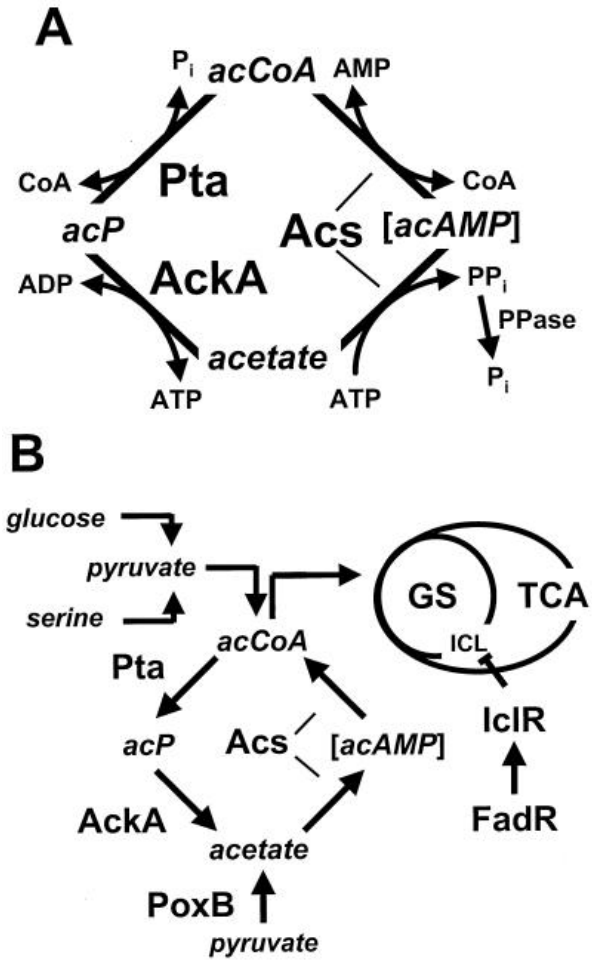

FIG 1.2 Pathways of acetate metabolism in *E. coli* (A) acAMP = acetyl-AMP; acCoA = acetyl-CoA; AckA = acetate kinase; acP = acetyl P; Acs = acetyl-CoA synthetase; CoA = coenzyme A; P_i = inorganic phosphate; PPi =pyrophosphate; PPase = pyrophosphatase; Pta =phosphotransacetylase. (B) Carbon flux and associated pathways during growth on glucose. GS = glyoxylate shunt; TCA = tricarboxylic acid cycle; PoxB = pyruvate oxidase; ICL = isocitrate lyase; IclR = repressor of the glyoxylate shunt operon *aceBAK*; FadR = regulator of fatty acid metabolism that also activates *iclR*. Taken with permission for reuse from (35).

Acetate metabolism in eukaryotes

ACS is central to the metabolism of almost all eukaryotic cells to activate acetate to acetyl-CoA (7). Eukaryotes usually have two isoforms, one localized to the mitochondria and another localized to the cytosol (36,37), although additional evidence suggests the cytosolic enzyme also resides with the nucleus (38). The mitochondrial enzyme is essential for maintaining energy homeostasis during ketogenic conditions in mammals (37), such as fasting or diabetes mellitus, when the liver releases large amounts of acetate into the bloodstream (39-41). The cytosolic isoform is associated with fatty acid synthesis, particularly supporting tumorogenesis (42), and has been of interest in understanding metabolism of tumor cells under hypoxic conditions (43). This isoform was also shown to be essential for yeast replicative longevity and predicted to produce acetyl-CoA within the nucleus for histone acetylation (38). ACS located within the plastid of *Arabidopsis* was suggested to recycle acetate as a toxic breakdown product of other fermentation pathways (44). In humans, endogenous sources of acetate that can be recycled via ACS include the breakdown of the neurotransmitter acetylcholine by acetylcholinesterase, deacetylation of histones in the nucleus, and catabolism of ethanol in the liver (45). Large concentrations of acetate are also produced by the gut microbiota which serve as a primary carbon source for adjacent intestinal cells, where glucose is limiting (46).

Regulation of ACS by reversible acetylation as found in bacteria is also conserved in the human enzymes (47). NAD^+-dependent deacetylases known as sirtuins are responsible for activation of ACS by deacetylation (28), but the acetyltransferase responsible for acetylation has yet to be identified. Sirtuins are known for regulating

gene silencing, energy homeostasis, and aging, suggesting a link between acetate metabolism and the aging process (45).

One ACS isoform is essential for growth of the fungal pathogen *Candida albicans* on a variety of carbon sources (48). *De novo* fatty acid synthesis via cytosolic ACS is essential in the bloodstream form of the parasite, *Trypanasoma brucei* (49). ACS was also recently identified in the cytosol of the protozoan parasite, *Leishmania donovanii* (50).

ACK was originally thought to be only a bacterial enzyme with the exception of the *Methanosarcina* genus of archaea, however it has now been identified in several eukaryotic species (51). The ACK-PTA pathway is found in the green algae *Chlamydomonas reinhardtii* (52) and the oomycete *Phytophthora ramorum* (51,53). *C. reinhardtii* contains two ACK/PTA pathways (54) that are differentially localized to the chloroplast and the mitochondria and function primarily for acetate production under dark, anoxic conditions (52).

In euascomycete and basidiomycete fungi, ACK partners with one or more XFP enzymes as part of a modified pentose phosphate pathway using xylulose-5-phosphate or fructose-6-phosphate as substrates (51). The only eukaryotic XFP to be characterized is from the pathogenic fungus *Cryptococcus neoformans*. This enzyme, one of two XFPs in *C. neoformans*, has been found to be allosterically regulated (55). A unique PP_i-dependent ACK [Eq. 10] in *Entamoeba histolytica* converts acetyl phosphate to acetate and PP_i (56). ACK activity has been detected in extracts of *E. histolytica* trophozoites, which suggests the enzyme is present under normal growth conditions. However, the source of the acetyl phosphate substrate is currently unknown as no known partner

enzymes are present within the genome. The hypothesized function is to provide PP_i for glycolysis, but its role remains a mystery.

Acetyl phosphate + P_i → acetate + PP_i [Eq. 10]

Fungi can also produce acetate from pyruvate through a pyruvate dehydrogenase bypass pathway composed of pyruvate decarboxylase (PDC; EC 4.1.1.1; Eq. 11) and acetaldehyde dehydrogenase (ALD; EC 1.2.1.5; Eq. 12). A deletion of two *ALD* genes in *Saccharomyces cerevisiae* decreased acetate formation during anaerobic growth on glucose, demonstrating a major role in acetate production (57). PDC is thought to occupy the branch point between oxidative metabolism through the TCA cycle and fermentative metabolism (58).

pyruvate → acetaldehyde + CO_2 [Eq. 11]

acetaldehyde + $NAD(P)^+$ + H_2O → acetate + NAD(P)H [Eq. 12]

Eukaryotic ACD is limited to a few protozoan parasites, having been positively identified in *Giardia lamblia* (59) and *E. histolytica (60)*, and putative *acd* genes have been identified in the genome sequences of *Plasmodium falciparum* and *Cryptosporidium muris*, corroborating the idea the ACD plays a role in the parasitic lifestyle. Like *E. histolytica, G. lamblia* is an amitochondriate protozoan parasite that relies on substrate-level phosphorylation for energy generation (61).

Acetate:succinate CoA transferase (ASCT; EC 2.8.3.8; Eq. 13) is present in hydrogenosomes of *Trichomonas vaginalis* (62), and mitochondria of Trypanasomatidae (63,64) and the parasitic helminth *Fasciola hepatica* (65). It functions by transferring CoA from acetyl-CoA to succinate, forming succinyl-CoA. This enzyme works in conjunction

with succinyl-CoA synthetase in order to produce ATP (Eq. 14). As for ACD, this specialized enzyme involved in acetate metabolism is associated with a few parasitic organisms, indicating the special role acetate metabolism can play in the parasitic lifestyle.

acetyl-CoA + succinate → succinyl-CoA + acetate [Eq. 13]

succinyl-CoA + ADP + Pi → succinate + CoA + ATP [Eq. 14]

Acetyl-CoA hydrolase (ACH; EC 3.1.2.1; Eq. 15) hydrolyzes acetyl-CoA, producing acetate and CoA. This reaction is not energy-conserving considering the high-energy thioester bond is cleaved to only low-energy products. ACH is proposed to function by aiding transfer of acetyl units between subcellular compartments (66).

acetyl-CoA + H_2O → acetate + CoA [Eq. 15]

In summary, several pathways exist for both production and utilization of acetate. The three main pathways (ACK/PTA, ACS, and ACD) are each found within all three domains of life. The balance between these two processes is tightly regulated in order to maintain proper carbon metabolism.

III. NDP-FORMING ACYL-COA SYNTHETASES

A newly recognized superfamily of NDP-forming acyl-CoA synthetases was identified by Sanchez *et al.* in 2000 (67). This family is comprised of several metabolic enzymes that either utilize NTP to generate an acyl-CoA molecule, or vice versa, use the cleavage of the thioester bond to generate an NTP (FIG 1.3A). Members of this enzyme family contain five subdomains – two CoA ligase domains, two ATP grasp domains, and a CoA binding domain. As the name suggests, the CoA binding domain is the location of the CoA binding pocket. The two ATP grasp domains form a cleft capable of opening and closing due to nucleotide binding, making these enzymes also part of the ATP-grasp family (68). The arrangement of these subdomains is unique between family members (FIG 1.3B), yet remarkably the overall mechanism remains the same.

Some members of this family have independent alpha and beta subunits that come together as a heteromer, while in other members the enzyme functions as a homodimer with fused alpha and beta subunits connected by a hinge region. Although both types usually maintain a similar quaternary structure, the significance of the hinge region has not been studied. Catalysis proceeds through a common mechanism involving a phosphoenzyme intermediate. The active site is separated into two regions, designated Site I and Site II, where different parts of the reaction take place (69). The NTP binds within the cleft of the two ATP-grasp domains within Site II and phosphorylates N-3 of the imidazole ring of the active site histidine (located within subdomain 2). The phosphoryl moiety is then transferred to the acyl substrate within Site I, forming a transient acyl-phosphate intermediate that transfers the acyl group to CoA.

The catalytic His residue is conserved throughout the entire superfamily with the exception of the acetyltransferases (67). Specific members of the superfamily will be discussed in the following sections.

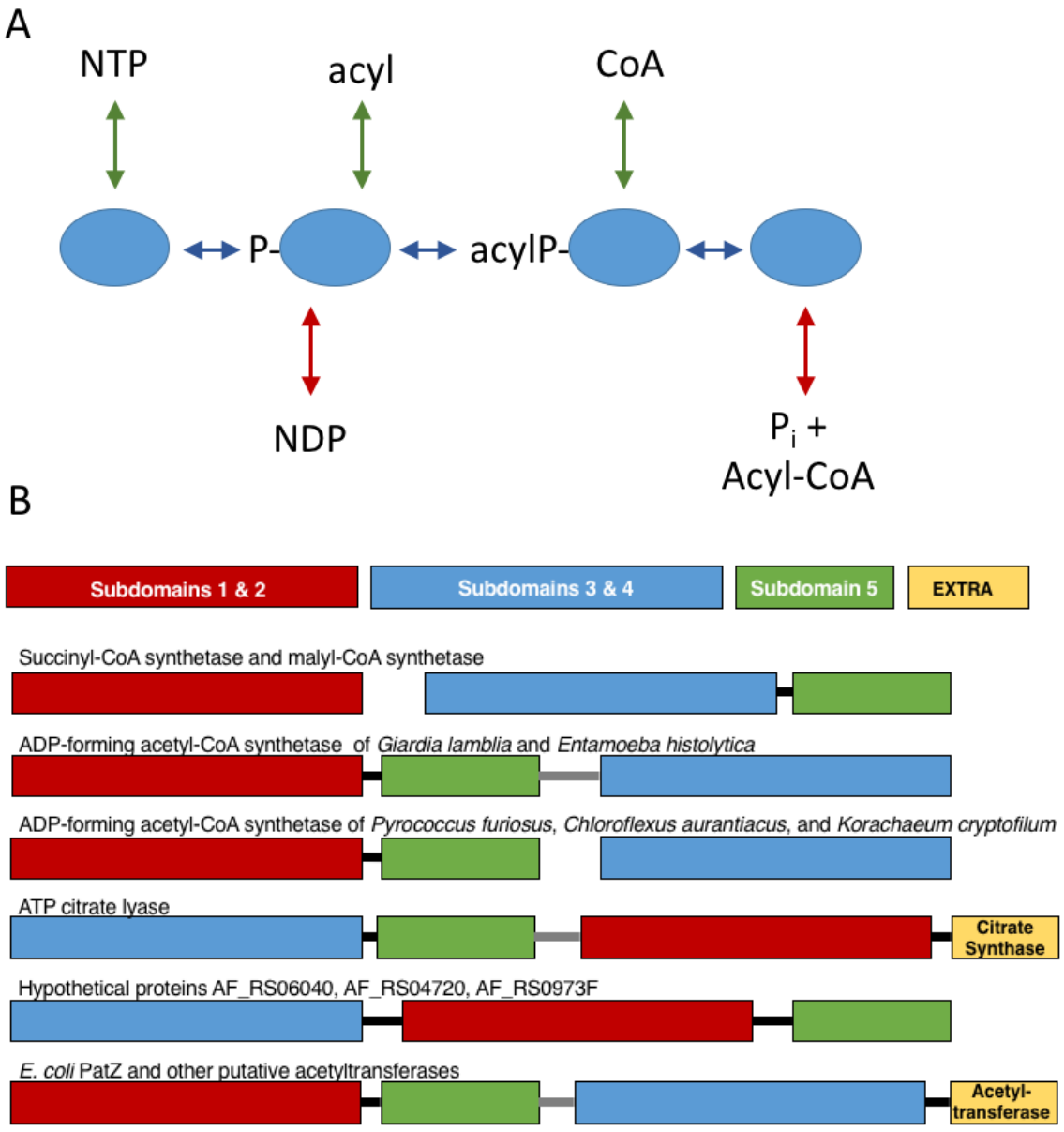

FIG 1.3 NDP-forming acyl-CoA synthetases. (A) Schematic of the general mechanism for this superfamily of enzymes. Green and red arrows indicate products/substrates in opposite directions of the reaction. (B) Domain organization of various enzymes within the superfamily. Gray connecting bars indicate a hinge region.

Succinyl-CoA synthetase

Succinyl-CoA synthetase (SCS; EC 6.2.1.4 and 6.2.1.5) is the most well-studied member of this superfamily of enzymes. Present in almost all organisms, SCS catalyzes the sole substrate-level phosphorylation reaction in the citric acid cycle. SCS functions as a thiolase, coupling cleavage of the thioester bond in succinyl-CoA to phosphorylation of a nucleoside diphosphate [Eq 16].

$$\text{succinyl-CoA} + \text{ADP/GDP} + P_i \leftrightarrow \text{succinate} + \text{CoA} + \text{ATP/GTP} \quad \text{[Eq 16]}$$

SCS functions as a heterotetramer composed of two alpha and two beta subunits (70-72). The structures of SCS enzymes from *E. coli* (73), pig heart (74), and *Thermus aquaticus (71)* have been determined to date. The first structure of SCS from *E. coli* was determined by X-ray crystallography in 1994 (73) and revealed phosphorylation of a His residue (His246) located on a loop region within the alpha subunit. The CoA bound to the alpha subunit was positioned with the free thiol oriented near the active site His. Since the nucleoside was shown to bind 30 Å away on the beta subunit (75), Fraser *et al.* (76) hypothesized that the loop containing the phosphorylated His swings between Site I within the alpha subunit to Site II within the beta subunit in order to accomplish a phosphoryl transfer to the nucleotide.

Structural characterization of pig heart SCS with the catalytic alpha His in both the dephosphorylated and phosphorylated states further supported this mechanism (74). In addition to the catalytic His residue, two Glu residues were implicated to stabilize the phosphorylated His intermediate in *E. coli* SCS (77). The carboxylate group of Glu208α interacts with the catalytic His at Site I by accepting a hydrogen bond at N1on the imidazole ring. This Glu residue also stabilizes the proton on N1 of the imidazole ring

when it is not phosphorylated. Glu197β has been hypothesized to function in a similar manner when the phosphorylated His moves to Site II and dephosphorylates.

While generally specific for succinyl-CoA, SCS varies in NDP specificity. *E. coli* SCS can use both ADP and GDP substrates but prefers ADP (78). *T. aquaticus* SCS can also use both ADP and GDP but prefers GDP (71). Mammals possess two isoforms of SCS, one specific for GDP and the other specific for ADP, that are present in different tissues (79,80). The nucleotide binding site was determined to be located within the beta subunit between the two ATP grasp subdomains (76). Analysis of the open and closed GTP-bound structures of pig heart SCS revealed a Gln residue located within the NDP binding pocket that interacts with the guanine base (81). That same position is replaced by Pro in both *E. coli* and *T. aquaticus* SCSs (71,75). However, a Glu residue within the binding pocket of the *T. aquaticus* SCS is replaced by Ala, allowing an additional water molecule to bind between the Pro and the guanine base (71).This interaction mimics that of the Gln residue in GTP-specific pig heart SCS and determines the preference for GDP.

ATP citrate lyase

ATP citrate lyase (ACL; EC 2.3.3.8) utilizes ATP hydrolysis in order to convert citrate to cytosolic acetyl-CoA and oxaloacetate(OAA) [Eq. 17]. First identified in rat liver in 1971 (82), this enzyme has been studied in multiple eukaryotic organisms including human (83-87), rat (88), fungi (89), yeast (90), plants (91), and green algae (92). Prokaryotic ACL has only been identified in autotrophic bacteria and archaea containing a reductive TCA cycle as a CO_2 assimilation pathway (90,93,94) and in sulfur-dependent archaea (95). This enzyme represents the link between cytosolic carbohydrate

metabolism and production of fatty acids. Characterization thus far suggests that ACL functions solely as a citrate lyase and does not catalyze the reverse citrate synthase activity (96).

$$\text{citrate} + \text{ATP} + \text{CoA} + H_2O \rightarrow \text{OAA} + \text{acetyl-CoA} + \text{ADP} + P_i \qquad \text{[Eq. 17]}$$

Knockdown of ACL in mammalian cells impairs glucose-dependent lipid synthesis, increases mitochondrial membrane potential, and decreases cell proliferation (97). ACL is required for normal growth and development in plants, resulting in a bonsai-phenotype of small stature and organ size when knocked down in *Arabidopsis* (98). ACL has been implicated in tumorigenesis (99) and has been suggested as a potential target for chemotherapeutic agents (100).

ACL consists of an N-terminal region composed of the five subdomains present in all NDP-forming acyl-CoA synthetases and a C-terminal region containing a citrate synthase domain (FIG 1.3B). ACL from the yeast *Rhodotorula gracilis* and bacterium *Chlorobium tepidum* were shown to be homotetramers (90,93). In the 1980's, attempts to purify and characterize ACL were complicated by the varying levels of phosphorylation observed. The enzyme is phosphorylated on serine and threonine residues (101,102) and this phosphorylation is regulated by hormones glucagon, insulin, and vasopressin in rats (101) and varies depending on tissue localization (101). Two protein kinases capable of phosphorylating ACL were identified (102,103). ATP citrate lyase kinase phosphorylates Thr446 and Ser454 of the human enzyme, while cAMP-dependent protein kinase phosphorylates Ser454. These residues are located within the hinge region between subdomains 5 and 1 (83). *In vitro* phosphorylation of recombinant bacterial ACL by protein kinase A increased maximal activity 3- to 6-fold (87). Potapova

et al. (87) suggested that phosphorylation only occurs on one of the four subunits, and a conformational change prevents phosphorylation on the remaining subunits.

The enzyme also responds to positive allosteric regulation by phosphorylated sugars, particularly fructose-6-phosphate (87). The increase in overall activity is most dramatic in the unphosphorylated enzyme. The presence of fructose-6-phosphate also caused a large reduction in K_m values for ATP and citrate, suggesting a conformational change that affects the binding sites of these two substrates. ACL from *Chlorobium limicola* consists of separate alpha and beta subunits encoded by neighboring genes, and lacks the region of phosphorylation (96).

NTP substrate preference varies among ACLs. *Hydrogenobacter thermophilu*s prefers ATP, but can utilize GTP at a lower rate (94). However, *C. tepidum* and *C. limicola* enzymes can only utilize ATP (93,96). Mammalian enzymes can bind GTP, but only utilize ATP for catalysis (104). Inhibition by ADP was first observed for the *H. thermophilus* ACL(94). Recombinant ACL from *C. limicola* was shown to be competitively inhibited by the presence of ADP (96,104).

Kinetics analysis of ACL purified from rat liver indicate a double displacement mechanism involving a phosphoenzyme intermediate is the most likely mechanism (88). Like other NDP-forming acyl-CoA synthetases, the mechanism is believed to proceed through a catalytic phosphohistidine analogous to the Hisα of SCS. Mutagenesis of His765 in human ACL abolished enzymatic activity, supporting the role of this residue as the critical phosphorylated intermediate. This was further confirmed with recombinant ACL from *C. limicola* in which alteration of the catalytic His residue to Ala resulted in complete loss of activity (105). Phosphorylation of the catalytic His residue in the

absence of citrate and CoA was still observed but at a much lower rate (~1%). However, phosphorylation of a His760Ala variant suggests there may be a second unproductive phosphorylation site located within the active site. The first ACL crystal structure was of a truncated version of the human enzyme (83). Structural analysis revealed the citrate binding site is located within subdomain 2 along with the supposed nucleotide binding site in subdomains 3 and 4, similar to *E. coli* SCS (FIG 1.3B). The enzyme was then crystallized with Mg^{2+}-ADP bound revealing the nucleotide binding site within the ATP grasp domains (106).

Acetyl-CoA synthetase

ADP-forming acetyl-CoA synthetases (ACD; EC 6.2.1.13; Eq. 1) are not widespread and are found primarily in acetate-producing archaea (17,18,107) and a few eukaryotic (59,108) and bacterial species (32). ACDs have been designated as either ACDI or ACDII based on substrate specificity. ACDI primarily reacts with acetyl-CoA while ACDII is capable of functioning on branched-chain acyl-CoAs or aryl-CoAs. As discussed previously, they catalyze the reversible conversion of acetyl-CoA to acetate, forming ATP via substrate level phosphorylation. Structural characterization was limited until recently when ACD1 from *Candidatus Korarchaeum cryptofilum* was crystallized under several conditions (69). ACD will be discussed further in later chapters.

Additional enzymes

Malyl-CoA synthetase (EC 6.2.1.9) catalyzes a reaction similar to that of SCS and is composed of the same arrangement of subdomains. Malate is converted to malyl-CoA as part of glyoxylate and dicarboxylate metabolism (109). Recombinant enzyme from *Pseudomonas* was purified and characterized, revealing a heterotetramer formation

of alpha-beta dimers (110). Mechanistic studies with [γ-^{32}P]ATP indicated a "half-of-the-sites" reactivity, meaning that only one active site was phosphorylated at a time (111).

Pimeloyl-CoA synthetase (EC 6.2.1.14) from *Pseudomonas mendocina* was originally reported as an AMP-forming enzyme (112); however, the original assay did not differentiate between AMP and ADP formation. Sequence analysis revealed strong similarity to the NDP-forming acyl-CoA synthetases as opposed to AMP forming enzymes, indicating pimeloyl-CoA synthetase is likely a member of this enzyme superfamily (67). Pimeloyl-CoA is the first intermediate in the biotin synthesis pathway. Recombinant pimeloyl-CoA synthetase from *P. mendocina* formed a tetrameric enzyme and exhibited typical Michaelis-Menten kinetics (112).

E. coli PatZ (formerly YfiQ) and *Salmonella enterica* Pat are protein acetyltransferases with significant homology to ACD. Each of the five subdomains of the NDP-forming acyl-CoA synthetase family is present in the same order as in ACD, along with a GCN5-related N-acetyltransferase domain (FIG 1.3B). PatZ is the only known acetyltransferase in *E. coli* and its function is to regulate AMP-forming acetyl-CoA synthetase by acetylation (113). The biochemical and kinetic characterization of *S. enterica* PAT revealed the enzyme exists as a monomer but forms a tetramer upon acetyl-CoA binding (114). *E. coli* PatZ demonstrated autoacetylation that changed the oligomerization from a tetramer to a more stable and more active octamer (115). The acetyltransferase proteins lack the primary catalytic His residue found in the rest of the superfamily, and instead that position contains an asparagine residue incapable of being phosphorylated.

Although some biochemical, functional, and structural analysis of this superfamily of enzymes has been accomplished already, many questions remain. The origin of domain shuffling is still a mystery, along with the division of enzymes as either separate subunits or fusions.

IV. *ENTAMOEBA HISTOLYTICA*

Entamoeba histolytica is a protozoan parasite responsible for amoebic colitis (dysentery) and liver abscess in humans. An estimated 500 million people are infected each year, with 50 million developing colitis and liver abscess, causing 40,000 – 100,000 deaths every year (116-118). It is the second leading cause of death by parasitic disease worldwide and is endemic to areas of Central and South America, Asia, Africa, and the Pacific Islands (116). *E. histolytica* cycles between two life stages: an infectious cyst and vegetative trophozoite (FIG 1.4). The environmentally-resistant cyst is typically ingested via contaminated food or water. The cyst passes through the digestive system into the small intestine where it undergoes excystation. Trophozoites then migrate to the large intestine and multiply via binary fission. *E. histolytica* typically maintains an asymptomatic infection in the colon, however it can break through the intestinal epithelial lining and travel through the bloodstream to other organs. Infection of the liver results in substantial tissue damage, leading to abscess and death. Some trophozoites undergo encystation in the colon and are expelled in order to continue transmission. Cysts are highly resistant to disinfectants and can persist for months outside the host in moist environments (119).

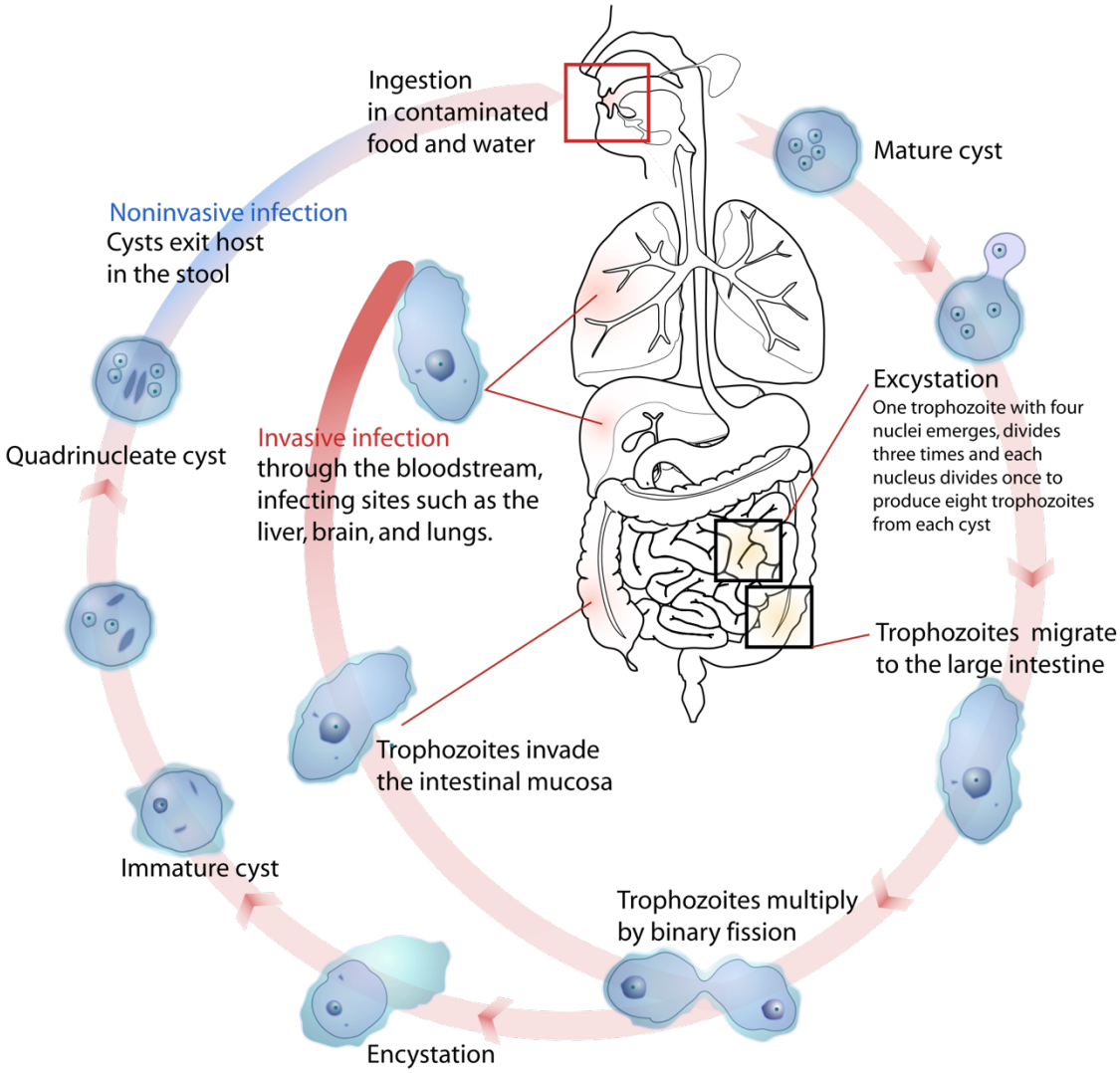

FIG 1.4 Life cycle of *Entamoeba histolytica*. The parasite cycles between the infectious cyst stage and the vegetative trophozoite that colonizes the human large intestine. Obtained from Wikimedia commons (File: Entamoebahistolyticalifecycle-en.svg)

Virulence and treatment

The colon is lined with a thick layer of mucin separating the intestinal microbiota from host epithelial cells. Adherence to this layer is essential for infection and is mediated by surface lectins that bind galactose (Gal) and N-acetyl-*D*-galactosamine (GalNAc) oligosaccharides (120). *E. histolytica* virulence is facilitated by contact-dependent cytotoxicity (121) and secreted proteins. Ingestion of microbes and host cells can occur via phagocytosis (122,123) or trogocytosis (124), and the resulting cellular material is degraded by a variety of enzymes within the phagolysosome (125).

The primary line of defense against invasive amoebiasis is metronidazole and other nitroimidazole derivatives (126). Originally discovered for the treatment of *Trichomonas vaginalis* infections, metronidazole targets anaerobic organisms. Upon entering the cell, metronidazole is reduced on the nitro group by reduced ferredoxin into short-lived cytotoxic intermediates (127,128). These compounds cause DNA strand breakage, eventually leading to disrupted transcription and cell death. Two pharmacokinetics studies showed 42% and 76% penetration of the drug into the colonic mucosa (129,130). Although largely effective, metronidazole has limitations because only 90% of patients respond to treatment, and parasites persist in 40-60% of treated patients (126). A second-line treatment of paromomycin or diloxanide furoate is necessary to completely clear infection (126). Furthermore, resistance to metronidazole has been demonstrated *in vitro* (131,132). Although this has not been observed clinically, the possibility is of growing concern. Efforts to develop new therapeutic targets as well as potential vaccines are currently underway (133-135).

Metabolism depends on the environment

E. histolytica possesses a uniquely reduced metabolism compared to typical eukaryotes, lacking mitochondria and several biosynthetic pathways (136). Consequently, the parasite relies heavily on scavenging essential nutrients including most amino acids, nucleic acids, lipids, and vitamins. Carbohydrate metabolism depends on availability within the environment. Trophozoites first emerge within the small intestine where glucose is prevalent and glycolysis is thought to provide the majority of energy for *E. histolytica* (137). However, as *E. histolytica* travels to the colon, the concentration of glucose is very low (138). Glucose transporters of epithelial cells in the small intestine have high affinity for glucose and most is removed before nutrients reach the colon (139). Consequently, the parasite must adapt to long-term glucose starvation in order to survive (140). Glucose starvation has been known to trigger cyst formation in other amoeboid species (141-143). Furthermore, *Entamoeba* competes with prevalent intestinal flora for nutrients (144). It has been suggested that *E. histolytica* secretes a beta-amylase enzyme to break down mucin oligosaccharides as a source of carbohydrates (145). In contrast, when *E. histolytica* invades the blood (146) or liver tissue (147), exogenous glucose is abundant, but the parasite must deal with other stresses. Also present in the colon are high concentrations of short-chain fatty acids, including acetate, that are known to be taken up in pH dependent manner by a related *Entamoeba* species (148).

Glycolysis

E. histolytica has several adaptations within its glycolytic pathway. The ATP-dependent phosphofructokinase (PFK; EC 2.7.9.1; Eq. 18) has been replaced by a

pyrophosphate (PP_i)-dependent phosphofructokinase (PP_i-PFK; 2.7.1.90; Eq. 19). PFK is typically an important point of regulation within glycolysis due to its irreversibility and allosteric regulation by AMP. However, PP_i-PFK is not allosterically regulated and constitutes a reversible reaction under physiological conditions (149-151).

Fructose-6-phosphate + ATP → fructose-1,6-bisphosphate + ADP [Eq. 18]

Fructose-6-phosphate + PP_i ←→ fructose-1,6-bisphosphate + Pi [Eq. 19]

Pyruvate phosphate dikinase (PPDK; EC 2.7.9.1; Eq. 20) is another PP_i-dependent enzyme which catalyzes the reversible conversion of phosphoenolpyruvate (PEP) to pyruvate replacing the typical pyruvate kinase (PK; 2.7.1.40; Eq. 21) (152).

PEP + AMP + PP_i ←→ pyruvate + ATP + P_i [Eq. 20]

PEP + ADP ←→ pyruvate + ATP [Eq. 21]

A potential benefit of using PP_i is the conservation of energy from PP_i-generating anabolic reactions. Also, since the typical “committed step” is now reversible under physiological conditions, these enzymes could be involved in both catabolic and anabolic processes (153). Another atypical glycolytic enzyme of unknown significance is the GDP-dependent phosphoglycerate kinase (GDP-PGK; EC 2.7.2.10), which displays a significant preference for GDP over ADP as the phosphoryl acceptor (154).

While these adaptations may confer an advantage to *Entamoeba*, they also require a change in the typical regulation of glycolysis. Each glycolytic enzyme of *E. histolytica* has been studied recombinantly (150,155). Elasticity analysis was used to understand how central carbon metabolism is regulated in live trophozoites of *E. histolytica*. The initial steps of hexose transporter, hexokinase, and glycogen degradation were determined to be the controlling steps (156).

As first observed by electron microscopy in 1970 (157), *Entamoeba* cells contain numerous glycogen granules in the cytoplasm. The high glycogen content observed when cells are cultured under high glucose serves as an energy reservoir that is capable of supporting glycolysis for up to 2 hours after glucose starvation before a significant decrease in ATP output or cell viability (156). Glycogen granules and the enzymes for their synthesis and degradation have all been characterized (158,159).

Most organisms employ the allosterically regulated pyruvate dehydrogenase complex to couple the conversion of pyruvate to acetyl-CoA and concomitantly produce NADH. However, multiple amitochondriate protozoan species lack a pyruvate dehydrogenase complex and instead complete the pyruvate to acetyl-CoA reaction via oxidative decarboxylation by pyruvate:ferrodoxin oxidoreductase (PFOR; EC 1.2.7.1). PFOR uses the cofactor ferredoxin as an electron acceptor to complete this reaction. This enzyme is typically found in Archaea, but has been identified in *E. histolytica* and *G. lamblia*. Both PFOR and ACD are thought to have been acquired by lateral gene transfer (160). EhPFOR has been studied in cell extracts (161).

Amino acid metabolism

E. histolytica lacks *de novo* synthesis pathways for the majority of amino acids. Consequently, it relies on scavenging in order to supply its amino acid requirements. Furthermore, the parasite is also capable of taking up amino acids to use them for energy generation (160,162). During glucose starvation, glycolysis-related genes are downregulated and amino acid consumption increases (162). Asparagine, aspartate, serine, alanine, tryptophan, cysteine, threonine, methionine, glutamine and glutamate can all be converted into either pyruvate or a 2-oxoacid (160). PFOR converts pyruvate

or 2-oxoacids to CoA esters, from which ACD can produce ATP and the corresponding acids.

Aspartate and asparagine are taken up in the presence or absence of glucose (162). Under long-term glucose shortage, methionine gamma-lyase and aspartate ammonia lyase are upregulated (163). Aspartate ammonia lyase converts aspartate to fumarate and ammonia, and asparaginase converts asparagine to aspartate and ammonia. Methionine gamma-lyase, a unique enzyme found only in *E. histolytica* and *Trichomonas vaginalis*, is capable of breaking down methionine or the potentially toxic homocysteine (160) to produce ammonia and 2-oxobutanoate. Flux analysis performed by Pineda *et al*. (156) indicated that amino acid catabolism cannot substitute for glucose to maintain ATP levels. However, the lack of a sufficient number of replicates brings these conclusions into question.

E. histolytica is capable of synthesizing just two amino acids, serine and cysteine. Cysteine serves a special role in *E. histolytica* in combatting oxidative stress. Typical eukaryotes contain glutathione as a low-molecular weight thiol capable of maintaining redox balance. However, *E. histolytica* does not contain glutathione and utilizes cysteine in this role instead (164). Cysteine has been deemed essential for growth, motility, adherence, and demonstrated protection against oxidative stress *in vitro* (165,166). Cysteine synthesis is critical to the parasite (167) and occurs via a two-step pathway from serine (168). Serine acetyltransferase (EC 2.3.1.30) converts serine to O-acetylserine by transferring the acetyl moiety from acetyl-CoA. Cysteine synthase (EC 4.2.99.8) then generates cysteine from O-acetylserine and sulfhydryl, releasing acetate.

This pathway is one source of excreted acetate, in addition to the pathways discussed later in this chapter.

Mitosome

Most eukaryotic organisms contain mitochondria that primarily function in ATP generation via oxidative phosphorylation and the electron transport chain. Several parasitic protozoan species do not have fully functional mitochondria (169), but instead retain highly reduced mitochondrion-related organelles (MROs). The principal functions of mitochondria have likely been lost due to adaptation to an anaerobic lifestyle. For some of these parasites such as *T. vaginalis*, this MRO is known as a hydrogenosome which produces molecular hydrogen and ATP (170). *E. histolytica* and *G. lamblia* possess the most degenerate MRO, known as a mitosome (170). Fe-S cluster synthesis was thought to be the solely retained function of mitosomes. However, the system found in *E. histolytica* does not originate from mitochondria but is found in nitrogen-fixing bacteria. Furthermore, the localization of this system in either the mitosome or cytosol is currently debated. However, a unique sulfate activation has been localized to the mitosome in *E. histolytica* (171,172). Investigations revealed that this sulfate activation pathway plays a role in proliferation (172) and encystation (173).

Excreted products

E. histolytica excretes three compounds during growth *in vitro*: acetate, ethanol, and alanine (160). The definitive function of alanine secretion is unknown, however it is thought to be a mechanism for eliminating excess nitrogen. Ethanol is produced via a bifunctional alcohol/acetaldehyde dehydrogenase(ADHE; E.C. 1.2.1.10, 1.1.1.1) enzyme that first converts acetyl-CoA to acetaldehyde and then to ethanol, regenerating a

molecule of NAD^+ at each step (174). There are three potential sources of excreted acetate: 1) as a byproduct of cysteine synthesis via cysteine synthase, 2) during additional ATP production via ADP-forming acetyl-CoA synthesis, or 3) by acetate kinase (FIG 1.5). The relative contributions of each of these pathways to acetate production is unknown.

E. histolytica possesses a unique PP_i-producing acetate kinase, and as discussed previously in this chapter, there is no known partner enzyme present in the genome (51,56,175). The source of the acetyl phosphate substrate has been postulated to come from ingested bacteria (175). The role of this enzyme remains to be determined, however, characterization of the recombinant enzyme indicates it functions primarily in PP_i and acetate formation. It is possible that PP_i is produced in order to supply the unique PP_i-dependent enzymes in glycolysis or that PP_i is used as a regulatory compound.

The balance between acetate and ethanol production is influenced by environmental oxygen concentrations. The first observations under anaerobic growth conditions indicated a ratio of ethanol:acetate production of 2:1 (176). This balance was then reversed to a 2:1 acetate:ethanol ratio under aerobic conditions. However, both of these observations were measured during monoxenic growth and the relative contributions from bacteria cannot be determined. Once axenic culture protocols were established, *E. histolytica* excretion was once again studied. Under aerobic growth, acetate was the major metabolite produced (60). After exposure to supraphysiological O_2 concentrations, *E. histolytica* showed a reduction in ethanol production and an increase in acetate production during the recovery period compared to unstressed cells (161).

PFOR and ADHE were both drastically inhibited by reactive oxygen species. Pineda *et al.* performed metabolic control analysis to understand the acetate and ethanol flux under moderate aerobic conditions, mimicking the environment encountered when invades tissue adjacent to the colon (177). They observed that PFOR and ADHE were major points of regulation of central carbon metabolism. The reported output of ethanol and acetate under typical *in vitro* growth conditions was 26 ± 7 and 3.6 ± 8 nmol min^{-1} mg^{-1} cell protein, respectively.

Recent knockdown of *ACD* in *E. histolytica* trophozoites revealed a significant reduction in acetate production in culture (178). Contributions to ATP were negligible, but ACD was shown to be important for maintaining acetyl-CoA/CoA homeostasis, especially under oxidative stress conditions when ADHE was inhibited. Knockdown of *ACK* showed no reduction in acetate production and no conclusions about the function of ACK could be made.

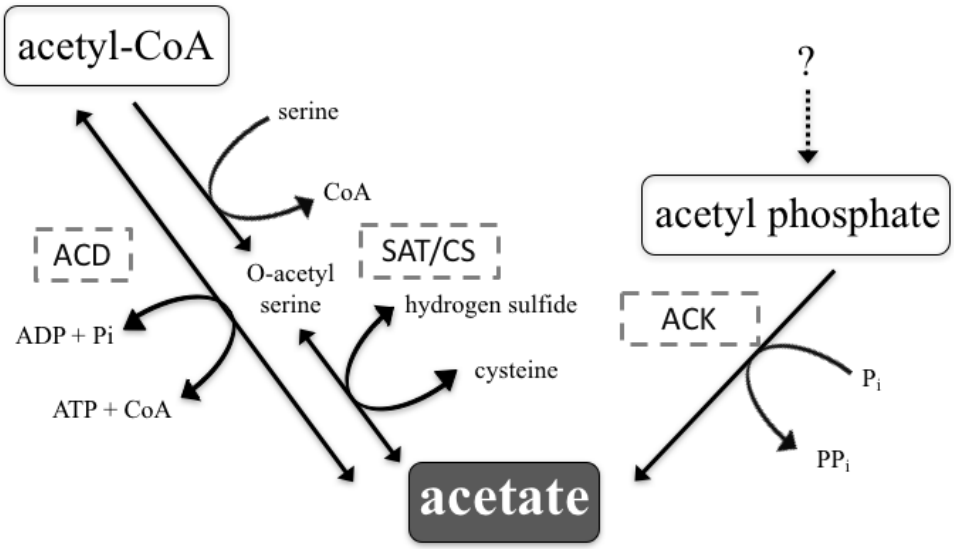

FIG 1.5 Acetate metabolism in *E. histolytica*. ACD = ADP-forming acetyl-CoA synthetase; SAT = serine acetyltransferase; CS = cysteine synthase; ACK = acetate kinase.

V. CONCLUSIONS

In summary, acetate metabolism is clearly an important process in many organisms, including parasitic protozoans. Both acetate production and assimilation occur under different conditions depending on the enzymes present and the cell's needs. ADP-forming acetyl-CoA synthetase functions in acetate metabolism and is part of a superfamily of NDP-forming acyl-CoA synthetases that catalyze a set of reactions involved in central carbon metabolism and often are involved in energy homeostasis. The metabolism of the amitochondriate parasite *Entamoeba histolytica* is severely limited, however an ACD enzyme is present. The research presented in the following chapters will explore the function and mechanism of *Eh*ACD.

VI. REFERENCES

1. Wolfe, A. J. (2005) The acetate switch. *Microbiol Mol Biol Rev* **69**, 12-50

2. Verdin, E., and Ott, M. (2015) 50 years of protein acetylation: from gene regulation to epigenetics, metabolism and beyond. *Nat Rev Mol Cell Biol* **16**, 258-264

3. McBrian, M. A., Behbahan, I. S., Ferrari, R., Su, T., Huang, T. W., Li, K., Hong, C. S., Christofk, H. R., Vogelauer, M., Seligson, D. B., and Kurdistani, S. K. (2013) Histone acetylation regulates intracellular pH. *Mol Cell* **49**, 310-321

4. Ferry, J. G. (2015) Acetate metabolism in anaerobes from the domain Archaea. *Life (Basel)* **5**, 1454-1471

5. Ferry, J. G. (1997) Enzymology of the fermentation of acetate to methane by *Methanosarcina thermophila*. *Biofactors* **6**, 25-35

6. Welte, C., Kroninger, L., and Deppenmeier, U. (2014) Experimental evidence of an acetate transporter protein and characterization of acetate activation in aceticlastic methanogenesis of *Methanosarcina mazei*. *FEMS Microbiol Lett* **359**, 147-153

7. Starai, V. J., and Escalante-Semerena, J. C. (2004) Acetyl-coenzyme A synthetase (AMP forming). *Cell Mol Life Sci* **61**, 2020-2030

8. Berger, S., Welte, C., and Deppenmeier, U. (2012) Acetate activation in *Methanosaeta thermophila*: characterization of the key enzymes pyrophosphatase and acetyl-CoA synthetase. *Archaea* **2012**, 315153

9. Anke, H., and Spector, L. B. (1975) Evidence for an acetyl-enzyme intermediate in the action of acetyl-CoA synthetase. *Biochem Biophys Res Commun* **67**, 767-773

10. Mayer, F., Kuper, U., Meyer, C., Daxer, S., Muller, V., Rachel, R., and Huber, H. (2012) AMP-forming acetyl coenzyme A synthetase in the outermost membrane of the hyperthermophilic crenarchaeon *Ignicoccus hospitalis*. *J Bacteriol* **194**, 1572-1581

11. Brasen, C., Urbanke, C., and Schonheit, P. (2005) A novel octameric AMP-forming acetyl-CoA synthetase from the hyperthermophilic crenarchaeon *Pyrobaculum aerophilum*. *FEBS Lett* **579**, 477-482

12. Brasen, C., and Schonheit, P. (2001) Mechanisms of acetate formation and acetate activation in halophilic archaea. *Arch Microbiol* **175**, 360-368

13. Brasen, C., and Schonheit, P. (2005) AMP-forming acetyl-CoA synthetase from the extremely halophilic archaeon *Haloarcula marismortui*: purification, identification and expression of the encoding gene, and phylogenetic affiliation. *Extremophiles* **9**, 355-365

14. Ingram-Smith, C., and Smith, K. S. (2007) AMP-forming acetyl-CoA synthetases in Archaea show unexpected diversity in substrate utilization. *Archaea* **2**, 95-107

15. Schäfer, T., Selig, M., and Schönheit, P. (1993) Acetyl-CoA synthetase (ADP forming) in archaea, a novel enzyme involved in acetate formation and ATP synthesis. *Arch. Microbiol.* **159**, 72-83

16. Brasen, C., Schmidt, M., Grotzinger, J., and Schonheit, P. (2008) Reaction mechanism and structural model of ADP-forming Acetyl-CoA synthetase from the hyperthermophilic archaeon *Pyrococcus furiosus*: evidence for a second active site histidine residue. *J Biol Chem* **283**, 15409-15418

17. Glasemacher, J., Bock, A. K., Schmid, R., and Schonheit, P. (1997) Purification and properties of acetyl-CoA synthetase (ADP-forming), an archaeal enzyme of acetate formation and ATP synthesis, from the hyperthermophile *Pyrococcus furiosus*. *Eur J Biochem* **244**, 561-567

18. Musfeldt, M., Selig, M., and Schonheit, P. (1999) Acetyl coenzyme A synthetase (ADP forming) from the hyperthermophilic Archaeon *Pyrococcus furiosus*: identification, cloning, separate expression of the encoding genes, acdAI and acdBI, in *Escherichia coli*, and in vitro reconstitution of the active heterotetrameric enzyme from its recombinant subunits. *J Bacteriol* **181**, 5885-5888

19. Mai, X., and Adams, M. W. (1996) Purification and characterization of two reversible and ADP-dependent acetyl coenzyme A synthetases from the hyperthermophilic archaeon *Pyrococcus furiosus*. *J Bacteriol* **178**, 5897-5903

20. Labes, A., and Schonheit, P. (2001) Sugar utilization in the hyperthermophilic, sulfate-reducing archaeon *Archaeoglobus fulgidus* strain 7324: starch degradation to acetate and CO_2 via a modified Embden-Meyerhof pathway and acetyl-CoA synthetase (ADP-forming). *Arch Microbiol* **176**, 329-338

21. Musfeldt, M., and Schonheit, P. (2002) Novel type of ADP-forming acetyl coenzyme A synthetase in hyperthermophilic archaea: heterologous expression and characterization of isoenzymes from the sulfate reducer *Archaeoglobus fulgidus* and the methanogen *Methanococcus jannaschii*. *J Bacteriol* **184**, 636-644

22. Awano, T., Wilming, A., Tomita, H., Yokooji, Y., Fukui, T., Imanaka, T., and Atomi, H. (2014) Characterization of two members among the five ADP-forming acyl coenzyme A (Acyl-CoA) synthetases reveals the presence of a 2-(Imidazol-

4-yl)acetyl-CoA synthetase in *Thermococcus kodakarensis*. *J Bacteriol* **196**, 140-147

23. Brasen, C., and Schonheit, P. (2004) Unusual ADP-forming acetyl-coenzyme A synthetases from the mesophilic halophilic euryarchaeon *Haloarcula marismortui* and from the hyperthermophilic crenarchaeon *Pyrobaculum aerophilum*. *Arch Microbiol* **182**, 277-287

24. Brasen, C., and Schonheit, P. (2004) Regulation of acetate and acetyl-CoA converting enzymes during growth on acetate and/or glucose in the halophilic archaeon *Haloarcula marismortui*. *FEMS Microbiol Lett* **241**, 21-26

25. Wolfe, A. J. (2010) Physiologically relevant small phosphodonors link metabolism to signal transduction. *Curr Opin Microbiol* **13**, 204-209

26. Suzuki, R., Kim, B. J., Shibata, T., Iwamoto, Y., Katayama, T., Ashida, H., Wakagi, T., Shoun, H., Fushinobu, S., and Yamamoto, K. (2010) Overexpression, crystallization and preliminary X-ray analysis of xylulose-5-phosphate/fructose-6-phosphate phosphoketolase from *Bifidobacterium breve*. *Acta Crystallogr Sect F Struct Biol Cryst Commun* **66**, 941-943

27. Abdel-Hamid, A. M., Attwood, M. M., and Guest, J. R. (2001) Pyruvate oxidase contributes to the aerobic growth efficiency of *Escherichia coli*. *Microbiology* **147**, 1483-1498

28. Hallows, W. C., Lee, S., and Denu, J. M. (2006) Sirtuins deacetylate and activate mammalian acetyl-CoA synthetases. *Proc Natl Acad Sci U S A* **103**, 10230-10235

29. Starai, V. J., and Escalante-Semerena, J. C. (2004) Identification of the protein acetyltransferase (Pat) enzyme that acetylates acetyl-CoA synthetase in *Salmonella enterica*. *J Mol Biol* **340**, 1005-1012

30. Starai, V. J., Celic, I., Cole, R. N., Boeke, J. D., and Escalante-Semerena, J. C. (2002) Sir2-dependent activation of acetyl-CoA synthetase by deacetylation of active lysine. *Science* **298**, 2390-2392

31. Chan, C. H., Garrity, J., Crosby, H. A., and Escalante-Semerena, J. C. (2011) In *Salmonella enterica*, the sirtuin-dependent protein acylation/deacylation system (SDPADS) maintains energy homeostasis during growth on low concentrations of acetate. *Mol Microbiol* **80**, 168-183

32. Schmidt, M., and Schonheit, P. (2013) Acetate formation in the photoheterotrophic bacterium *Chloroflexus aurantiacus* involves an archaeal type ADP-forming acetyl-CoA synthetase isoenzyme I. *FEMS Microbiol Lett* **349**, 171-179

33. McInerney, M. J., Rohlin, L., Mouttaki, H., Kim, U., Krupp, R. S., Rios-Hernandez, L., Sieber, J., Struchtemeyer, C. G., Bhattacharyya, A., Campbell, J. W., and Gunsalus, R. P. (2007) The genome of *Syntrophus aciditrophicus*: life at the thermodynamic limit of microbial growth. *Proc Natl Acad Sci U S A* **104**, 7600-7605

34. Kosaka, T., Kato, S., Shimoyama, T., Ishii, S., Abe, T., and Watanabe, K. (2008) The genome of *Pelotomaculum thermopropionicum* reveals niche-associated evolution in anaerobic microbiota. *Genome Res* **18**, 442-448

35. Kumari, S., Beatty, C. M., Browning, D. F., Busby, S. J., Simel, E. J., Hovel-Miner, G., and Wolfe, A. J. (2000) Regulation of acetyl coenzyme A synthetase in *Escherichia coli*. *J Bacteriol* **182**, 4173-4179

36. van den Berg, M. A., de Jong-Gubbels, P., Kortland, C. J., van Dijken, J. P., Pronk, J. T., and Steensma, H. Y. (1996) The two acetyl-coenzyme A synthetases of *Saccharomyces cerevisiae* differ with respect to kinetic properties and transcriptional regulation. *J Biol Chem* **271**, 28953-28959

37. Fujino, T., Kondo, J., Ishikawa, M., Morikawa, K., and Yamamoto, T. T. (2001) Acetyl-CoA synthetase 2, a mitochondrial matrix enzyme involved in the oxidation of acetate. *J Biol Chem* **276**, 11420-11426

38. Falcon, A. A., Chen, S., Wood, M. S., and Aris, J. P. (2010) Acetyl-coenzyme A synthetase 2 is a nuclear protein required for replicative longevity in *Saccharomyces cerevisiae*. *Mol Cell Biochem* **333**, 99-108

39. Buckley, B. M., and Williamson, D. H. (1977) Origins of blood acetate in the rat. *Biochem J* **166**, 539-545

40. Seufert, C. D., Graf, M., Janson, G., Kuhn, A., and Soling, H. D. (1974) Formation of free acetate by isolated perfused livers from normal, starved and diabetic rats. *Biochem Biophys Res Commun* **57**, 901-909

41. Yamashita, H., Kaneyuki, T., and Tagawa, K. (2001) Production of acetate in the liver and its utilization in peripheral tissues. *Biochim Biophys Acta* **1532**, 79-87

42. Yoshii, Y., Furukawa, T., Saga, T., and Fujibayashi, Y. (2015) Acetate/acetyl-CoA metabolism associated with cancer fatty acid synthesis: overview and application. *Cancer Lett* **356**, 211-216

43. Yoshii, Y., Furukawa, T., Yoshii, H., Mori, T., Kiyono, Y., Waki, A., Kobayashi, M., Tsujikawa, T., Kudo, T., Okazawa, H., Yonekura, Y., and Fujibayashi, Y. (2009) Cytosolic acetyl-CoA synthetase affected tumor cell survival under hypoxia: the possible function in tumor acetyl-CoA/acetate metabolism. *Cancer Sci* **100**, 821-827

44. Lin, M., and Oliver, D. J. (2008) The role of acetyl-coenzyme a synthetase in *Arabidopsis*. *Plant Physiol* **147**, 1822-1829

45. Shimazu, T., Hirschey, M. D., Huang, J. Y., Ho, L. T., and Verdin, E. (2010) Acetate metabolism and aging: An emerging connection. *Mech Ageing Dev* **131**, 511-516

46. Zambell, K. L., Fitch, M. D., and Fleming, S. E. (2003) Acetate and butyrate are the major substrates for de novo lipogenesis in rat colonic epithelial cells. *J Nutr* **133**, 3509-3515

47. Schwer, B., Bunkenborg, J., Verdin, R. O., Andersen, J. S., and Verdin, E. (2006) Reversible lysine acetylation controls the activity of the mitochondrial enzyme acetyl-CoA synthetase 2. *Proc Natl Acad Sci U S A* **103**, 10224-10229

48. Carman, A. J., Vylkova, S., and Lorenz, M. C. (2008) Role of acetyl coenzyme A synthesis and breakdown in alternative carbon source utilization in *Candida albicans*. *Eukaryot Cell* **7**, 1733-1741

49. Mazet, M., Morand, P., Biran, M., Bouyssou, G., Courtois, P., Daulouede, S., Millerioux, Y., Franconi, J. M., Vincendeau, P., Moreau, P., and Bringaud, F. (2013) Revisiting the central metabolism of the bloodstream forms of *Trypanosoma brucei*: production of acetate in the mitochondrion is essential for parasite viability. *PLoS Negl Trop Dis* **7**, e2587

50. Soumya, N., Kumar, I. S., Shivaprasad, S., Gorakh, L. N., Dinesh, N., Swamy, K. K., and Singh, S. (2015) AMP-acetyl CoA synthetase from *Leishmania donovani*: identification and functional analysis of 'PX4GK' motif. *Int J Biol Macromol* **75**, 364-372

51. Ingram-Smith, C., Martin, S. R., and Smith, K. S. (2006) Acetate kinase: not just a bacterial enzyme. *Trends Microbiol* **14**, 249-253

52. Yang, W., Catalanotti, C., D'Adamo, S., Wittkopp, T. M., Ingram-Smith, C. J., Mackinder, L., Miller, T. E., Heuberger, A. L., Peers, G., Smith, K. S., Jonikas, M. C., Grossman, A. R., and Posewitz, M. C. (2014) Alternative acetate production pathways in *Chlamydomonas reinhardtii* during dark anoxia and the dominant role of chloroplasts in fermentative acetate production. *Plant Cell* **26**, 4499-4518

53. Taylor, T., Ingram-Smith, C., and Smith, K. S. (2015) Biochemical and Kinetic Characterization of the Eukaryotic Phosphotransacetylase Class IIa Enzyme from *Phytophthora ramorum*. *Eukaryot Cell* **14**, 652-660

54. Atteia, A., van Lis, R., Gelius-Dietrich, G., Adrait, A., Garin, J., Joyard, J., Rolland, N., and Martin, W. (2006) Pyruvate formate-lyase and a novel route of eukaryotic ATP synthesis in *Chlamydomonas mitochondria*. *J Biol Chem* **281**, 9909-9918

55. Glenn, K., Ingram-Smith, C., and Smith, K. S. (2014) Biochemical and kinetic characterization of xylulose 5-phosphate/fructose 6-phosphate phosphoketolase 2 (Xfp2) from *Cryptococcus neoformans*. *Eukaryot Cell* **13**, 657-663

56. Fowler, M. L., Ingram-Smith, C., and Smith, K. S. (2012) Novel pyrophosphate-forming acetate kinase from the protist E*ntamoeba histolytica*. *Eukaryot Cell* **11**, 1249-1256

57. Saint-Prix, F., Bonquist, L., and Dequin, S. (2004) Functional analysis of the ALD gene family of *Saccharomyces cerevisiae* during anaerobic growth on glucose: the $NADP^+$-dependent Ald6p and Ald5p isoforms play a major role in acetate formation. *Microbiology* **150**, 2209-2220

58. Hajipour, G., Schowen, K. B., and Schowen, R. L. (1999) The linkage of catalysis and regulation in enzyme action: oxidative diversion in the hysteretically regulated yeast pyruvate decarboxylase. *Bioorg Med Chem* **7**, 887-894

59. Sanchez, L. B., and Muller, M. (1996) Purification and characterization of the acetate forming enzyme, acetyl-CoA synthetase (ADP-forming) from the amitochondriate protist, *Giardia lamblia*. *FEBS Lett* **378**, 240-244

60. Reeves, R. E., Warren, L. G., Susskind, B., and Lo, H. S. (1977) An energy-conserving pyruvate-to-acetate pathway in *Entamoeba histolytica*. Pyruvate synthase and a new acetate thiokinase. *J Biol Chem* **252**, 726-731

61. Lindmark, D. G. (1980) Energy metabolism of the anaerobic protozoon *Giardia lamblia*. *Mol Biochem Parasitol* **1**, 1-12

62. van Grinsven, K. W., Rosnowsky, S., van Weelden, S. W., Putz, S., van der Giezen, M., Martin, W., van Hellemond, J. J., Tielens, A. G., and Henze, K. (2008) Acetate:succinate CoA-transferase in the hydrogenosomes of *Trichomonas vaginalis*: identification and characterization. *J Biol Chem* **283**, 1411-1418

63. Riviere, L., van Weelden, S. W., Glass, P., Vegh, P., Coustou, V., Biran, M., van Hellemond, J. J., Bringaud, F., Tielens, A. G., and Boshart, M. (2004) Acetyl:succinate CoA-transferase in procyclic *Trypanosoma brucei*. Gene identification and role in carbohydrate metabolism. *J Biol Chem* **279**, 45337-45346

64. Van Hellemond, J. J., Opperdoes, F. R., and Tielens, A. G. (1998) Trypanosomatidae produce acetate via a mitochondrial acetate:succinate CoA transferase. *Proc Natl Acad Sci U S A* **95**, 3036-3041

65. van Grinsven, K. W., van Hellemond, J. J., and Tielens, A. G. (2009) Acetate:succinate CoA-transferase in the anaerobic mitochondria of *Fasciola hepatica. Mol Biochem Parasitol* **164**, 74-79

66. Chen, Y., Zhang, Y., Siewers, V., and Nielsen, J. (2015) Ach1 is involved in shuttling mitochondrial acetyl units for cytosolic C2 provision in *Saccharomyces cerevisiae* lacking pyruvate decarboxylase. *FEMS Yeast Res* **15**

67. Sanchez, L. B., Galperin, M. Y., and Muller, M. (2000) Acetyl-CoA synthetase from the amitochondriate eukaryote *Giardia lamblia* belongs to the newly recognized superfamily of acyl-CoA synthetases (Nucleoside diphosphate-forming). *J Biol Chem* **275**, 5794-5803

68. Fawaz, M. V., Topper, M. E., and Firestine, S. M. (2011) The ATP-grasp enzymes. *Bioorg Chem* **39**, 185-191

69. Weiße, R. H., Faust, A., Schmidt, M., Schonheit, P., and Scheidig, A. J. (2016) Structure of NDP-forming Acetyl-CoA synthetase ACD1 reveals a large rearrangement for phosphoryl transfer. *Proc Natl Acad Sci U S A* **113**, E519-528

70. Wolodko, W. T., Kay, C. M., and Bridger, W. A. (1986) Active enzyme sedimentation, sedimentation velocity, and sedimentation equilibrium studies of succinyl-CoA synthetases of porcine heart and *Escherichia coli. Biochemistry* **25**, 5420-5425

71. Joyce, M. A., Hayakawa, K., Wolodko, W. T., and Fraser, M. E. (2012) Biochemical and structural characterization of the GTP-preferring succinyl-CoA synthetase from *Thermus aquaticus*. *Acta Crystallogr D Biol Crystallogr* **68**, 751-762

72. Bridger, W. A. (1971) Evidence for two types of subunits in succinyl coenzyme A synthetase. *Biochem Biophys Res Commun* **42**, 948-954

73. Wolodko, W. T., Fraser, M. E., James, M. N., and Bridger, W. A. (1994) The crystal structure of succinyl-CoA synthetase from *Escherichia coli* at 2.5-A resolution. *J Biol Chem* **269**, 10883-10890

74. Fraser, M. E., James, M. N., Bridger, W. A., and Wolodko, W. T. (2000) Phosphorylated and dephosphorylated structures of pig heart, GTP-specific succinyl-CoA synthetase. *J Mol Biol* **299**, 1325-1339

75. Joyce, M. A., Fraser, M. E., James, M. N., Bridger, W. A., and Wolodko, W. T. (2000) ADP-binding site of *Escherichia coli* succinyl-CoA synthetase revealed by x-ray crystallography. *Biochemistry* **39**, 17-25

76. Joyce, M. A., Fraser, M. E., Brownie, E. R., James, M. N., Bridger, W. A., and Wolodko, W. T. (1999) Probing the nucleotide-binding site of *Escherichia coli* succinyl-CoA synthetase. *Biochemistry* **38**, 7273-7283

77. Fraser, M. E., Joyce, M. A., Ryan, D. G., and Wolodko, W. T. (2002) Two glutamate residues, Glu 208 alpha and Glu 197 beta, are crucial for

phosphorylation and dephosphorylation of the active-site histidine residue in succinyl-CoA synthetase. *Biochemistry* **41**, 537-546

78. Fraser, M. E., James, M. N., Bridger, W. A., and Wolodko, W. T. (1999) A detailed structural description of *Escherichia coli* succinyl-CoA synthetase. *J Mol Biol* **285**, 1633-1653

79. Johnson, J. D., Muhonen, W. W., and Lambeth, D. O. (1998) Characterization of the ATP- and GTP-specific succinyl-CoA synthetases in pigeon. The enzymes incorporate the same alpha-subunit. *J Biol Chem* **273**, 27573-27579

80. Lambeth, D. O., Tews, K. N., Adkins, S., Frohlich, D., and Milavetz, B. I. (2004) Expression of two succinyl-CoA synthetases with different nucleotide specificities in mammalian tissues. *J Biol Chem* **279**, 36621-36624

81. Fraser, M. E., Hayakawa, K., Hume, M. S., Ryan, D. G., and Brownie, E. R. (2006) Interactions of GTP with the ATP-grasp domain of GTP-specific succinyl-CoA synthetase. *J Biol Chem* **281**, 11058-11065

82. Mardh, S., Ljungstrom, O., Hogstedt, S., and Zetterqvist, O. (1971) Studies on a rat-liver cell-sap protein yielding 3-[32P]-phosphohistidine after incubation with [32P]ATP and alkaline hydrolysis. Identification of the protein as ATP citrate lyase. *Biochim Biophys Acta* **251**, 419-426

83. Sun, T., Hayakawa, K., Bateman, K. S., and Fraser, M. E. (2010) Identification of the citrate-binding site of human ATP-citrate lyase using X-ray crystallography. *J Biol Chem* **285**, 27418-27428

84. Elshourbagy, N. A., Near, J. C., Kmetz, P. J., Wells, T. N., Groot, P. H., Saxty, B. A., Hughes, S. A., Franklin, M., and Gloger, I. S. (1992) Cloning and expression of a human ATP-citrate lyase cDNA. *Eur J Biochem* **204**, 491-499

85. Fan, F., Williams, H. J., Boyer, J. G., Graham, T. L., Zhao, H., Lehr, R., Qi, H., Schwartz, B., Raushel, F. M., and Meek, T. D. (2012) On the catalytic mechanism of human ATP citrate lyase. *Biochemistry* **51**, 5198-5211

86. Lord, K. A., Wang, X. M., Simmons, S. J., Bruckner, R. C., Loscig, J., O'Connor, B., Bentley, R., Smallwood, A., Chadwick, C. C., Stevis, P. E., and Ciccarelli, R. B. (1997) Variant cDNA sequences of human ATP:citrate lyase: cloning, expression, and purification from baculovirus-infected insect cells. *Protein Expr Purif* **9**, 133-141

87. Potapova, I. A., El-Maghrabi, M. R., Doronin, S. V., and Benjamin, W. B. (2000) Phosphorylation of recombinant human ATP:citrate lyase by cAMP-dependent protein kinase abolishes homotropic allosteric regulation of the enzyme by citrate and increases the enzyme activity. Allosteric activation of ATP:citrate lyase by phosphorylated sugars. *Biochemistry* **39**, 1169-1179

88. Houston, B., and Nimmo, H. G. (1984) Purification and some kinetic properties of rat liver ATP citrate lyase. *Biochem J* **224**, 437-443

89. Pfitzner, A., Kubicek, C. P., and Rohr, M. (1987) Presence and regulation of ATP:citrate lyase from the citric acid producing fungus *Aspergillus niger*. *Arch Microbiol* **147**, 88-91

90. Shashi, K., Bachhawat, A. K., and Joseph, R. (1990) ATP:citrate lyase of *Rhodotorula gracilis:* purification and properties. *Biochim Biophys Acta* **1033**, 23-30

91. Rangasamy, D., and Ratledge, C. (2000) Compartmentation of ATP:citrate lyase in plants. *Plant Physiol* **122**, 1225-1230

92. Chen, C., and Gibbs, M. (1992) Some Enzymes and Properties of the Reductive Carboxylic Acid Cycle Are Present in the Green Alga *Chlamydomonas reinhardtii* F-60. *Plant Physiol* **98**, 535-539

93. Wahlund, T. M., and Tabita, F. R. (1997) The reductive tricarboxylic acid cycle of carbon dioxide assimilation: initial studies and purification of ATP-citrate lyase from the green sulfur bacterium *Chlorobium tepidum. J Bacteriol* **179**, 4859-4867

94. Ishii, M., Igarashi, Y., and Kodama, T. (1989) Purification and characterization of ATP:citrate lyase from *Hydrogenobacter thermophilus* TK-6. *J Bacteriol* **171**, 1788-1792

95. Beh, M. S., G.; Huber, R.; Stetter, K. O.; Fuchs, G. (1993) Enzymes of the reductive citric acid cycle in the autotrophic eubacterium *Aquifex pyrophilus* and in the archaebacterium *Thermoproteus neutrophilus. Arch Microbiol* **160**, 306-311

96. Kanao, T., Fukui, T., Atomi, H., and Imanaka, T. (2001) ATP-citrate lyase from the green sulfur bacterium *Chlorobium limicola* is a heteromeric enzyme composed of two distinct gene products. *Eur J Biochem* **268**, 1670-1678

97. Bauer, D. E., Hatzivassiliou, G., Zhao, F., Andreadis, C., and Thompson, C. B. (2005) ATP citrate lyase is an important component of cell growth and transformation. *Oncogene* **24**, 6314-6322

98. Fatland, B. L., Nikolau, B. J., and Wurtele, E. S. (2005) Reverse genetic characterization of cytosolic acetyl-CoA generation by ATP-citrate lyase in Arabidopsis. *Plant Cell* **17**, 182-203

99. Migita, T., Narita, T., Nomura, K., Miyagi, E., Inazuka, F., Matsuura, M., Ushijima, M., Mashima, T., Seimiya, H., Satoh, Y., Okumura, S., Nakagawa, K., and Ishikawa, Y. (2008) ATP citrate lyase: activation and therapeutic implications in non-small cell lung cancer. *Cancer Res* **68**, 8547-8554

100. Khwairakpam, A. D., Shyamananda, M. S., Sailo, B. L., Rathnakaram, S. R., Padmavathi, G., Kotoky, J., and Kunnumakkara, A. B. (2015) ATP citrate lyase (ACLY): a promising target for cancer prevention and treatment. *Curr Drug Targets* **16**, 156-163

101. Pierce, M. W., Palmer, J. L., Keutmann, H. T., and Avruch, J. (1981) ATP-citrate lyase. Structure of a tryptic peptide containing the phosphorylation site directed by glucagon and the cAMP-dependent protein kinase. *J Biol Chem* **256**, 8867-8870

102. Ramakrishna, S., Pucci, D. L., and Benjamin, W. B. (1981) ATP-citrate lyase kinase and cyclic AMP-dependent protein kinase phosphorylate different sites on ATP-citrate lyase. *J Biol Chem* **256**, 10213-10216

103. Guy, P. S., Cohen, P., and Hardie, D. G. (1981) Purification and physicochemical properties of ATP citrate (pro-3S) lyase from lactating rat mammary gland and studies of its reversible phosphorylation. *Eur J Biochem* **114**, 399-405

104. Tuhackova, Z., and Krivanek, J. (1996) GTP, a nonsubstrate of ATP citrate lyase, is a phosphodonor for the enzyme histidine autophosphorylation. *Biochem Biophys Res Commun* **218**, 61-66

105. Kanao, T., Fukui, T., Atomi, H., and Imanaka, T. (2002) Kinetic and biochemical analyses on the reaction mechanism of a bacterial ATP-citrate lyase. *Eur J Biochem* **269**, 3409-3416

106. Sun, T., Hayakawa, K., and Fraser, M. E. (2011) ADP-Mg2+ bound to the ATP-grasp domain of ATP-citrate lyase. *Acta Crystallogr Sect F Struct Biol Cryst Commun* **67**, 1168-1172

107. Scott, J. W., Poole, F. L., and Adams, M. W. (2014) Characterization of ten heterotetrameric NDP-dependent acyl-CoA synthetases of the hyperthermophilic archaeon *Pyrococcus furiosus*. *Archaea* **2014**, 176863

108. Jones, C. P., and Ingram-Smith, C. (2014) Biochemical and kinetic characterization of the recombinant ADP-forming acetyl coenzyme A synthetase from the amitochondriate protozoan *Entamoeba histolytica*. *Eukaryot Cell* **13**, 1530-1537

109. Friedrich, M., and Schink, B. (1995) Electron transport phosphorylation driven by glyoxylate respiration with hydrogen as electron donor in membrane vesicles of a glyoxylate-fermenting bacterium. *Arch Microbiol* **163**, 268-275

110. Surendranathan, K. K., and Hersch, L. B. (1983) Malate thiokinase. Evidence for a random site reaction mechanism. *J Biol Chem* **258**, 3794-3798

111. Hersh, L. B., and Peet, M. (1981) Half-of-the-sites reactivity in the malate thiokinase reaction. *J Biol Chem* **256**, 1732-1737

112. Binieda, A., Fuhrmann, M., Lehner, B., Rey-Berthod, C., Frutiger-Hughes, S., Hughes, G., and Shaw, N. M. (1999) Purification, characterization, DNA sequence and cloning of a pimeloyl-CoA synthetase from *Pseudomonas mendocina* 35. *Biochem J* **340 (Pt 3)**, 793-801

113. Castano-Cerezo, S., Bernal, V., Rohrig, T., Termeer, S., and Canovas, M. (2015) Regulation of acetate metabolism in *Escherichia coli* BL21 by protein N(epsilon)-lysine acetylation. *Appl Microbiol Biotechnol* **99**, 3533-3545

114. Thao, S., and Escalante-Semerena, J. C. (2011) Biochemical and thermodynamic analyses of *Salmonella enterica* Pat, a multidomain, multimeric N(epsilon)-lysine acetyltransferase involved in carbon and energy metabolism. *MBio* **2**

115. de Diego Puente, T., Gallego-Jara, J., Castano-Cerezo, S., Bernal Sanchez, V., Fernandez Espin, V., Garcia de la Torre, J., Manjon Rubio, A., and Canovas Diaz, M. (2015) The Protein Acetyltransferase PatZ from *Escherichia coli* Is Regulated by Autoacetylation-induced Oligomerization. *J Biol Chem* **290**, 23077-23093

116. Stanley, S. L., Jr. (2003) Amoebiasis. *Lancet* **361**, 1025-1034

117. Baxt, L. A., and Singh, U. (2008) New insights into *Entamoeba histolytica* pathogenesis. *Curr Opin Infect Dis* **21**, 489-494

118. (1997) *Entamoeba* taxonomy. *Bull World Health Organ* **75**, 291-294

119. McDonnell, G., and Russell, A. D. (1999) Antiseptics and disinfectants: activity, action, and resistance. *Clin Microbiol Rev* **12**, 147-179

120. Marie, C., and Petri, W. A., Jr. (2014) Regulation of virulence of *Entamoeba histolytica. Annu Rev Microbiol* **68**, 493-520

121. Ralston, K. S., and Petri, W. A., Jr. (2011) Tissue destruction and invasion by *Entamoeba histolytica*. *Trends Parasitol* **27**, 254-263

122. Orozco, E., Guarneros, G., Martinez-Palomo, A., and Sanchez, T. (1983) *Entamoeba histolytica*. Phagocytosis as a virulence factor. *J Exp Med* **158**, 1511-1521

123. Rodriguez, M. A., and Orozco, E. (1986) Isolation and characterization of phagocytosis- and virulence-deficient mutants of *Entamoeba histolytica*. *J Infect Dis* **154**, 27-32

124. Ralston, K. S., Solga, M. D., Mackey-Lawrence, N. M., Somlata, Bhattacharya, A., and Petri, W. A., Jr. (2014) Trogocytosis by *Entamoeba histolytica* contributes to cell killing and tissue invasion. *Nature* **508**, 526-530

125. Okada, M., Huston, C. D., Oue, M., Mann, B. J., Petri, W. A., Jr., Kita, K., and Nozaki, T. (2006) Kinetics and strain variation of phagosome proteins of *Entamoeba histolytica* by proteomic analysis. *Mol Biochem Parasitol* **145**, 171-183

126. Petri, W. A., Jr. (2003) Therapy of intestinal protozoa. *Trends Parasitol* **19**, 523-526

127. Muller, M. (1983) Mode of action of metronidazole on anaerobic bacteria and protozoa. *Surgery* **93**, 165-171

128. Edwards, D. I. (1979) Mechanism of antimicrobial action of metronidazole. *J Antimicrob Chemother* **5**, 499-502

129. Kling, P. A., and Burman, L. G. (1989) Serum and tissue pharmacokinetics of intravenous metronidazole in surgical patients. *Acta Chir Scand* **155**, 347-350

130. Martin, C., Sastre, B., Mallet, M. N., Bruguerolle, B., Brun, J. P., De Micco, P., and Gouin, F. (1991) Pharmacokinetics and tissue penetration of a single 1,000-milligram, intravenous dose of metronidazole for antibiotic prophylaxis of colorectal surgery. *Antimicrob Agents Chemother* **35**, 2602-2605

131. Samarawickrema, N. A., Brown, D. M., Upcroft, J. A., Thammapalerd, N., and Upcroft, P. (1997) Involvement of superoxide dismutase and pyruvate:ferredoxin oxidoreductase in mechanisms of metronidazole resistance in *Entamoeba histolytica*. *J Antimicrob Chemother* **40**, 833-840

132. Wassmann, C., Hellberg, A., Tannich, E., and Bruchhaus, I. (1999) Metronidazole resistance in the protozoan parasite *Entamoeba histolytica* is associated with increased expression of iron-containing superoxide dismutase and peroxiredoxin and decreased expression of ferredoxin 1 and flavin reductase. *J Biol Chem* **274**, 26051-26056

133. Quach, J., St-Pierre, J., and Chadee, K. (2014) The future for vaccine development against *Entamoeba histolytica*. *Hum Vaccin Immunother* **10**, 1514-1521

134. Ali, V., and Nozaki, T. (2007) Current therapeutics, their problems, and sulfur-containing-amino-acid metabolism as a novel target against infections by "amitochondriate" protozoan parasites. *Clin Microbiol Rev* **20**, 164-187

135. Debnath, A., Ndao, M., and Reed, S. L. (2013) Reprofiled drug targets ancient protozoans: drug discovery for parasitic diarrheal diseases. *Gut Microbes* **4**, 66-71

136. Loftus, B., Anderson, I., Davies, R., Alsmark, U. C., Samuelson, J., Amedeo, P., Roncaglia, P., Berriman, M., Hirt, R. P., Mann, B. J., Nozaki, T., Suh, B., Pop, M., Duchene, M., Ackers, J., Tannich, E., Leippe, M., Hofer, M., Bruchhaus, I.,

Willhoeft, U., Bhattacharya, A., Chillingworth, T., Churcher, C., Hance, Z., Harris, B., Harris, D., Jagels, K., Moule, S., Mungall, K., Ormond, D., Squares, R., Whitehead, S., Quail, M. A., Rabbinowitsch, E., Norbertczak, H., Price, C., Wang, Z., Guillen, N., Gilchrist, C., Stroup, S. E., Bhattacharya, S., Lohia, A., Foster, P. G., Sicheritz-Ponten, T., Weber, C., Singh, U., Mukherjee, C., El-Sayed, N. M., Petri, W. A., Jr., Clark, C. G., Embley, T. M., Barrell, B., Fraser, C. M., and Hall, N. (2005) The genome of the protist parasite *Entamoeba histolytica. Nature* **433**, 865-868

137. Reeves, R. E. (1984) Metabolism of *Entamoeba histolytica* Schaudinn, 1903. *Adv Parasitol* **23**, 105-142

138. Hirayama, A., Kami, K., Sugimoto, M., Sugawara, M., Toki, N., Onozuka, H., Kinoshita, T., Saito, N., Ochiai, A., Tomita, M., Esumi, H., and Soga, T. (2009) Quantitative metabolome profiling of colon and stomach cancer microenvironment by capillary electrophoresis time-of-flight mass spectrometry. *Cancer Res* **69**, 4918-4925

139. Kellett, G. L., Brot-Laroche, E., Mace, O. J., and Leturque, A. (2008) Sugar absorption in the intestine: the role of GLUT2. *Annu Rev Nutr* **28**, 35-54

140. Baumel-Alterzon, S., and Ankri, S. (2014) *Entamoeba histolytica* adaptation to glucose starvation: a matter of life and death. *Curr Opin Microbiol* **20**, 139-145

141. Byers, T. J., Akins, R. A., Maynard, B. J., Lefken, R. A., and Martin, S. M. (1980) Rapid growth of *Acanthamoeba* in defined media; induction of encystment by glucose-acetate starvation. *J Protozool* **27**, 216-219

142. Singh, U., and Ehrenkaufer, G. M. (2009) Recent insights into *Entamoeba* development: identification of transcriptional networks associated with stage conversion. *Int J Parasitol* **39**, 41-47

143. Vazquezdelara-Cisneros, L. G., and Arroyo-Begovich, A. (1984) Induction of encystation of *Entamoeba invadens* by removal of glucose from the culture medium. *J Parasitol* **70**, 629-633

144. Cummings, J. H., and Macfarlane, G. T. (1997) Role of intestinal bacteria in nutrient metabolism. *JPEN J Parenter Enteral Nutr* **21**, 357-365

145. Thibeaux, R., Weber, C., Hon, C. C., Dillies, M. A., Ave, P., Coppee, J. Y., Labruyere, E., and Guillen, N. (2013) Identification of the virulence landscape essential for *Entamoeba histolytica* invasion of the human colon. *PLoS Pathog* **9**, e1003824

146. Gunst, J., and Van den Berghe, G. (2010) Blood glucose control in the intensive care unit: benefits and risks. *Semin Dial* **23**, 157-162

147. Appelboom, J. W., Brodsky, W. A., and Rehm, W. S. (1959) The concentration of glucose in mammalian liver. *J Gen Physiol* **43**, 467-479

148. Byers, J., and Eichinger, D. (2008) Acetylation of the *Entamoeba* histone H4 N-terminal domain is influenced by short-chain fatty acids that enter trophozoites in a pH-dependent manner. *Int J Parasitol* **38**, 57-64

149. Reeves, R. E., Serrano, R., and South, D. J. (1976) 6-phosphofructokinase (pyrophosphate). Properties of the enzyme from *Entamoeba histolytica* and its reaction mechanism. *J Biol Chem* **251**, 2958-2962

150. Saavedra, E., Encalada, R., Pineda, E., Jasso-Chavez, R., and Moreno-Sanchez, R. (2005) Glycolysis in *Entamoeba histolytica*. Biochemical characterization of recombinant glycolytic enzymes and flux control analysis. *FEBS J* **272**, 1767-1783

151. Siebers, B., Klenk, H. P., and Hensel, R. (1998) PP_i-dependent phosphofructokinase from *Thermoproteus tenax*, an archaeal descendant of an ancient line in phosphofructokinase evolution. *J Bacteriol* **180**, 2137-2143

152. Reeves, R. E. (1968) A new enzyme with the glycolytic function of pyruvate kinase. *J Biol Chem* **243**, 3202-3204

153. Armstrong, P. M., Aspock, H., Baughman, R. P., Behr, C., Combes, C., De Bont, J., Dubremetz, J. F., Freeman, J., Frenkel, J. K., Gessner, A., Gustaffson, M., Haas, W., Halton, D. W., Hanel, H., Hansen, O., Harder, A., Kaneshiro, E. S., Kohler, P., Londer Shausen, M., Mackenstedt, U., Mehlhorn, H., Pereira da Silva, L. H., Raether, W., Reiter-Owana, I., Richter, D., Rollinghoff, M., Schaub, G., Schneider, T., Seitz, H. M., Spielman, A., Spinder, K. D., Taraschewski, H., Tielens, A. G. M., Turberg, A., Vercruysse, J., Voigt, W. P., Walldorf, V., and Wernsdorfer, W. H. (2001) Energy Metabolism. in *Encyclopedic Reference of Parasitology* (Mehlhorn, H. ed., 2 Ed., Springer, Berlin Heidelberg

154. Reeves, R. E., and South, D. J. (1974) Phosphoglycerate kinase (GTP). An enzyme from *Entamoeba histolytica* selective for guanine nucleotides. *Biochem Biophys Res Commun* **58**, 1053-1057

155. Bruchhaus, I., Jacobs, T., Denart, M., and Tannich, E. (1996) Pyrophosphate-dependent phosphofructokinase of *Entamoeba histolytica*: molecular cloning, recombinant expression and inhibition by pyrophosphate analogues. *Biochem J* **316 (Pt 1)**, 57-63

156. Pineda, E., Encalada, R., Vazquez, C., Nequiz, M., Olivos-Garcia, A., Moreno-Sanchez, R., and Saavedra, E. (2015) *In vivo* identification of the steps that control energy metabolism and survival of *Entamoeba histolytica. FEBS J* **282**, 318-331

157. Rosenbaum, R. M., and Wittner, M. (1970) Ultrastructure of bacterized and axenic trophozoites of *Entamoeba histolytica* with particular reference to helical bodies. *J Cell Biol* **45**, 367-382

158. Werries, E., Franz, A., and Geisemeyer, S. (1990) Detection of glycogen-debranching system in trophozoites of *Entamoeba histolytica*. *J Protozool* **37**, 576-580

159. Werries, E., and Thurn, I. (1989) Breakdown of glucopolysaccharides in *Entamoeba histolytica* by phosphorylase. *J Protozool* **36**, 607-612

160. Clark, C. G., Alsmark, U. C., Tazreiter, M., Saito-Nakano, Y., Ali, V., Marion, S., Weber, C., Mukherjee, C., Bruchhaus, I., Tannich, E., Leippe, M., Sicheritz-Ponten, T., Foster, P. G., Samuelson, J., Noel, C. J., Hirt, R. P., Embley, T. M., Gilchrist, C. A., Mann, B. J., Singh, U., Ackers, J. P., Bhattacharya, S., Bhattacharya, A., Lohia, A., Guillen, N., Duchene, M., Nozaki, T., and Hall, N. (2007) Structure and content of the *Entamoeba histolytica* genome. *Adv Parasitol* **65**, 51-190

161. Pineda, E., Encalada, R., Rodriguez-Zavala, J. S., Olivos-Garcia, A., Moreno-Sanchez, R., and Saavedra, E. (2010) Pyruvate:ferredoxin oxidoreductase and bifunctional aldehyde-alcohol dehydrogenase are essential for energy metabolism under oxidative stress in *Entamoeba histolytica. FEBS J* **277**, 3382-3395

162. Zuo, X., and Coombs, G. H. (1995) Amino acid consumption by the parasitic, amoeboid protists *Entamoeba histolytica* and *E. invadens*. *FEMS Microbiol Lett* **130**, 253-258

163. Baumel-Alterzon, S., Weber, C., Guillen, N., and Ankri, S. (2013) Identification of dihydropyrimidine dehydrogenase as a virulence factor essential for the survival of *Entamoeba histolytica* in glucose-poor environments. *Cell Microbiol* **15**, 130-144

164. Fahey, R. C., Newton, G. L., Arrick, B., Overdank-Bogart, T., and Aley, S. B. (1984) *Entamoeba histolytica*: a eukaryote without glutathione metabolism. *Science* **224**, 70-72

165. Gillin, F. D., and Diamond, L. S. (1981) *Entamoeba histolytica* and *Giardia lamblia*: effects of cysteine and oxygen tension on trophozoite attachment to glass and survival in culture media. *Exp Parasitol* **52**, 9-17

166. Gillin, F. D., and Diamond, L. S. (1980) Attachment and short-term maintenance of motility and viability of *Entamoeba histolytica* in a defined medium. *J Protozool* **27**, 220-225

167. Agarwal, S. M., Jain, R., Bhattacharya, A., and Azam, A. (2008) Inhibitors of Escherichia coli serine acetyltransferase block proliferation of *Entamoeba histolytica* trophozoites. *Int J Parasitol* **38**, 137-141

168. Nozaki, T., Asai, T., Sanchez, L. B., Kobayashi, S., Nakazawa, M., and Takeuchi, T. (1999) Characterization of the gene encoding serine acetyltransferase, a regulated enzyme of cysteine biosynthesis from the protist parasites *Entamoeba histolytica* and *Entamoeba dispar*. Regulation and possible function of the cysteine biosynthetic pathway in *Entamoeba*. *J Biol Chem* **274**, 32445-32452

169. Muller, M. (1992) Energy metabolism of ancestral eukaryotes: a hypothesis based on the biochemistry of amitochondriate parasitic protists. *Biosystems* **28**, 33-40

170. Makiuchi, T., and Nozaki, T. (2014) Highly divergent mitochondrion-related organelles in anaerobic parasitic protozoa. *Biochimie* **100**, 3-17

171. Mi-ichi, F., Abu Yousuf, M., Nakada-Tsukui, K., and Nozaki, T. (2009) Mitosomes in *Entamoeba histolytica* contain a sulfate activation pathway. *Proc Natl Acad Sci U S A* **106**, 21731-21736

172. Mi-ichi, F., Makiuchi, T., Furukawa, A., Sato, D., and Nozaki, T. (2011) Sulfate activation in mitosomes plays an important role in the proliferation of *Entamoeba histolytica*. *PLoS Negl Trop Dis* **5**, e1263

173. Mi-ichi, F., Miyamoto, T., Takao, S., Jeelani, G., Hashimoto, T., Hara, H., Nozaki, T., and Yoshida, H. (2015) *Entamoeba* mitosomes play an important role in encystation by association with cholesteryl sulfate synthesis. *Proc Natl Acad Sci U S A* **112**, E2884-2890

174. Lo, H. S., and Reeves, R. E. (1978) Pyruvate-to-ethanol pathway in *Entamoeba histolytica*. *Biochem J* **171**, 225-230

175. Reeves, R. E., and Guthrie, J. D. (1975) Acetate kinase (pyrophosphate). A fourth pyrophosphate-dependent kinase from *Entamoeba histolytica*. *Biochem Biophys Res Commun* **66**, 1389-1395

176. Montalvo, F. E., Reeves, R. E., and Warren, L. G. (1971) Aerobic and anaerobic metabolism in *Entamoeba histolytica*. *Exp Parasitol* **30**, 249-256

177. Pineda, E., Encalada, R., Olivos-Garcia, A., Nequiz, M., Moreno-Sanchez, R., and Saavedra, E. (2013) The bifunctional aldehyde-alcohol dehydrogenase controls ethanol and acetate production in *Entamoeba histolytica* under aerobic conditions. *FEBS Lett* **587**, 178-184

178. Pineda, E., Vazquez, C., Encalada, R., Nozaki, T., Sato, E., Hanadate, Y., Nequiz, M., Olivos-Garcia, A., Moreno-Sanchez, R., and Saavedra, E. (2016) Roles of acetyl-CoA synthetase (ADP-forming) and acetate kinase (PPi-forming)

in ATP and PPi supply in *Entamoeba histolytica*. *Biochim Biophys Acta* **1860**, 1163-1172

BIOCHEMICAL AND KINETIC CHARACTERIZATION OF THE RECOMBINANT ADP-FORMING ACETYL-COA SYNTHETASE FROM THE AMITOCHONDRIATE PROTOZOAN *ENTAMOEBA HISTOLYTICA*

Cheryl P. Jones and Cheryl Ingram-Smith

I. ABSTRACT

Entamoeba histolytica, an amitochondriate protozoan parasite that relies on glycolysis as a key pathway for ATP generation, has developed an unique extended PP_i-dependent glycolytic pathway in which ADP-forming acetyl-CoA synthetase (ACD; Acetate:CoA ligase (ADP-forming) [EC 6.2.1.13]) converts acetyl-CoA to acetate to produce additional ATP and recycle CoA. We have characterized the recombinant *E. histolytica* ACD and have shown that the enzyme is bidirectional, allowing it to potentially play a role in ATP production or in utilization of acetate. In the acetate-forming direction, acetyl-CoA is the preferred substrate and propionyl-CoA was used with lower efficiency. In the acetyl-CoA forming direction, acetate is the preferred substrate, with a lower efficiency observed with propionate. The enzyme can utilize both ADP/ATP and GDP/GTP in the respective directions of the reaction. ATP and PP_i were found to inhibit the acetate-forming direction of the reaction with IC_{50} values of 0.81 ± 0.17 mM and 0.75 ± 0.20 mM, respectively, which are both in the range of their physiological concentrations. ATP and PP_i displayed mixed inhibition versus each of the three

substrates, acetyl-CoA, ADP, and phosphate. This is the first example of regulation of ACD enzymatic activity, and possible roles for this are discussed.

Citation: Jones, C. P., and Ingram-Smith, C. (2014) Biochemical and kinetic characterization of the recombinant ADP-forming acetyl coenzyme A synthetase from the amitochondriate protozoan *Entamoeba histolytica*. *Eukaryotic Cell* **13**, 1530-1537.

II. INTRODUCTION

Entamoeba histolytica, a protozoan parasite that causes amoebic dysentery and amoebic liver abscess in humans, is a leading cause of morbidity and mortality due to parasitic disease worldwide, second only to malaria (1).This parasite has a two-stage life cycle, existing as infectious cysts or motile trophozoites that can reside in the anaerobic confines of the human colon and cause disease. After ingestion of cysts and excystation to release trophozoites, asymptomatic infection can occur when trophozoites remain confined to the intestine. However, the parasite can break through the epithelial lining of the intestine and enter the bloodstream, resulting in an invasive infection. Cell lysis, phagocytosis, and trogocytosis all play a role in pathogenicity and contribute sources of nutrients to this metabolically limited parasite (2).

E. histolytica lacks a functional TCA cycle and oxidative phosphorylation, and consequently relies on substrate-level phosphorylation to provide high-energy compounds. This amitochondriate protozoan utilizes an unusual PP_i-dependent glycolytic pathway (FIG 2.1) in which ATP-dependent phosphofructokinase is replaced by PP_i-dependent phosphofructokinase, and pyruvate kinase is replaced by a PP_i-dependent pyruvate phosphate dikinase (3-5). The pyruvate end-product of glycolysis is converted to acetyl-CoA by pyruvate:ferredoxin oxidoreductase (PFOR) rather than pyruvate dehydrogenase. Acetyl-CoA can then be broken down to ethanol by a bifunctional aldehyde-alcohol dehydrogenase (ADHE) (6) or to acetate by ADP-forming acetyl-CoA synthetase (ACD; Acetate:CoA ligase (ADP-forming); EC 6.2.1.13) [Eq. 1].

$$\text{acetyl-CoA} + \text{ADP} + P_i \leftrightarrows \text{acetate} + \text{CoA} + \text{ATP} \qquad \text{[Eq. 1]}$$

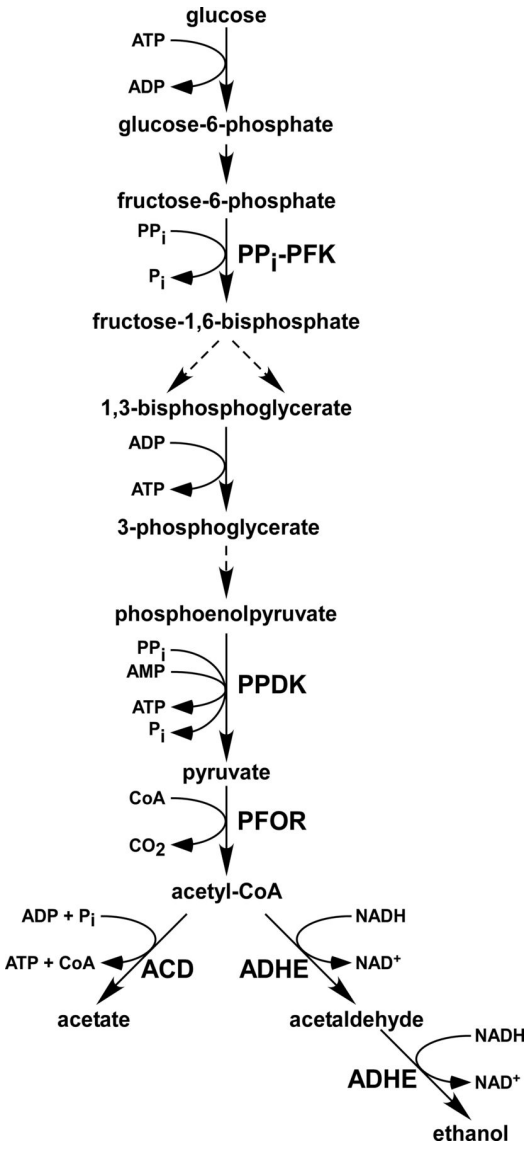

FIG 2.1 The PP_i-dependent extended glycolytic pathway of *E. histolytica*. Relevant steps that produce or utilize ATP and PP_i are shown, and enzymes that catalyze reactions specific to this pathway are indicated. Dotted arrows represent multiple steps that are not shown. Abbreviations: PP_i-PFK, pyrophosphate-dependent phosphofructokinase; PPDK, pyruvate phosphate dikinase; PFOR, pyruvate:ferredoxin oxidoreductase; ACD, ADP-forming acetyl-CoA synthetase; ADHE, bifunctional aldehyde-alcohol dehydrogenase.

This extended PP_i-dependent glycolytic pathway increases ATP output per glucose molecule to three when ethanol is produced and to five when acetate is the product. ACD was first identified as an acetate-forming activity in *E. histolytica* extracts, and the partially purified enzyme was shown to have activity in both directions of the reaction (7). The only other characterized eukaryotic ACD is that from the amitochondriate *Giardia lamblia* (8-10), for which only substantial acetate-forming activity was detected (10).

Although not widespread, ACD has been identified in all three domains and is postulated for the conversion of acetyl-CoA to acetate. In archaea, ACD was first identified in *Pyrococcus furiosus* (11,12), a thermophilic anaerobe that ferments carbohydrates and peptides, and has now been identified in a number of other archaea, including the thermophilic anaerobes *Pyrococcus woesei*, *Desulfurococcus amylolyticus*, *Hyperthermus butylicus*, and *Thermococcus celer* (13,14), the hyperthermophilic anaerobic sulfate reducer *Archaeoglobus fulgidus* (15), and the halophilic aerobe *Halobacterium saccharovorum* (13,14). Native ACD has been purified from *P. furiosus* (11,12) and *Haloarcula marismortui* (16), and recombinant ACDs from *P. furiosus* (17), *A. fulgidus* (18), *Methanococcus jannaschii* (18), *H. marismortui* (16), *Pyrobaculum aerophilum* (16), and *Thermococcus kodakarensis* (19) have been characterized.

A similar role for ACD in acetate production has been proposed in bacteria. Most bacteria have phosphotransacetylase (PTA) and acetate kinase (ACK), which form a predominant pathway for acetate production from acetyl-CoA. ACD from the phototrophic *Chloroflexus aurantiacus* has recently been purified and the recombinant enzyme characterized (20). The syntrophs *Pelotomaculum thermopropionicum* (21) and *Syntrophus aciditrophicus* (22), and the propionic acid producing *Propionibacterium*

acidipropionici (23) all lack genes for the PTA-ACK pathway and instead have *acd* genes. ACD has been identified in proteome analysis of *P. acidipropionici* cells grown under acetate-producing conditions, but the enzyme has not been purified or characterized (23). Likewise, the acetate-producing archaea listed above that have ACD lack genes encoding the PTA-ACK pathway.

ACD is part of a superfamily of nucleoside diphosphate-forming acyl-CoA synthetases, which includes the closely related citric acid cycle enzyme succinyl-CoA synthetase (SCS; EC 6.2.1.4) as well as ATP citrate lyase (EC 2.3.3.8) and malate thiokinase (EC 6.3.1.9) (9). SCS has been extensively studied kinetically and structurally (24-26), and a three-step enzymatic mechanism has been proposed (27) [Steps 1-3]:

Step 1: succinyl-CoA + P_i ⇆ E~succinyl-P + CoA

Step 2: E~succinyl-P ⇆ E-His~P + succinate

Step 3: E-His~P + ADP ⇆ ATP

Based on their studies with *P. furiosus* ACD, Brasen *et al.* (28) proposed that ACD proceeds through a mechanism similar to that of SCS, but with an additional step in which the phosphoryl group is transferred from a His residue on the α subunit to a His residue on the β subunit before transfer to ADP in the final step to produce ATP.

Here we report the biochemical and kinetic characterization of the recombinantly produced ACD from the intestinal parasite *E. histolytica,* revealing its ability to function in either acetate production or utilization *in vitro*. Our results confirm that both the acetyl-CoA forming and acetate-forming activities of ACD are present in cell lysate from *E. histolytica* trophozoites. Inhibition studies suggest *E. histolytica* ACD (*Eh*ACD) is regulated through inhibition by ATP and PP_i in the acetate-forming direction.

III. MATERIALS AND METHODS

Materials

Chemicals were purchased from Sigma-Aldrich, VWR International, Gold Biotechnology, Fisher Scientific, Atlanta Biological, Life Technologies, and J R Scientific.

Growth of *E. histolytica* trophozoites and preparation of cell lysate

E. histolytica strain HM-1:IMSS (kindly provided by Dr. Lesly Temesvari, Clemson University) was cultured axenically at 37°C in TYI-S-33 medium (29). Cells were harvested by incubation on ice for 10 minutes and centrifugation at ~350 x g for 5 minutes at 4°C. The pellet was resuspended in 0.8 ml lysis buffer (50 mM Tris-HCl [pH 7.3], 1 mM AEBSF, 0.015 mM E-64, 0.02 mM Pepstatin A, 5 mM 1,10-Phenanthroline) and disrupted by five cycles of freezing in a dry ice/ethanol bath and thawing at 37°C. The cell lysate was kept on ice, and enzymatic activity was assayed immediately using the DTNB and hydroxamate assays described below. Total protein concentration was determined using the Bradford method (30) with bovine serum albumin as standard.

Production and purification of *E. histolytica* ACD

A codon-optimized *E. histolytica acd* gene was synthesized by Genscript and cloned into pET21b (Novagen) for production of recombinant *E. histolytica* ACD in *Escherichia coli*. The pET21b-*ACD* plasmid was transformed into *E. coli* Rosetta2(DE3)pLysS cells (Novagen) and cultures were grown in Luria-Bertani medium (LB) containing 50 μg ml^{-1} ampicillin and 34 μg ml^{-1} chloramphenicol shaking at 200 rpm at 37°C to A_{600} ~0.8. Protein production was initiated by the addition of isopropyl β-D-1-thiogalactopyranoside (IPTG) to a final concentration of 0.5 mM. Cultures were grown

overnight at ambient temperature and harvested by centrifugation. Cells were suspended in ice-cold buffer A (25 mM Tris-HCl, 150 mM NaCl, 10% glycerol, 20 mM imidazole [pH 7.4]) and disrupted by two passages through a French pressure cell at 138 MPa. The cell lysate was clarified via ultracentrifugation at ~ 98,000 x *g* for 1 hour at 4°C, and cell-free extract was applied to a 5 ml HisTrap HP nickel affinity column (GE Healthcare) equilibrated with buffer A. After extensive washing with buffer A to remove unbound protein, the column was developed with a linear gradient from 0 to 0.5M imidazole in buffer A. Fractions containing active enzyme were pooled, dialyzed overnight in buffer (25 mM Tris-HCl, 10% glycerol, [pH 7.0]), aliquoted, and stored at -80°C. The enzyme was judged to be electrophoretically pure by SDS-PAGE analysis. Protein concentration was determined from the absorbance at 280 nm using the Take3 Micro-volume plate (BioTek).

Determination of molecular mass

The native molecular mass of *Eh*ACD was determined by gel filtration chromatography through a Superose 12 column (GE Healthcare) pre-equilibrated with 50 mM Tris-HCl, 150 mM NaCl [pH 7.0]. The column was calibrated with cytochrome C (12.4 kDa), carbonic anhydrase (29 kDa), albumin (66 kDa), amylase (200 kDa), apoferritin (443 kDa), and thyroglobulin (669 kDa), and developed at a flow rate of 0.5 ml per minute.

Determination of kinetic parameters for *Eh*ACD

Pseudo-first order reaction kinetics determinations were performed in both directions of the reactions. Enzymatic activity in the acetate-forming direction was determined by measuring the release of CoASH from acyl-CoA using Ellman's thiol

reagent (5,5'-dithio-bis-[2-nitrobenzoic acid], DTNB) (31). Production of NTB^{2-} by CoASH cleavage of DTNB was measured spectrophotometrically at 412 nm. Reaction mixtures (50 mM Tris-HCl, 0.3 mM DTNB, 6 mM HEPES (used to solubilize DTNB) [pH 7.3]) with varied substrate concentrations were pre-incubated at 37°C for 5.5 minutes. Assays were performed in 96-well plates in 0.2 ml reaction volumes. Reactions were initiated by the addition of enzyme, and absorbance was measured every 4 seconds at 37°C using a Synergy HT Multi-Mode Microplate Reader (BioTek). Initial velocities were converted to μmol CoASH formed using an extinction coefficient of $\varepsilon = 13.6\ mM^{-1}\ cm^{-1}$ for the thiophenolate NTB^{2-} anion. One unit of activity is defined as 1 µmol product per minute per mg protein. In determination of kinetic parameters for acetate formation, non-varied substrate concentrations were held at 0.3 mM acetyl-CoA, 8 mM KH_2PO_4, and 5 mM $MgCl_2$:ADP or 6 mM $MgCl_2$:GDP. For propionate formation, non-varied substrate concentrations were held at 0.3 mM propionyl-CoA, 12.5 mM KH_2PO_4, and 3 mM $MgCl_2$:ADP.

Activity in the acetate-forming direction was confirmed using the hexokinase/glucose-6-phosphate dehydrogenase coupled assay (32). This assay couples ATP formation to the reduction of $NADP^+$ to NADPH, which is measured spectrophotometrically at 340 nm. Reaction mixtures (100 mM Tris-HCl [pH 7.3], 5.5 mM glucose, 1 mM $NADP^+$, 0.2 mM DTT) with varied concentrations of substrates were pre-incubated at 37°C for 5.5 minutes, hexokinase and glucose-6-phosphate dehydrogenase were added, and the reactions were initiated by the addition of ACD. Assays were performed in 96-well plates in 0.2 ml reaction volumes and absorbance was measured every 4 seconds at 37°C using a Synergy HT Multi-Mode Microplate Reader (BioTek).

Initial velocities were converted to μmol ATP formed using an extinction coefficient ε = 6.22 mM^{-1} cm^{-1} for NADPH. Concentrations of non-varied substrate used for both the DTNB assay and coupled enzyme assay were identical.

Enzymatic activity for detection of acetyl-CoA formation was determined using the hydroxamate assay (33,34). Reaction mixtures (50 mM Tris-HCl [pH 7.5], 300 mM hydroxylamine-HCl [pH 7.0]) with varied substrate concentrations were pre-incubated at 37°C for 5.5 minutes and reactions were initiated by the addition of enzyme. Reactions (0.15 ml) were terminated by the addition of one volume of stop solution (2.5% $FeCl_3$,2 N HCl,10% trichloroacetic acid) and the absorbance at 540 nm was measured. Product formation was determined by comparison to an acetyl-CoA standard curve. For acyl substrates prepared in ethanol, the final concentration of ethanol in the reaction was kept to 2.5%, which was determined not to affect enzymatic activity. One unit of activity is defined as 1 μmol of acetyl-CoA produced per minute per mg protein. In determination of kinetic parameters for acetyl-CoA formation, the non-varied substrates were held at 100 mM acetate, 1 mM CoA, 20 mM $MgCl_2$:ATP, and 25 mM $MgCl_2$:GTP. For determination of kinetic parameters for propionyl-CoA formation, the non-varied substrates were held at the following concentrations: 250 mM propionate, 3 mM CoA, and 20 mM $MgCl_2$:ATP.

Apparent kinetic parameters were determined by varying the concentration of a single substrate while the concentrations of the other two substrates were held constant. For determination of the apparent steady-state kinetic parameters K_m, k_{cat}, and k_{cat}/K_m and their standard deviations, nonlinear regression in KaleidaGraph (Synergy Software) was used to fit the data to the Michaelis-Menten equation.

Determination of inhibition parameters

Various metabolic intermediates were tested as effectors of ACD. IC_{50} values (the effector concentration that provides half maximal inhibition) for inhibitors were determined at K_m substrate concentrations by measuring the decrease in enzymatic activity as a function of increasing concentrations of inhibitor. Non-linear regression analysis in GraphPad Prism 5 (GraphPad Software) was used to fit the data to the log [inhibitor] vs. response curve to determine IC_{50} values. To examine the mode of inhibition, enzymatic activity was assayed in each direction in a four-by-four matrix of varied inhibitor concentrations versus varied concentrations of one substrate, with the other two substrates held constant. Linear regression in KaleidaGraph (Synergy Software) was used to resolve the point of intersection of the inverse plots.

IV. RESULTS

General characterization

The limited characterization of partially purified native *E. histolytica* ACD reported by Reeves *et al.* (7) indicated the enzyme has a narrow nucleotide specificity. To allow a more thorough characterization of the *E. histolytica* ACD (*Eh*ACD), we produced the recombinant enzyme in *E. coli*. A codon-optimized gene was synthesized by Genscript and cloned into the pET21b *E. coli* expression vector (Novagen), which encodes for addition of a C-terminal His_6 tag to the recombinant protein. The calculated subunit molecular mass of the recombinant His-tagged protein is 78999 Da. The molecular mass of the purified enzyme was estimated to be ~150 kDa by gel filtration chromatography, suggesting *Eh*ACD is dimeric as for the *G. lamblia* ACD (10). The optimum temperature for ACD activity was determined to be 55°C in the acetyl-CoA forming direction but could not be determined in the acetate-forming direction due to limitations of the equipment used for measurements. This unexpectedly high optimal temperature may be an artifact from the assay conditions or represent unusual stability of this protein, but was not analyzed further. However, activity was routinely assayed at 37°C, the temperature *E. histolytica* trophozoites would typically encounter within the human host. The enzyme had approximately 70% activity at this temperature versus its optimum temperature.

The requirement for a divalent cation was examined and ACD was found to have the highest activity with Mg^{2+} and Mn^{2+} and substantial activity with Co^{2+} in both directions of the reaction, but only weak activity with Ni^{2+}, Zn^{2+}, Ca^{2+}, and Cu^{2+} (FIG 2.2). The preference for Mg^{2+}, Mn^{2+}, and Co^{2+} is similar to that of other ACDs (10,11,18).

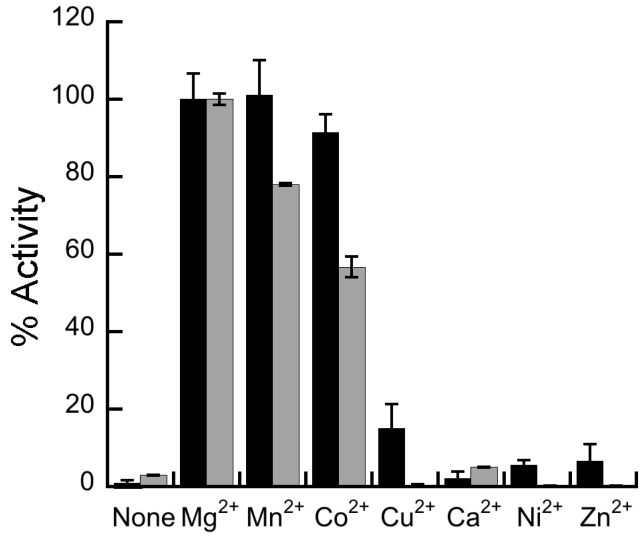

FIG 2.2 Divalent cation specificity of *Eh*ACD. Activities were determined in each direction of the reaction using saturating substrate conditions in the presence or absence of metals (3 mM final concentration in the acetate-forming direction and 20 mM final concentration in the acetyl-CoA forming direction). Activities are normalized to the activity observed with Mg^{2+}. Black bars: activity in the acetate-forming direction. Gray bars: activity in the acetyl-CoA forming direction. Activities are the mean ± SD of three replicates.

ACD enzymatic activity was observed in both directions of the reaction, and the reaction rate was linearly dependent on enzyme concentration. Specific activity in the acetate-forming direction (85 ± 1.2 μmol min^{-1} mg^{-1}) was approximately half that observed in the acetyl-CoA forming direction (180 ± 2.0 μmol min^{-1} mg^{-1}). Similarly, measurement of ACD specific activity in *E. histolytica* cell extract showed that activity in the acetate-forming direction was approximately half that in the acetyl-CoA forming direction (0.14 ± 0.022 μmol min^{-1} mg^{-1} versus 0.29 ± 0.004 μmol min^{-1} mg^{-1}). In contrast, ACD activity in *Giardia* cell extracts could only be detected in the direction of acetate formation (10). Although the purified recombinant *Giardia* ACD had activity in both directions of the reaction, the acetyl-CoA forming activity was ~4% of the acetate-forming activity (9).

*Eh*ACD has a limited acyl-CoA substrate range, with the highest activity observed with acetyl-CoA and lower activity observed with propionyl-CoA (16 ± 2.8% activity versus that with acetyl-CoA). Less than 1% activity was observed with isobutyryl-CoA and isovaleryl-CoA at 0.3 mM final concentration, and no activity was observed with butyryl-CoA, succinyl-CoA, or phenylacetyl-CoA. ADP and GDP gave the highest activity (100 ± 1.0% and 106 ± 3.7% activity, respectively), although activity was also observed with IDP (28 ± 3.8%), CDP (7.0 ± 0.2%), and UDP (2.8 ± 0.1%); no activity was observed with TDP as substrate. PP_i was tested with AMP as the phosphoryl acceptor but no activity was observed under the conditions tested.

In the acyl-CoA forming direction, acetate was the favored substrate, and propionate and butyrate could also be used with relative activities of 72 ± 1.5%, and 5.6 ± 0.2%, respectively, versus acetate. Less than 4% activity was observed with

isobutyrate, valerate, isovalerate, hexanoate, heptanoate, octanoate, succinate, or phenylacetate as the acyl substrate. Activity observed with ATP (representing 100% activity) was nearly double that with GTP (57 ± 0.4%) and substantially higher than the activities observed with ITP (15 ± 0.2%), CTP (4.1 ± 0.3%), or UTP (1.6 ± 0.2%); no activity was observed with TTP or PP_i.

Kinetic parameters

Kinetic parameters for *Eh*ACD were determined in both the acetate-forming and acetyl-CoA forming directions (TABLE 2.1). Activity decreased above 6 mM ADP or 25 mM ATP in the respective directions of the reaction, so the concentrations of these substrates were held below saturation in determination of kinetic parameters. Under these conditions, acetyl-CoA and P_i in the acetate/ATP forming direction and acetate and CoA in the acetyl-CoA forming direction followed Michaelis-Menten like kinetics. The enzyme displayed similar K_m values for acetyl-CoA and propionyl-CoA in the acetate-forming direction of the reaction. However, the turnover rate k_{cat} was approximately 5-fold higher with acetyl-CoA versus propionyl-CoA, resulting in ~4-fold higher catalytic efficiency with acetyl-CoA. The K_m for P_i was similar with acetyl-CoA or propionyl-CoA as the acyl substrate, but the K_m for ADP was reduced ~2-fold with propionyl-CoA versus acetyl-CoA. Similar K_m and k_{cat} values were observed with ADP and GDP (TABLE 2.1). The K_m values observed for *Eh*ACD are similar to those reported for the *Giardia* ACD (0.02 mM, 0.23 mM, and 1.59 mM for acetyl-CoA, ADP, and P_i, respectively) (10).

As the enzyme assay used for determination of kinetic parameters in the acetate-forming direction of the reaction measures CoA release in the first step, we confirmed our results using a coupled enzyme assay that measures ATP production in the last step

TABLE 2.1 Apparent kinetic parameters for *Eh*ACD in each direction of the reaction.

Varied Substrate	K_m (mM)	k_{cat} (sec^{-1})	k_{cat}/K_m (sec^{-1} mM^{-1})
Acetate-forming direction			
Acetyl-CoA	0.04 ± 0.001	110 ± 1.6	2600 ± 370
Phosphate	1.8 ± 0.18	120 ± 7.8	65 ± 2.3
ADP	1.6 ± 0.15	140 ± 1.2	89 ± 7.9
GDP	1.9 ± 0.14	170 ± 5.2	90 ± 8.3
Propionyl-CoA	0.032 ± 0.002	21 ± 0.6	650 ± 63
Phosphate	1.5 ± 0.09	18 ± 0.6	12 ± 0.5
ADP	0.71 ± 0.09	24 ± 0.3	34 ± 3.4
Acetyl-CoA forming direction			
Acetate	14 ± 0.6	240 ± 2.7	16 ± 0.5
CoA	0.20 ± 0.01	220 ± 4.3	1100 ± 57
ATP	12 ± 0.4	320 ± 4.4	27 ± 0.7
GTP	10 ± 0.1	180 ± 1.6	18 ± 0.1
Propionate	29 ± 1.4	190 ± 1.5	6.3 ± 0.3
CoA	1.6 ± 0.05	260 ± 2.0	160 ± 4.3
ATP	7.2 ± 0.7	240 ± 7.1	33 ± 2.2

of the reaction. Similar K_m and k_{cat} values were observed with this assay (acetyl-CoA, 0.017 ± 0.001 mM, 130 ± 14 sec^{-1}; KH_2PO_4, 2.1 ± 0.21 mM, 180 ± 16 sec^{-1}; ADP, 0.94 ± 0.16 mM, 140 ± 7.2 sec^{-1}).

In the acetyl-CoA forming direction of the reaction, the K_m for acetate was ~2-fold higher than that for propionate (TABLE 2.1); however, the k_{cat} values were similar for both substrates, unlike in the opposite direction. Thus, the catalytic efficiency of *Eh*ACD with acetate was only 2.6-fold higher than with propionate. The K_m for CoA was ~2-fold elevated with propionate versus acetate as the acyl substrate, but the K_m for ATP was slightly reduced. The K_m values for ATP and GTP were similar, but the turnover rate was 1.8-fold reduced with GTP. The overall catalytic efficiency with ATP was only 1.5-fold higher than with GTP, indicating that both are suitable substrates. Although weak activity was observed with butyrate, kinetic parameters could not be determined as the enzyme was unsaturable for butyrate even at concentrations as high as 1 M.

Enzyme inhibition

Since ACD can function to produce either ATP or acetyl-CoA, regulation of this enzyme may be important for maintaining proper levels of these metabolites in the cell. An array of metabolic intermediates was tested as effectors for ACD (FIG 2.3). ATP and PP_i were found to be potent inhibitors in the acetate-forming direction of the reaction, producing greater than 95% inhibition at 10 mM final concentration (FIG 2.3). Additionally, 50% or less activity was observed in the presence of 10 mM glyoxylate (32 ± 2%), NAD^+ (47 ± 3%), or glucose-6-phosphate (50 ± 5%). In the acetyl-CoA forming direction, only weak to moderate inhibition was observed with any of the compounds tested (FIG 2.3). PP_i had only a moderate effect in this direction, reducing activity to 64 ±

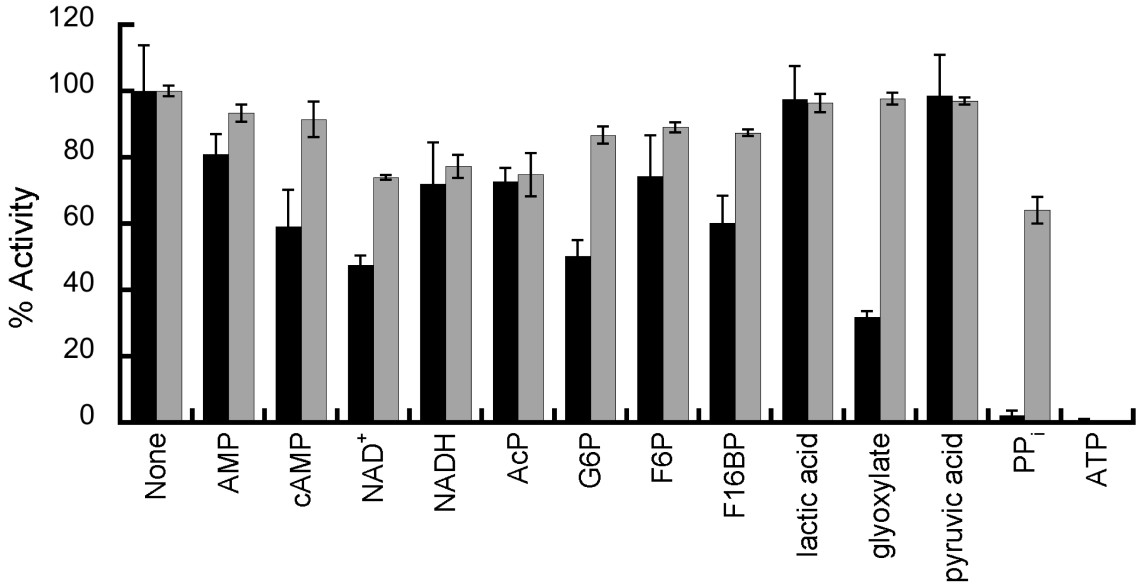

FIG 2.3 Effect of various metabolites on *Eh*ACD activity. Activities were determined in each direction of the reaction using K_m concentrations of substrate in the presence or absence of the indicated metabolites at a final concentration of 10 mM. Note that ATP was tested only in the acetate-forming direction since it serves as a substrate in the acetyl-CoA forming direction. Activities are normalized to the activity observed in the absence of added metabolites. Black bars: activity in the acetate-forming direction. Gray bars: activity in the acetyl-CoA forming direction. Activities are the mean ± SD of three replicates. Abbreviations: cAMP, cyclic AMP; AcP, acetyl phosphate; G6P, glucose 6-phosphate; F6P, fructose 6-phosphate; F16BP, fructose 1,6-bisphosphate.

4% when present at 10 mM final concentration in the reaction. ATP is a substrate in this direction, and although it does inhibit at higher concentrations, we did not examine this further.

In addition to the intermediates shown in FIG 2.3, glyceraldehyde-3-phosphate, phosphoenolpyruvate, and oxaloacetate were tested but only in the acetyl-CoA forming direction because they interfere with the assays used for the acetate-forming direction. None of these compounds resulted in any substantial inhibition in this direction, with 85 ± 0.3%, 85 ± 5.1%, and 90 ± 1.4% activity observed, respectively. IC_{50} values for ATP and PP_i in the acetate-forming direction were determined to be 0.81 ± 0.17 mM for ATP and 0.83 ± 0.27 mM for PP_i. The estimated intracellular concentrations of ATP and PP_i in *E. histolytica* trophozoites grown in the presence of glucose are 5 ± 2 mM and 0.45 mM (35), respectively, suggesting that regulation of the acetate-forming activity of ACD by ATP and PP_i is biologically relevant. The mode of inhibition by each of these compounds was determined by kinetic analysis in which the concentration of inhibitor was varied versus one substrate and the concentrations of the other two substrates were held constant. These analyses suggest mixed inhibition by ATP (FIG 2.4) and PP_i (FIG 2.5) versus each substrate.

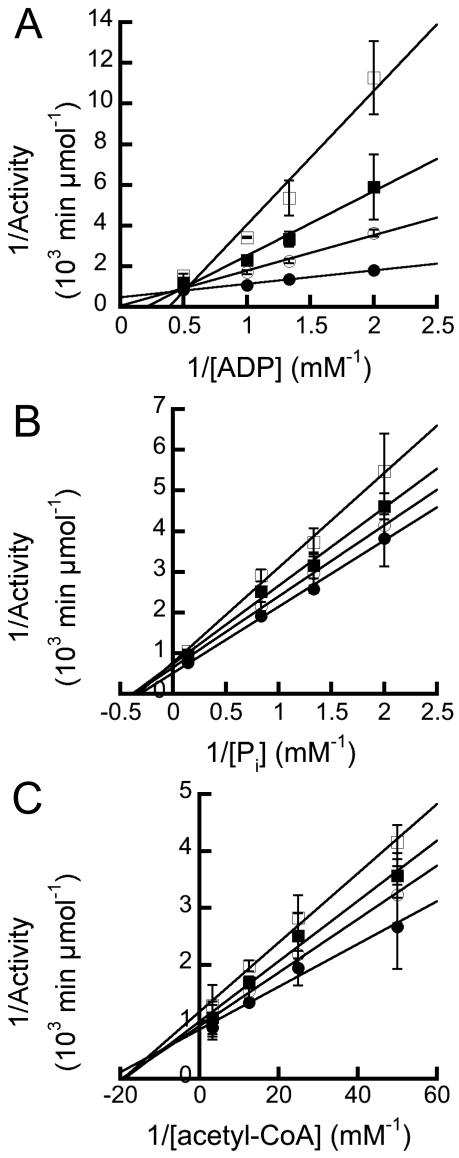

FIG 2.4 The inhibitory effect of ATP versus ADP, acetyl-CoA, and phosphate in the acetate-forming direction. Activity was determined in the presence of varying ATP concentrations with concentration of one substrate varied and the others held constant. ATP concentrations used were 0 mM (●), 0.2 mM (○), 0.35 mM (■), and 0.5 mM (□). ATP inhibition patterns observed versus (A) ADP, (B) acetyl-CoA, and (C) KH_2PO_4. Activities are the mean ± SD of three replicates.

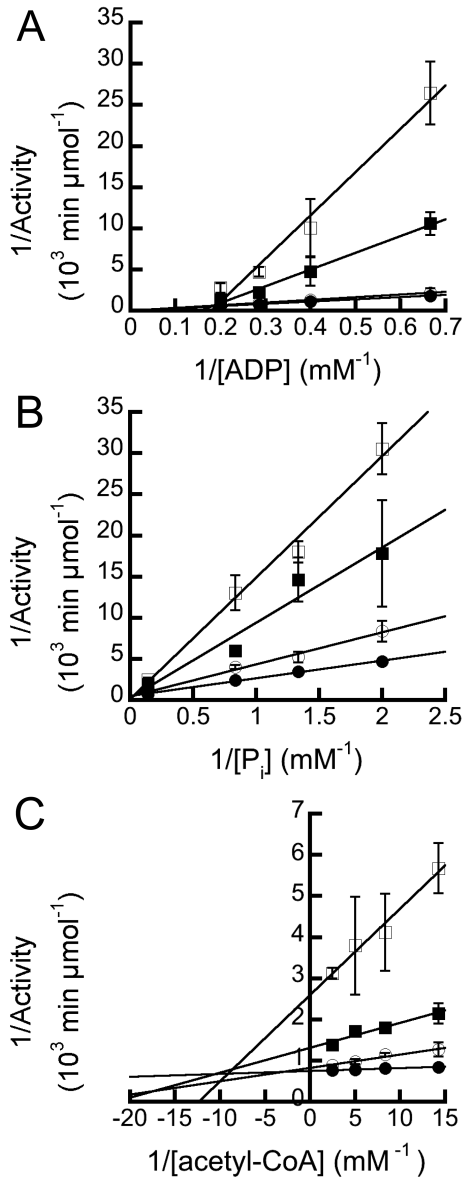

FIG 2.5 The inhibitory effect of PP_i on ADP, acetyl-CoA, and phosphate in the acetate-forming direction. Activity was determined in the presence of varying PP_i concentrations with concentration of one substrate varied and the others held constant. PP_i concentrations used were 0.6 mM (●), 2 mM (○), 3.5 mM (■), and 6 mM (□). PP_i inhibition patterns observed versus (A) ADP, (B) acetyl-CoA, and (C) KH_2PO_4. Activities are the mean ± SD of three replicates.

V. DISCUSSION

Substrate specificity of *Eh*ACD and comparison to other characterized ACDs

Although ACD is not widespread, characterization of *P. furiosus* ACDs has demonstrated that there are at least two different isoforms (11,12). This was confirmed by characterization of additional enzymes from *A. fulgidus* (18) and *T.kodakarensis* (19). The ACD I isoforms prefer acetate and acetyl-CoA and can typically utilize propionate, butyrate, and propionyl-CoA as well, but do not tend to use longer or branched chain acyl/acyl-CoA derivatives (11,12,16,18,20). The ACD II isoforms prefer longer acyl/acyl-CoA derivatives such as phenylacetyl-CoA/phenylacetate and indoleacetate as substrates (12,18,19). Based on our characterization of recombinant *Eh*ACD and the previous characterization of the partially purified native *Eh*ACD (7), this enzyme belongs to the ACD I class. The *Giardia* enzyme also appears to belong to this class (10).

All ACDs utilize ADP but the ability to accept GDP as a substrate varies (11,12,16). In contrast to SCS which has an isozyme specific for each (24), and the *G. lamblia* ACD which functions only with ADP (10), *Eh*ACD is able to utilize ADP and GDP interchangeably with similar K_m and k_{cat} values for each. However, *Eh*ACD may be more likely to utilize ADP *in vivo* since the estimated intracellular concentration of ADP is higher than that for GDP (3.3 ± 1.2 mM versus 0.7 mM, respectively (35)). Furthermore, the intracellular concentration for ADP is above the K_m value for ADP whereas that the intracellular GDP concentration is below the K_m value. Like *Eh*ACD, *Entamoeba* phosphoglycerate kinase can use both ADP and GDP but shows a strong preference for

GDP as judged by an order of magnitude difference between the K_m values for these substrates (4).

In the acetyl-CoA forming direction of the reaction, the enzyme does not show a clear preference for ATP or GTP as the kinetic parameters with each substrate are similar. The fact that the intracellular concentrations of ATP and GTP (5 ± 2 mM and 1.8 mM, respectively (35)) are both below the K_m values for these substrates may suggest that the acetate/ATP-forming direction of the reaction is favored in the cell, even though the purified enzyme has similar activity in both directions. The higher catalytic efficiency observed with either substrate in the acetate-forming direction versus the acetyl-CoA forming direction is consistent with this.

A comparison of the characterized ACD I enzymes reveals a great deal of variability. All of the characterized enzymes catalyze the acetate/ATP forming reaction, but an acetyl-CoA forming activity was not detected or was very low for the ACDs from *G. lamblia* (8-10), *P. aerophilum* (16), and *M. jannaschii* (18). A range of K_m values has been observed for each substrate in both directions of the reaction (TABLE 2.2). Within the archaea, for which six ACD I enzymes have been characterized, the K_m for a given substrate in the acetyl-CoA forming direction showed up to an 11-fold range in values. In the acetate/ATP forming direction, K_m values ranged up to 41-fold for acetyl-CoA. The K_m values observed for the single characterized bacterial ACD from *C. aurantiacus* were within the range of values observed with the archaeal enzymes. Likewise, the K_m values observed for the *G. lamblia* enzyme were within or near those for the archaeal enzymes.

For *Eh*ACD, the K_m values for acetyl-CoA and P_i were comparable to those for other enzymes, but the K_m for ADP was substantially higher. In the acetyl-CoA forming

TABLE 2.2 A comparison of K_m values for characterized ACD I enzymes

Substrate	Archaeal ACDs K_m (μM)	Bacterial ACD[f] K_m (μM)	Giardia ACD[g] K_m (μM)	*Eh*ACD K_m (μM)
Acetyl-CoA	10[a] – 410[b]	37	20	40
Phosphate	100[d] – 1300[b,c]	1000	1590	1800
ADP	7[a] – 150[d]	91	230	1600
Acetate	340[a] – 1700[b]	900	NA	14000
CoA	5.6[e] – 60[b]	24	NA	200
ATP	56[e] – 477[d]	570	NA	12000

[a] *Archaeoglobus fulgidus* (18)
[b] *Haloarcula marismortui* (16)
[c] *Pyrobaculum aerophilum* (16)
[d] *Pyrococcus furiosus* (12)
[e] *Thermococcus kodakarensis* (19)
[f] *Chloroflexus aurantiacus* (20)
[g] *Giardia lamblia* (10)

ND, no activity detected in the direction of acetyl-CoA formation.

direction, the K_m value for CoA was slightly above the range observed for other ACDs. However, the K_m for acetate was 8-fold higher than the highest K_m observed for any other ACD, and the K_m for ATP was over 20-fold higher. This may suggest that acetyl-CoA formation is not the preferred direction of the reaction and that *E. histolytica* may employ this direction only under specific environmental or physiological conditions (see below).

Role of the extended glycolytic pathway

The PP_i-dependent extended glycolytic pathway branches after production of acetyl-CoA from pyruvate. In one branch, ACD is responsible for production of acetate and ATP; in the other, acetyl-CoA is metabolized to ethanol by ADHE (6). Montalvo *et al.* (36) and Reeves *et al.* (7) showed that ethanol and acetate are produced at approximately a 2:1 ratio under anaerobic conditions versus a 1:2 ratio under aerobic conditions. More recently, Pineda *et al.* (37) found an ethanol to acetate ratio of 3.9:1 produced in cells growing under standard conditions. Upon exposure to oxygen saturated medium, however, the flux through acetate increased for up to 90 minutes. The flux through ethanol decreased but gradually recovered over time. Overall, these results suggest ethanol and acetate are both important end products of glycolysis, and that flux through both of these pathways may be necessary to generate sufficient ATP while still providing for NAD^+ recycling.

ACD may also play a role in ATP production from amino acid catabolism

In addition to increasing ATP production from glycolysis, the presence of ACD and PFOR allows certain amino acids to be catabolized for ATP production. *E. histolytica* trophozoites scavenge a number of amino acids. Asparagine, aspartate, and

tryptophan are broken down to pyruvate, and methionine, threonine, and homocysteine are broken down to 2-oxobutanoate (38). PFOR converts these products respectively to acetyl-CoA and propionyl-CoA (7,39,40), which can then serve as substrates of ACD for ATP production.

Regulation of ACD activity

Although metabolic flux analysis using kinetic modeling suggested that ACD has little regulatory effect over glycolysis (35), its roles in amino acid degradation were not taken into account. Contrarily, one might expect that ACD's position in the extended glycolytic pathway of *E. histolytica* makes it a prime site for regulation in order to properly maintain ATP and acetyl-CoA concentrations. In fact, we have found that *Eh*ACD is regulated by both ATP and PP_i in the acetate-forming direction with IC_{50} concentrations that are within the physiological range based on the estimated intracellular concentrations for each (35). An excess of ATP would indicate that energy needs of the cell are being met, and thus additional ATP production by ACD would be unnecessary. This would prevent costly depletion of acetyl-CoA, which could instead be used by other pathways.

PP_i serves as a phosphoryl donor for two PP_i-dependent glycolytic enzymes in *E. histolytica* (4). A buildup of PP_i may signal a backup in glycolysis that would again warrant inhibition of ACD to prevent depletion of acetyl-CoA. Finally, regulation of ACD by two components of the glycolytic pathway may provide a means for shunting acetyl-CoA to ADHE for ethanol production to regenerate NAD^+, thus maintaining a proper balance between these two alternative pathways.

Differences between *G. lamblia* and *E. histolytica* allow these microorganisms to occupy diverse habitats

Although *E. histolytica* and *G. lamblia* rely on similar extended PP_i-dependent glycolytic pathways, the *E. histolytica* ACD is able to function in both the acetate-forming and acetyl-CoA forming directions of the reaction, whereas the *Giardia* enzyme is limited to just the acetate-forming direction (10). This divergence may have arisen due to the different environments these parasites inhabit during infection. *Entamoeba* trophozoites reside in the mucus layer of the colon where bacterial microflora produce high amounts of the small chain fatty acids (SCFA) acetate, propionate, and butyrate (41). *Giardia* colonizes the small intestine in which the SCFA concentration is relatively low (41), and thus it is unlikely that ACD will be needed to function in acetate utilization.

The total SCFA concentration in the human colon is approximately 100-120 mM, with relative molar ratios of 57:22:21 acetate:propionate:butyrate (41), giving approximate concentrations of 57-68 mM for acetate, 22-26 mM for propionate, and 21-25 mM for butyrate. Acetate and propionate concentrations are thus in a range that would suggest ACD's activity in the acetyl-CoA forming direction may be physiologically relevant and that ACD may switch from acetate/ATP production when glucose is present to SCFA utilization when glucose becomes limiting.

Concluding remarks

Although we have speculated on the roles of ACD in *Entamoeba*, experimental confirmation still remains. In addition to *Entamoeba* and *Giardia*, ACD may also be present in other parasites including *Cryptosporidium muris*, *Blastocystis hominis*, and *Plasmodium falciparum*. The possible existence of ACD in *Plasmodium* is of particular

interest, not only because of its enormous public health significance, but also because they retain fully functional mitochondria. Within the complex life cycle of *Plasmodium*, the intraerythrocyte stages rely primarily on the incomplete oxidation of blood glucose by glycolysis to produce ATP (42,43), and thus ACD may play a similar role as in *Entamoeba*. Whether ACD plays similar roles in other parasites must still be investigated, and may provide insight into energy metabolism in these important eukaryotic pathogens.

VI. ACKNOWLEDGEMENTS

We gratefully acknowledge Kerry Smith (Clemson University) for helpful discussions on this research and comments on the preparation of this manuscript. Support for this research was provided by National Science Foundation Award #0920274 (Kerry Smith, PI, and C.I.-S., co-I), a National Science Foundation Graduate Research Fellowship award to C. J., and Clemson University.

VII. REFERENCES

1. Organization, W. H. (1997) Amoebiasis. *Weekly Epidemiology Records* **72**, 97-100

2. Marie, C., and Petri, W. A., Jr. (2014) Regulation of Virulence of *Entamoeba histolytica*. *Annual review of microbiology* **68**, 493-520

3. Reeves, R. E., Serrano, R., and South, D. J. (1976) 6-phosphofructokinase (pyrophosphate). Properties of the enzyme from *Entamoeba histolytica* and its reaction mechanism. *The Journal of biological chemistry* **251**, 2958-2962

4. Saavedra, E., Encalada, R., Pineda, E., Jasso-Chavez, R., and Moreno-Sanchez, R. (2005) Glycolysis in *Entamoeba histolytica*. Biochemical characterization of recombinant glycolytic enzymes and flux control analysis. *The FEBS journal* **272**, 1767-1783

5. Saavedra-Lira, E., and Perez-Montfort, R. (1996) Energy production in *Entamoeba histolytica*: new perspectives in rational drug design. *Archives of medical research* **27**, 257-264

6. Lo, H. S., and Reeves, R. E. (1978) Pyruvate-to-ethanol pathway in *Entamoeba histolytica*. *The Biochemical journal* **171**, 225-230

7. Reeves, R. E., Warren, L. G., Susskind, B., and Lo, H. S. (1977) An energy-conserving pyruvate-to-acetate pathway in *Entamoeba histolytica*. Pyruvate synthase and a new acetate thiokinase. *J Biol Chem* **252**, 726-731

8. Lindmark, D. G. (1980) Energy metabolism of the anaerobic protozoon *Giardia lamblia*. *Mol Biochem Parasitol* **1**, 1-12

9. Sanchez, L. B., Galperin, M. Y., and Muller, M. (2000) Acetyl-CoA synthetase from the amitochondriate eukaryote *Giardia lamblia* belongs to the newly recognized superfamily of acyl-CoA synthetases (Nucleoside diphosphate-forming). *J Biol Chem* **275**, 5794-5803

10. Sanchez, L. B., and Muller, M. (1996) Purification and characterization of the acetate forming enzyme, acetyl-CoA synthetase (ADP-forming) from the amitochondriate protist, *Giardia lamblia*. *FEBS Lett* **378**, 240-244

11. Glasemacher, J., Bock, A. K., Schmid, R., and Schonheit, P. (1997) Purification and properties of acetyl-CoA synthetase (ADP-forming), an archaeal enzyme of acetate formation and ATP synthesis, from the hyperthermophile *Pyrococcus furiosus*. *Eur J Biochem* **244**, 561-567

12. Mai, X., and Adams, M. W. (1996) Purification and characterization of two reversible and ADP-dependent acetyl coenzyme A synthetases from the hyperthermophilic archaeon *Pyrococcus furiosus*. *J Bacteriol* **178**, 5897-5903

13. Schafer, T., and Schonheit, P. (1991) Pyruvate metabolism of the hyperthermophilic archaebacterium *Pyrococcus furiosus*. Acetate formation from acetyl-CoA and ATP synthesis are catalyzed by an acetyl-CoA synthetase (ADP-forming). *Archives of microbiology* **155**, 366-377

14. Schafer, T., Selig, M., and Schonheit, P. (1993) Acetyl-CoA synthetase (ADP-forming) in archaea, a novel enzyme involved in acetate formation and ATP synthesis. *Archives of microbiology* **159**, 72-83

15. Labes, A., and Schonheit, P. (2001) Sugar utilization in the hyperthermophilic, sulfate-reducing archaeon *Archaeoglobus fulgidus* strain 7324: starch degradation to acetate and CO_2 via a modified Embden-Meyerhof pathway and acetyl-CoA synthetase (ADP-forming). *Archives of microbiology* **176**, 329-338

16. Brasen, C., and Schonheit, P. (2004) Unusual ADP-forming acetyl-coenzyme A synthetases from the mesophilic halophilic euryarchaeon *Haloarcula marismortui* and from the hyperthermophilic crenarchaeon *Pyrobaculum aerophilum*. *Arch Microbiol* **182**, 277-287

17. Musfeldt, M., Selig, M., and Schonheit, P. (1999) Acetyl coenzyme A synthetase (ADP forming) from the hyperthermophilic Archaeon *Pyrococcus furiosus*: identification, cloning, separate expression of the encoding genes, acdAI and acdBI, in *Escherichia coli*, and in vitro reconstitution of the active heterotetrameric enzyme from its recombinant subunits. *J Bacteriol* **181**, 5885-5888

18. Musfeldt, M., and Schonheit, P. (2002) Novel type of ADP-forming acetyl coenzyme A synthetase in hyperthermophilic archaea: heterologous expression and characterization of isoenzymes from the sulfate reducer *Archaeoglobus fulgidus* and the methanogen *Methanococcus jannaschii*. *J Bacteriol* **184**, 636-644

19. Awano, T., Wilming, A., Tomita, H., Yokooji, Y., Fukui, T., Imanaka, T., and Atomi, H. (2014) Characterization of two members among the five ADP-forming acyl coenzyme A (Acyl-CoA) synthetases reveals the presence of a 2-(Imidazol-4-yl)acetyl-CoA synthetase in *Thermococcus kodakarensis*. *Journal of bacteriology* **196**, 140-147

20. Schmidt, M., and Schonheit, P. (2013) Acetate formation in the photoheterotrophic bacterium *Chloroflexus aurantiacus* involves an archaeal type ADP-forming acetyl-CoA synthetase isoenzyme I. *FEMS Microbiol Lett* **349**, 171-179

21. Kosaka, T., Kato, S., Shimoyama, T., Ishii, S., Abe, T., and Watanabe, K. (2008) The genome of *Pelotomaculum thermopropionicum* reveals niche-associated evolution in anaerobic microbiota. *Genome Res* **18**, 442-448

22. McInerney, M. J., Rohlin, L., Mouttaki, H., Kim, U., Krupp, R. S., Rios-Hernandez, L., Sieber, J., Struchtemeyer, C. G., Bhattacharyya, A., Campbell, J. W., and Gunsalus, R. P. (2007) The genome of *Syntrophus aciditrophicus*: life at the thermodynamic limit of microbial growth. *Proc Natl Acad Sci U S A* **104**, 7600-7605

23. Parizzi, L. P., Grassi, M. C., Llerena, L. A., Carazzolle, M. F., Queiroz, V. L., Lunardi, I., Zeidler, A. F., Teixeira, P. J., Mieczkowski, P., Rincones, J., and Pereira, G. A. (2012) The genome sequence of *Propionibacterium acidipropionici* provides insights into its biotechnological and industrial potential. *BMC genomics* **13**, 562

24. Fraser, M. E., James, M. N., Bridger, W. A., and Wolodko, W. T. (1999) A detailed structural description of *Escherichia coli* succinyl-CoA synthetase. *J Mol Biol* **285**, 1633-1653

25. Fraser, M. E., Joyce, M. A., Ryan, D. G., and Wolodko, W. T. (2002) Two glutamate residues, Glu 208 alpha and Glu 197 beta, are crucial for phosphorylation and dephosphorylation of the active-site histidine residue in succinyl-CoA synthetase. *Biochemistry* **41**, 537-546

26. Wolodko, W. T., Fraser, M. E., James, M. N., and Bridger, W. A. (1994) The crystal structure of succinyl-CoA synthetase from *Escherichia coli* at 2.5-A resolution. *J Biol Chem* **269**, 10883-10890

27. Bridger, W. A. (1974) *Succinyl-CoA Synthetase*, 3rd ed., Academic Press, New York

28. Brasen, C., Schmidt, M., Grotzinger, J., and Schonheit, P. (2008) Reaction mechanism and structural model of ADP-forming Acetyl-CoA synthetase from the hyperthermophilic archaeon *Pyrococcus furiosus*: evidence for a second active site histidine residue. *J Biol Chem* **283**, 15409-15418

29. Diamond, L. S., Harlow, D. R., and Cunnick, C. C. (1978) A new medium for the axenic cultivation of *Entamoeba histolytica* and other *Entamoeba*. *Trans R Soc Trop Med Hyg* **72**, 431-432

30. Bradford, M. M. (1976) A rapid and sensitive method for the quantitation of microgram quantities of protein utilizing the principle of protein-dye binding. *Analytical biochemistry* **72**, 248

31. Srere, P. A. (1963) Citryl-CoA. An Substrate for the Citrate-Cleavage Enzyme. *Biochim Biophys Acta* **73**, 523-525

32. Bowman, C. M., Valdez, R. O., and Nishimura, J. S. (1976) Acetate kinase from *Veillonella alcalescens*. Regulation of enzyme activity by succinate and substrates. *The Journal of biological chemistry* **251**, 3117-3121

33. Lipmann, F., and Tuttle, L. C. (1945) A specific micromethod for determination of acyl phosphates. *The Journal of biological chemistry* **159**, 21-28

34. Rose, I. A., Grunberg-Manago, M., Korey, S. F., and Ochoa, S. (1954) Enzymatic phosphorylation of acetate. *The Journal of biological chemistry* **211**, 737-756

35. Saavedra, E., Marin-Hernandez, A., Encalada, R., Olivos, A., Mendoza-Hernandez, G., and Moreno-Sanchez, R. (2007) Kinetic modeling can describe in vivo glycolysis in *Entamoeba histolytica*. *FEBS J* **274**, 4922-4940

36. Montalvo, F. E., Reeves, R. E., and Warren, L. G. (1971) Aerobic and anaerobic metabolism in *Entamoeba histolytica*. *Exp Parasitol* **30**, 249-256

37. Pineda, E., Encalada, R., Rodriguez-Zavala, J. S., Olivos-Garcia, A., Moreno-Sanchez, R., and Saavedra, E. (2010) Pyruvate:ferredoxin oxidoreductase and bifunctional aldehyde-alcohol dehydrogenase are essential for energy metabolism under oxidative stress in *Entamoeba histolytica*. *FEBS J* **277**, 3382-3395

38. Zuo, X., and Coombs, G. H. (1995) Amino acid consumption by the parasitic, amoeboid protists *Entamoeba histolytica* and *E. invadens. FEMS Microbiol Lett* **130**, 253-258

39. Anderson, I. J., and Loftus, B. J. (2005) *Entamoeba histolytica*: observations on metabolism based on the genome sequence. *Exp Parasitol* **110**, 173-177

40. Clark, C. G., Alsmark, U. C., Tazreiter, M., Saito-Nakano, Y., Ali, V., Marion, S., Weber, C., Mukherjee, C., Bruchhaus, I., Tannich, E., Leippe, M., Sicheritz-Ponten, T., Foster, P. G., Samuelson, J., Noel, C. J., Hirt, R. P., Embley, T. M., Gilchrist, C. A., Mann, B. J., Singh, U., Ackers, J. P., Bhattacharya, S., Bhattacharya, A., Lohia, A., Guillen, N., Duchene, M., Nozaki, T., and Hall, N. (2007) Structure and content of the *Entamoeba histolytica* genome. *Adv Parasitol* **65**, 51-190

41. Cummings, J. H., Pomare, E. W., Branch, W. J., Naylor, C. P., and Macfarlane, G. T. (1987) Short chain fatty acids in human large intestine, portal, hepatic and venous blood. *Gut* **28**, 1221-1227

42. Fry, M., and Beesley, J. E. (1991) Mitochondria of mammalian *Plasmodium* spp. *Parasitology* **102 Pt 1**, 17-26

43. van Dooren, G. G., Stimmler, L. M., and McFadden, G. I. (2006) Metabolic maps and functions of the *Plasmodium* mitochondrion. *FEMS microbiology reviews* **30**, 596-630

CHAPTER 3

INVESTIGATING THE MECHANISM OF ADP-FORMING ACETYL-COA SYNTHETASE FROM THE PROTOZOAN PARASITE *ENTAMOEBA HISTOLYTICA*

Cheryl P. Jones, Kirin Khan, and Cheryl Ingram-Smith

I. ABSTRACT

ADP-forming acetyl-CoA synthetase catalyzes the reversible conversion of acetyl-CoA to acetate to generate ATP via substrate level phosphorylation or to activate acetate to acetyl-CoA. Investigation of the *Pyrococcus furiosus* ACD suggested a novel four-step mechanism involving two phosphohistidine intermediates. The *Pyrococcus* enzyme is an $\alpha_2\beta_2$ heterotetramer with one phosphorylated His in each subunit. In this study, the enzymatic mechanism of *E. histolytica* ACD was investigated through kinetic characterization of site-altered variants. The homodimeric *E. histolytica* enzyme has α and β domains fused into a single subunit. Our results indicate that of the two proposed phosphorylation sites, only His252 (equivalent to Hisα of *P. furiosus* ACD) is essential but His533 (equivalent to Hisβ) is important for activity but not essential. Glu213, proposed to be involved in phosphorylation of Hisα, was also shown to be essential and replacements at this position resulted in complete loss of activity. Asp674, thought to play a role in stabilization of the phosphorylated His, plays an important role in catalysis

as replacement with Ala resulted in substantial loss of activity that was partially recovered by more conservative replacement with Glu. Our kinetic data, isotopic labeling and distance calculations within the active site of the recently solved structure of Candidatus *Korarchaeum cryptofilum* ACDI challenge the proposed four-step mechanism and suggest that there is a single essential phosphorylated His, at least for ACD enzymes with fused α and β domains.

II. INTRODUCTION

ADP-forming acetyl-CoA synthetase (ACD; E.C 6.2.1.13), belonging to the NDP-forming acyl-CoA synthetase enzyme superfamily (1), is an acetate thiokinase capable of substrate-level phosphorylation (Eq. 1). Previously characterized ACD enzymes vary in their substrate preference and ability to catalyze the reverse reaction (2-5), leading to the designation of ACD I and II subtypes based on substrate utilization (6).

$$\text{acetyl-CoA} + \text{NDP} + P_i \rightleftharpoons \text{acetate} + \text{CoA} + \text{ATP} \qquad \text{[Eq. 1]}$$

ACD has been identified in a number of acetate-producing prokaryotes, including multiple archaeal species (2,7,8) and the bacterium *Chloroflexus aurantiacus* (4), that lack the traditional acetate kinase/phosphotransacetylase pathway for acetate production. ACD is also present in the parasitic protozoan species *Entamoeba histolytica* (9) and *Giardia lamblia* (10) which are both anaerobic intestinal parasites that lack mitochondria. In *E. histolytica*, ACD may function in energy conservation by providing ATP via substrate level phosphorylation (11) and CoA recycling (12), but may also function in the reverse direction for acetate utilization (11). Putative ACD sequences have also been identified in other parasitic protozoan species such as *Plasmodium falciparum* and *Cryptosporidium muris* (11).

Succinyl-CoA synthetase (SCS; EC 6.2.1.4), the most well-studied member of the enzyme superfamily to which ACD belongs, consists of five domains arranged in two subunits designated as alpha and beta. These five subunits are present in ACD but are arranged differently within the primary sequence (FIG 3.1A). SCS is a heterotetrameric

A

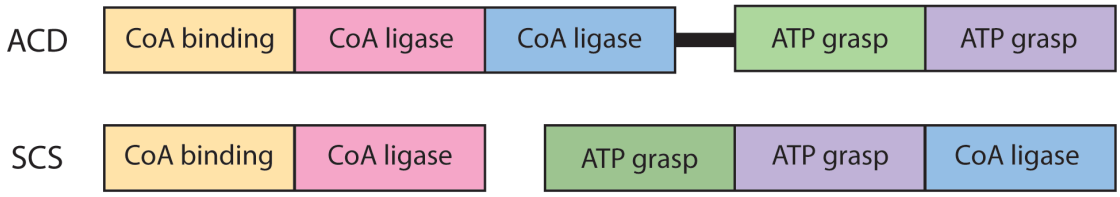

B

		HISα:			HISβ:	
E. coli SCS	239α	PKGKPMG**H**AGAIIA	252α	50β	HAGGRGK-AGGV	60β
E. histolytica	245	GAAAAMS**H**TGSLAG	258	529	PDIM**H**KTDVGGV	540
G. lamblia	256	GAAAASS**H**TGALAG	269	545	PQII**H**KSDCGGV	556
P. falciparum	281	AAEAAIS**H**TGSMVG	294	594	DKIT**H**KKDIGGV	605
C. muris	273	AYKAAAS**H**TGSLVG	286	564	RTFT**H**KSDIGGV	575
P. furiosus	250α	GAKAAAS**H**TGSLAG	263α	67β	PQII**H**KSDAGGV	78β
Ca. K. cryptofilum	247α	GARAAAS**H**TGSIAG	260α	64β	PQVV**H**KSDVGGV	75β

		GLUα:			ASPβ:	
E. coli SCS	203α	IVMIG**E**IGGSA	213α	193β	LALIEINPLVI	203β
E. histolytica	208	ILMYI**E**SIKDA	218	670	ISEV**D**INPLAV	680
G. lamblia	219	ILLYL**E**SIVDG	229	693	ITEL**D**MNPLLV	703
P. falciparum	208	ILLYV**E**SIGDM	218	739	INEC**D**INPLYV	749
C. muris	236	ILMYI**E**SIGNA	246	712	VLEC**D**INPLCI	722
P. furiosus	213α	ILIYM**E**GVKDG	223α	208β	IKEI**D**INPIFA	218β
Ca. K. cryptofilum	208α	IMIYL**E**GIAPG	218α	205β	IAEM**D**LNPVIA	215β

FIG 3.1 Comparison of ACD and SCS. (A) Diagram of the domain organization in ACD and SCS. Each is comprised of five domains arranged in a unique pattern. The optional hinge region present in some ACD enzymes is represented by the black rectangle. (B) Sequence alignment of *E. coli* SCS and ACD from multiple organisms. α and β indicate the respective subunit for those enzymes in which the alpha and beta domains are separate subunits.

enzyme with two active sites, one residing in each alpha-beta dimer (13). Most prokaryotic ACDs exist as a heterotetramer of two alpha and two beta subunits, as for SCS (1). The only known exception with more than two α-β units is ACD from *C. aurantiacus*, which is a homotetramer (4). Eukaryotic *G. lamblia* and *E. histolytica* ACDs (3,11), along with Archaeal *Archaeoglobus fulgidus* and *Methanococcus janaschii* ACDs (14), are encoded by a single gene and have fused alpha and beta domains connected by a novel hinge region. This represents a unique adaptation that adds complexity to this class of enzymes.

Structural analyses of SCS from *E. coli* (15), pig heart (16) and *Thermus aquaticus* (17,18) have revealed the active site and substrate binding sites. The three-step mechanism of SCS proceeds through a single phosphorylated enzyme intermediate.

Step 1: succinyl-CoA + P_i + E ⇌ E~succinyl-P + CoA

Step 2: E~succinyl-P ⇌ E-Hisα-P + succinate

Step 3: E-Hisα-P + ADP ⇌ E + ATP

The succinyl-CoA and phosphate binding pockets are located in the alpha subunit of SCS in a region designated as Site I. After binding succinyl-CoA, a succinyl-phosphate intermediate is formed and CoA is released (Step 1). The phosphoryl group is then transferred to a His residue (Hisα) located within a loop in the alpha subunit (designated as the phosphohistidine loop) and succinate is released (Step 2). It was postulated that a conformational change subsequently swings this phosphohistidine loop from its Site I position to a position closer to the nucleotide binding site of the beta subunit (Site II) (15). The phosphoryl group is then transferred to a nucleotide diphosphate and the

newly formed nucleotide triphosphate is released (Step 3). Two additional glutamate residues of *E. coli* SCS have been investigated and determined to be crucial for the phosphorylation and dephosphorylation of the active site histidine (19).

The mechanism of ACD was originally thought to be analogous to that of SCS; however, Brasen *et al.* (20) observed phosphorylation of both alpha and beta subunits of *P. furiosus* ACD (*Pf*ACD) when incubated with ^{32}P-labeled ATP or P_i. They proposed a four-step mechanism containing an additional phosphoryl transfer step (Step 3) to a separate His residue located in the beta subunit (Hisβ).

Step 1: acetyl-CoA + P_i + E ⇌ E~acetyl-P + CoA

Step 2: E~acetyl-P ⇌ E-Hisα-P + acetate

Step 3: E-Hisα-P ⇌ E-Hisβ-P

Step 4: E-Hisβ-P + ADP ⇌ E + ATP

Recently, the first structural characterization of an ACD from the hyperthermophilic archaea *Candidatus Korachaeum cryptofilum* (*ckc*ACD) was performed (21). This enzyme was crystallized with different ligands to reveal nine structures that include multiple structures showing the phosphorylated Hisα intermediate. This study confirmed the postulated swinging mechanism of the phosphohistidine loop from Site I to Site II of the active site.

In this study, we investigate the role of four primary residues within *E. histolytica* ACD (*Eh*ACD) and assess their roles through kinetic characterization of site-altered enzyme variants and isotopic labeling to examine phosphorylation. Our results contradict

the proposed four-step mechanism for *Pf*ACD and instead agree with the original three-step mechanism proposed for SCS (15).

III. MATERIALS AND METHODS

Materials

Chemicals were purchased from Sigma-Aldrich, VWR International, Gold Biotechnology, Fisher Scientific, Life Technologies, and J R Scientific. Primers were purchased from Integrated DNA Technologies

Sequence alignment

Putative ACD amino acid sequences were identified by PSI-BLAST (http://blast.ncbi.nlm.nih.gov/Blast.cgi?PAGE=Proteins) (22) using the *E. histolytica* ACD sequence as the query (GI: 67481881). Sequences were aligned using ClustalW (http://www.ebi.ac.uk/Tools/msa/clustalo/) (23).

Site-directed mutagenesis of *acd*

Site-directed mutagenesis of an *Escherichia coli* codon-optimized *E. histolytica* *acd* gene was performed using the Quikchange Lightning Kit (Stratagene, Inc.) according to manufacturer's specifications. Primers used are listed in TABLE 3.1. Alterations were confirmed by sequencing by Clemson University Genomics Institute (CUGI).

Heterologous production of enzyme variants

Plasmids were transformed into *E. coli* Rosetta2(DE3)pLysS cells (Novagen). ACD and its variants were purified as in (11). Briefly, cells with the altered or unaltered pET21b-ACD constructs were grown in LB medium and protein production was induced by the addition of IPTG. Cells were resuspended in ice-cold buffer A (25 mM Tris-HCl, 500 mM NaCl, 10% glycerol, 25 mM imidazole [pH 7.3]) and disrupted. Cell-free extract

TABLE 3.1 Primers used for site-directed mutagenesis.

Variant	Dir	Primer Sequence
$His^{252}Ala$	F	5' GCAGCGGCCATGAGTGCTACCGGTAGCCTGGCC 3'
	R	5' GGCCAGGCTACCGGTAGCACTCATGGCCGCTGC 3'
$His^{533}Ala$	F	5' GAGTCCGGATATTATGGCTAAAACCGATGTTGG 3'
	R	5' CCAACATCGGTTTTAGCCATAATATCCGGACTC 3'
$His^{533}Asp$	F	5' GAGTCCGGATATTATGGATAAAACCGATGTTGGCGG 3'
	R	5' CCGCCAACATCGGTTTTATCCATAATATCCGGACTC 3'
$His^{533}Glu$	F	5' GAGTCCGGATATTATGGCGAAAACCGATGTTGGCGG 3'
	R	5' CCGCCAACATCGGTTTTCTCCATAATATCCGGACTC 3'
$His^{533}Lys$	F	5' GAGTCCGGATATTATGAAGAAAACCGATGTTGGCGG 3'
	R	5' CCGCCAACATCGGTTTTCTTCATAATATCCGGACTC 3'
$His^{533}Asn$	F	5' GAGTCCGGATATTATGAACAAAACCGATGTTGGCGG 3'
	R	5' CCGCCAACATCGGTTTTGTTCATAATATCCGGACTC 3'
$His^{533}Gln$	F	5' GAGTCCGGATATTATGCAGAAAACCGATGTTGGCGG 3'
	R	5' CCGCCAACATCGGTTTTCTGCATAATATCCGGACTC 3'
$His^{533}Arg$	F	5' GAGTCCGGATATTATGCGTAAAACCGATGTTGGCGG 3'
	R	5' CCGCCAACATCGGTTTTACGCATAATATCCGGACTC 3'
$Asp^{674}Ala$	F	5' CCCGGAAATCTCTGAAGTTGCTATTAATCCGCTGGCCGTG 3'
	R	5' CACGGCCAGCGGATTAATAGCAACTTCAGAGATTTCCGGG 3'
$Asp^{674}Glu$	F	5' GAAATCTCTGAAGTTGAAATTAATCCGCTGGCC 3'
	R	5' CCGCCAACATCGGTTTTACGCATAATATCCGGACTC 3'
$Asp^{674}Asn$	F	5' GAAATCTCTGAAGTTAATATTAATCCGCTGGCC 3'
	R	5' GGCCAGCGGATTAATATTAACTTCAGAGATTTC 3'
$Glu^{213}Ala$	F	5' GTCTATCCTGATGTACATCGCAAGTATCAAAGATGCCAAA 3'
	R	5' TTTGGCATCTTTGATACTTGCGATGTACATCAGGATAGAC 3'
$Glu^{213}Asp$	F	5' TCCTGATGTACATCGACAGTATCAAAGATGCC 3'
	R	5' GGCATCTTTGATACTGTCGATGTACATCAGGA 3'
$Glu^{213}Gln$	F	5' TCCTGATGTACATCCAAAGTATCAAAGATGCC 3'
	R	5' GGCATCTTTGATACTTTGGATGTACATCAGGA 3'

was applied to a 5 ml HisTrap HP nickel affinity column (GE Healthcare) equilibrated with buffer A and protein was eluted using a linear gradient from 0.025-0.5M imidazole. Fractions containing enzyme were pooled, dialyzed overnight in 25 mM Tris-HCl, 10% glycerol [pH 7.3], aliquoted, and stored at -80°C. Enzyme was verified to be electrophoretically pure by SDS-PAGE analysis . Protein concentration was determined spectrophotometrically using the Take3 Micro-volume plate (BioTek).

Determination of kinetic parameters

Enzymatic activity in the acetate-forming direction was determined by measuring release of CoASH from acyl-CoA using Ellman's thiol reagent (5,5'-dithio-bis-[2-nitrobenzoic acid], DTNB) (24). Production of NTB^{2-} by CoASH cleavage of DTNB was measured spectrophotometrically at 412 nm. Assays were performed in 96-well plates in 0.2 ml reaction volumes. Reaction mixtures contained 50 mM Tris-HCl, 0.3 mM DTNB, and 6 mM HEPES (used to solubilize DTNB) [pH 7.3]) with varied substrate concentrations. Reactions were pre-incubated at 37°C for 5.5 minutes and initiated by the addition of enzyme. Absorbance was measured every 4 seconds at 37°C using a Synergy HT Multi-Mode Microplate Reader (BioTek). Initial velocities were converted to μmol CoASH formed using an extinction coefficient of $\varepsilon = 13.6\ mM^{-1}\ cm^{-1}$ for the thiophenolate NTB^{2-} anion. One unit of activity is defined as 1 µmol product per minute per mg protein.

Enzymatic activity in the acetyl-CoA forming direction was determined using the hydroxamate assay (25,26). Reaction mixtures contained 50 mM Tris-HCl [pH 7.3] and 300 mM hydroxylamine-HCl [pH 7.0] with varied substrate concentrations in a volume of 0.15 ml. Reactions were pre-incubated at 37°C for 5.5 minutes, initiated by the addition

of enzyme and incubated at 37°C, and terminated after a specified amount of time by the addition of one volume of stop solution (2.5% $FeCl_3$/2 N HCl/10% trichloroacetic acid). Product formation was determined by absorbance at 540 nm and comparison to a standard curve. One unit of activity is defined as 1 μmol of acetyl-CoA produced per minute per mg protein. Saturating substrate concentrations for each variant are summarized in TABLE 3.2.

Apparent kinetic parameters were determined by varying the concentration of a single substrate while the other substrates were held at constant saturating concentrations. For determination of the apparent steady-state kinetic parameters K_m and k_{cat} and their standard deviations, nonlinear regression in KaleidaGraph (Synergy Software) was used to fit the data to the Michaelis-Menten equation.

Radiolabeled phosphorylation assay

In order to detect phosphorylated enzyme intermediates, 17 μg enzyme was incubated for 15 minutes at 37°C with either 2.5 μCi of [γ-^{32}P]ATP (10 mM) or 1 μCi $^{32}P_i$ (4 mM) and 0.3 mM acetyl-CoA. Mixtures also contained 50 mM Tris-HCl [pH 8.0]. An equal volume of 2X SDS buffer (5% β-mercaptoethanol, 2% SDS, 25% glycerol, 0.625 M Tris-HCl pH6.8, 0.01% bromophenol blue) was added to the solution and 15 μl was subjected to SDS-PAGE. The gel was dried overnight and autoradiographed. Image quantification was performed using ImageJ. Statistical analysis was performed using paired one-tail t-tests.

Distance Calculations

The *ckc*ACDI-c structure (4XZ3) was obtained from the PDB database. Distance was measured between two atoms using the 'monitor distance' function in Accelrys Discovery Studio 3.5.

TABLE 3.2 Optimized assay conditions for wild type and variant enzymes.

	Acetyl-CoA forming direction						*Acetate-forming direction*			
Enzyme	μg enz	Time (min)	mM acetate	mM CoA	mM MgATP		μg enz	μM AcCoA	mM P_i	mM MgADP
WT	1.1	15	100	1	20		0.019	300	8	5
$His^{533}Arg$	13.4	15	75	0.4	12.5		0.36	300	8	3
$His^{533}Lys$	7.4	25	100	0.8	15		0.74	300	8	5
$His^{533}Ala$	8.2	10	4	0.6	12.5		0.82	200	8	3
$His^{533}Asn$	9.1	45	50	0.2	20		1.52	300	8	5
$His^{533}Gln$	10.2	45	30	0.3	15		1.13	300	10	4
$His^{533}Asp$	27.8	45	75	0.4	12.5		11.1	300	8	5
$His^{533}Glu$	24.8	50	5	0.8	15		9.9	300	6	3
$Asp^{674}Ala$	21	10	6	1	20		0.82	300	10	3
$Asp^{674}Asn$	17.9	30	5	0.2	20		1.5	300	8	6
$Asp^{674}Glu$	0.91	20	200	0.7	25		0.09	300	8	5

IV. RESULTS

His^{252} (Hisα) and His^{533} (Hisβ), the two His residues proposed to be directly phosphorylated during the ACD reaction (20), are conserved among ACDs but only Hisα is conserved across the NDP-forming acyl-CoA synthetase superfamily (FIG 3.1B). These residues were individually changed to alanine and the variants were assayed for activity in each direction of the reaction. Similar to what was observed with *P. furiosus* ACD (20), the His252Ala variant was not active in either direction confirming this residue is essential for activity (FIG 3.2A). Surprisingly, the His533Ala variant retained weak activity in both directions.

To investigate this further, additional variants were created in which His533 was altered to the positively charged residues Arg and Lys, the neutral Asn and Gln, and negatively charged Asp and Glu. Although each of the His533 variants had less than 25% activity compared to wild-type, activity corresponded to the charge of the replacement residue (FIG 3.2A). Substitution of His with a positively charged residue resulted in higher activity than replacement with an uncharged residue. Replacement with a negatively charged residue was the most deleterious (FIG 3.2A).

Apparent kinetic parameters were determined for the His533 variants in both directions of the reaction. In the acetate-forming direction (TABLE 3.3), K_m values for acetyl-CoA and ADP were slightly decreased for the variants versus the wild type. The K_m values for P_i were more variable, ranging from a 10- to 12-fold decrease observed with the His533Glu and His533Arg variants to a 1.8-fold increase with the His533Lys

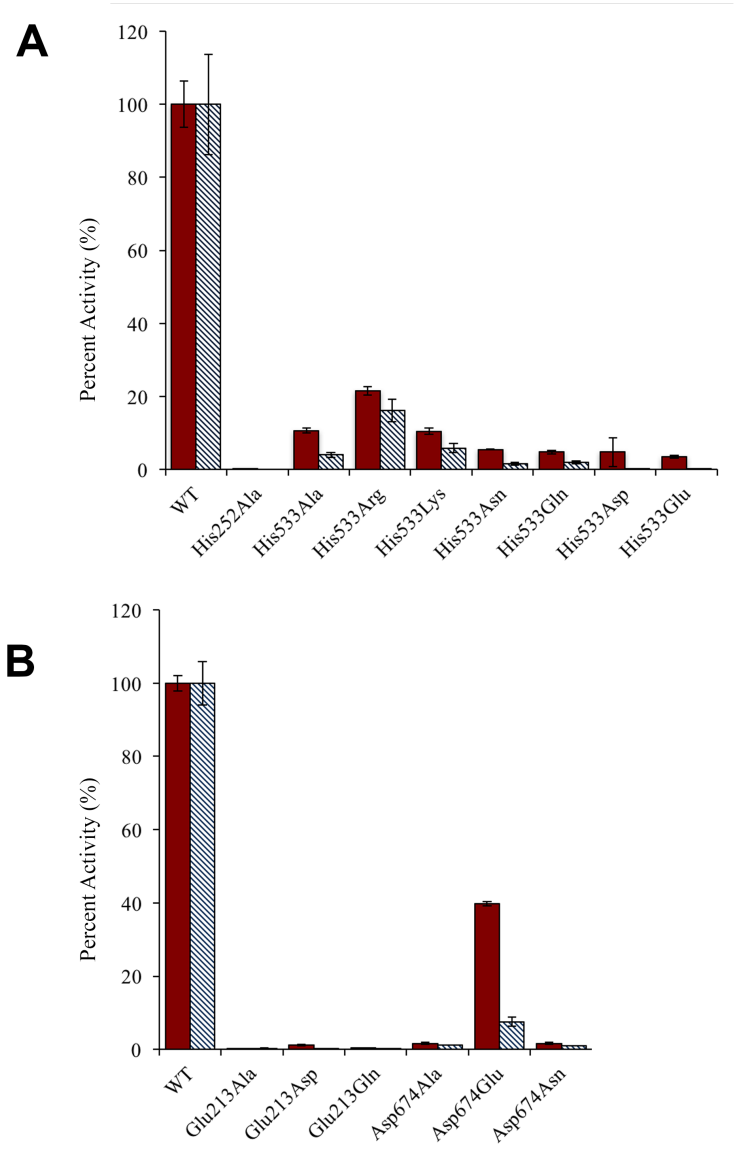

FIG 3.2 Percent activity of *Eh*ACD variants. Activity was determined in the acetyl-CoA forming direction (solid red) and in the acetate-forming direction (blue diagonal pattern). Activities are represented as a percentage of the activity observed for the wild type enzyme (100%). Activity was normalized to wild-type. (A) Activity of the His252 and His533 variants. (B) Activity of the Glu213 and Asp674 variants.

TABLE 3.3 Apparent kinetic parameters of the His533 variants in the acetate-forming direction.

Acetate-forming direction		K_m (mM)	Fold Change	k_{cat} (sec^{-1})	Fold Change
Acetyl-CoA	WT[#]	0.043 ± 0.005		111 ± 2	
	$His^{533}Arg$	0.016 ± 0.003	**-2.7x**	17.6 ± 1.4	**-6.3x**
	$His^{533}Lys$	0.030 ± 0.003	**-1.4x**	2.35 ± 0.21	**-47x**
	$His^{533}Ala$	0.010 ± 0.001	**-4.3x**	2.68 ± 0.09	**-41x**
	$His^{533}Asn$	0.015 ± 0.0003	**-2.9x**	1.39 ± 0.06	**-80x**
	$His^{533}Gln$	0.019 ± 0.004	**-2.3x**	1.73 ± 0.13	**-64x**
	$His^{533}Asp$	0.027 ± 0.008	**-1.6x**	1.62 ± 0.17	**-69x**
	$His^{533}Glu$	0.012 ± 0002	**-3.6x**	0.12 ± 0.001	**-925x**
ADP	WT[#]	1.56 ± 0.15		138 ± 1	
	$His^{533}Arg$	0.64 ± 0.18	**-2.4x**	19.6 ± 1.8	**-7x**
	$His^{533}Lys$	0.97 ± 0.14	**-0.6x**	3.27 ± 0.46	**-42x**
	$His^{533}Ala$	0.41 ± 0.03	**-3.8x**	2.80 ± 0.14	**-49x**
	$His^{533}Asn$	0.57 ± 0.15	**-2.7x**	1.37 ± 0.08	**-101x**
	$His^{533}Gln$	1.28 ± 0.08	**-1.2x**	2.48 ± 0.10	**-56x**
	$His^{533}Asp$	0.60 ± 0.08	**-2.6x**	1.71 ± 0.09	**-81x**
	$His^{533}Glu$	1.19 ± 0.08	**-1.3x**	0.27 ± 0.03	**-511x**
P_i	WT[#]	1.77 ± 0.18		115 ± 8	
	$His^{533}Arg$	0.15 ± 0.03	**-11.8x**	13.9 ± 1.0	**-8.3x**
	$His^{533}Lys$	3.25 ± 0.35	**+1.8x**	3.12 ± 0.37	**-37x**
	$His^{533}Ala$	0.75 ± 0.10	**-2.4x**	2.26 ± 0.09	**-51x**
	$His^{533}Asn$	0.94 ± 0.25	**-1.9x**	1.49 ± 0.11	**-77x**
	$His^{533}Gln$	0.86 ± 0.21	**-2x**	1.76 ± 0.12	**-63x**
	$His^{533}Asp$	0.25 ± 0.08	**-7x**	1.66 ± 0.14	**-69x**
	$His^{533}Glu$	0.18 ± 0.04	**-9.8x**	0.22 ± 0.01	**-523x**

[#] as reported in (11)

variant when compared to wild-type (TABLE 3.3). However, k_{cat} values displayed significant decreases for all of the variants. The most severe decrease in k_{cat} value was observed for the His533Glu variant, and the least severe decrease was observed with the His533Arg variant (TABLE 3.3).

In the acetyl-CoA forming direction of the reaction (TABLE 3.4), K_m values for CoA were only mildly affected with the exception of the His533Gln and His533Asp variants, both of which displayed an 18-fold reduction for CoA. Likewise, the K_m values for ATP were not substantially affected, except for the His533Asp variant for which the K_m was decreased 10-fold.K_m values for acetate showed the greatest effect for all variants, ranging from an 8- to 45-fold decrease compared to wild-type (TABLE 3.4). The k_{cat} values for all of the His533 variants were greatly reduced, ranging from ~40-fold decreased (His533Arg) to over 1300-fold decreased (His533Asp). Replacement of His 533 with a positively charged residue had the least deleterious effect whereas replacement with a negatively charged residue had the most severe effect (TABLE 3.4).

Glu212α and Glu197β were originally identified in *E. coli* SCS for their role in phosphorylation and dephosphorylation of the catalytic Hisα residue (16). Therefore, we wanted to investigate the potential roles of the homologous residues in *Eh*ACD, Glu213 and Asp674. Substitution of Glu213 with Ala, Asn, or Asp resulted in little to no activity (FIG 3.2B), suggesting that this residue is essential.

Asp674 is analogous to *E. coli* SCS Glu197β and *P. furiosus* ACDI Asp212β (FIG 3.1). Substitution of Asp674 with Ala or Asn markedly reduced activity that was partially rescued when replaced with Glu (FIG 3.2B), consistent with corresponding changes in *P. furiosus* ACD (20) and *E. coli* SCS (19). Apparent kinetic parameters for

TABLE 3.4 Apparent kinetic parameters of the His533 variants in the acetyl-CoA forming direction.

Acetyl-CoA forming direction		K_m (mM)	Fold Change	k_{cat} (sec^{-1})	Fold Change
Acetate	WT[#]	14 ± 0.61		233 ± 2.7	
	$His^{533}Arg$	1.7 ± 0.8	**-8x**	5.6 ± 0.09	**-42x**
	$His^{533}Lys$	0.84 ± 0.60	**-17x**	3.4 ± 0.04	**-69x**
	$His^{533}Ala$	0.68 ± 0.10	**-21x**	3.3 ± 0.09	**-71x**
	$His^{533}Asn$	0.76 ± 0.70	**-18x**	1.5 ± 0.02	**-160x**
	$His^{533}Gln$	0.55 ± 0.20	**-25x**	1.2 ± 0.02	**-194x**
	$His^{533}Asp$	0.31 ± 0.02	**-45x**	0.18 ± 0.01	**-1294x**
	$His^{533}Glu$	0.40 ± 0.01	**-35x**	0.26 ± 0.002	**-896x**
CoA	WT[#]	0.20 ± 0.01		328 ± 5.3	
	$His^{533}Arg$	0.10 ± 0.004	**-2x**	7.0 ± 0.15	**-47x**
	$His^{533}Lys$	0.13 ± 0.01	**-1.5x**	4.1 ± 0.04	**-80x**
	$His^{533}Ala$	0.07 ± 0.01	**-3x**	4.2 ± 0.08	**-78x**
	$His^{533}Asn$	0.08 ± 0.004	**-2.5x**	2.0 ± 0.1	**-161x**
	$His^{533}Gln$	0.011 ± 0.001	**-18x**	1.3 ± 0.03	**-252x**
	$His^{533}Asp$	0.011 ± 0.001	**-18x**	0.25 ± 0.01	**-1312x**
	$His^{533}Glu$	0.26 ± 0.02	**+1.3x**	0.27 ± 0.003	**-1215x**
ATP	WT[#]	12 ± 0.40		320 ± 4.4	
	$His^{533}Arg$	2.5 ± 0.16	**-5x**	6.6 ± 0.06	**-48x**
	$His^{533}Lys$	1.7 ± 0.10	**-7x**	3.7 ± 0.09	**-86x**
	$His^{533}Ala$	2.2 ± 0.10	**-5x**	3.3 ± 0.03	**-97x**
	$His^{533}Asn$	7.7 ± 0.6	**-1.6x**	2.0 ± 0.10	**-160x**
	$His^{533}Gln$	2.5 ± 0.13	**-5x**	1.4 ± 0.03	**-230x**
	$His^{533}Asp$	1.2 ± 0.20	**-10x**	0.25 ± 0.01	**-1280x**
	$His^{533}Glu$	3.9 ± 0.10	**-3x**	0.28 ± 0.002	**-1140x**

[#] as reported in (11)

the Asp674 variants revealed only weak changes in K_m for any substrate in either direction of the reaction with the exception of acetate, for which K_m values decreased over 10-fold for the Asp674Ala and Asp674Glu variants (TABLE 3.5). The Asp674Glu variant showed very modest reductions in k_{cat} as compared to the Asp674Ala and Asp674Asn variants, suggesting that the negative charge is important at this position (TABLE 3.5).

Our kinetic results suggest that His252 and Glu213 residues are essential residues; however, His533 and Asp674 are important for catalysis but not critical. Thus, we wanted to analyze the influence of these residues on phosphorylation of the enzyme during catalysis. Phosphorylation was assessed using isotopic labeling with either [γ-^{32}P]ATP or $^{32}P_i$ + acetyl-CoA and analyzed using autoradiography. Phosphorylation of wild type *Eh*ACD was observed under both conditions (FIG 3.3). The His252Ala variant was not phosphorylated by [γ-^{32}P]ATP or $^{32}P_i$ + acetyl-CoA (FIG 3.3A), consistent with the lack of activity of this variant. In contrast, the His533Ala variant was phosphorylated from both directions. Quantitative analysis indicated that this variant was phosphorylated at levels similar to the wild type enzyme by $^{32}P_i$ + acetyl-CoA, and ~20% less by [γ-^{32}P]ATP (FIG 3.3C). Phosphorylation was abolished in His252Ala, confirming that this residue is essential for formation of the phosphorylated enzyme intermediate (FIG 3.3A). A time course of phosphorylation for the wild-type and the His533Ala enzymes showed no discernible difference in labeling between 15 seconds and 15 minutes, as judged by autoradiography (data not shown).

Phosphorylation of the Asp674Ala variant was observed by both $^{32}P_i$ + acetyl-CoA and [γ-^{32}P]ATP (FIG 3.3B). Labeling by $^{32}P_i$ + acetyl-CoA was reduced to 62 ± 3.5%

and to 47 ± 5.3% versus the wild type enzyme using [γ-^{32}P]ATP (FIG 3.3D). In contrast, the Glu213Ala variant was phosphorylated by [γ-^{32}P]ATP but not by $^{32}P_i$ + acetyl-CoA (FIG 3.3B). Labeling by [γ-^{32}P]ATP was similar to that for the wild type enzyme, whereas labeling by $^{32}P_i$ was absent (FIG 3.3D). This is consistent with the lack of enzymatic activity for the Glu213 variants.

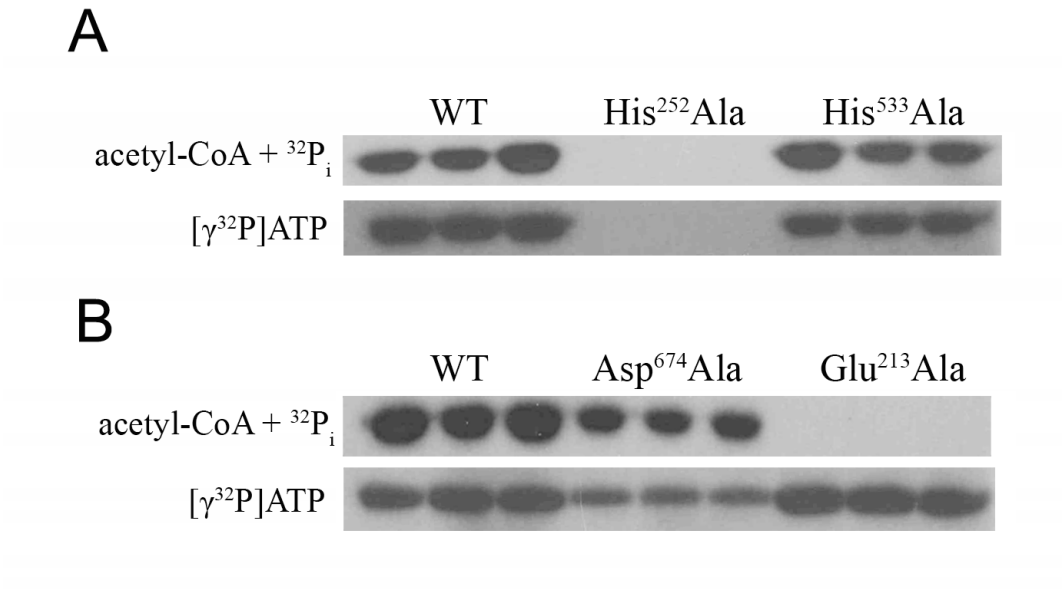

FIG 3.3 Isotopic labeling of *Eh*ACD to detect phosphorylation. Enzymes were labeled with ^{32}P in the presence of acetyl-CoA + P_i (top panels) or ATP (bottom panels). (A) Analysis of the His252Ala and His533Ala variants versus wild type. (B) Analysis of the Glu213Ala and Asp674Ala variants.

TABLE 3.5 Apparent kinetic parameters of the Asp674 variants in both directions of the reaction.

Acetyl-CoA forming direction		K_m (mM)	Fold Change	k_{cat} (sec^{-1})	Fold Change
Acetate	WT[#]	14 ± 0.61		233 ± 2.7	
	$Asp^{674}Ala$	1.3 ± 0.10	**-11x**	2.9 ± 0.1	**-80x**
	$Asp^{674}Asn$	0.96 ± 0.05	**-15x**	1.3 ± 0.1	**-179x**
	$Asp^{674}Glu$	3.9 ± 0.25	**-3.6x**	50.3 ± 1.8	**-4.6x**
CoA	WT[#]	0.20 ± 0.01		328 ± 5.3	
	$Asp^{674}Ala$	0.12 ± 0.01	**-1.7x**	4.2 ± 0.1	**-78x**
	$Asp^{674}Asn$	0.041 ± 0.004	**-5x**	1.2 ± 0.1	**-273x**
	$Asp^{674}Glu$	0.24 ± 0.02	**+1.2x**	44.3 ± 0.1	**-7.4x**
ATP	WT[#]	12 ± 0.4		320 ± 4.4	
	$Asp^{674}Ala$	4.0 ± 0.4	**-3x**	3.2 ± 0.03	**-99x**
	$Asp^{674}Asn$	2.8 ± 0.2	**-4x**	1.2 ± 0.02	**-267x**
	$Asp^{674}Glu$	4.6 ± 0.2	**-2.6x**	53.0 ± 1.2	**-6x**
Acetate-forming direction					
Acetyl-CoA	WT[#]	0.043 ± 0.005		111 ± 2	
	$Asp^{674}Ala$	0.012 ± 0.002	**-3.6x**	2.45 ± 0.18	**-45x**
	$Asp^{674}Asn$	0.016 ± 0.002	**-2.7x**	1.26 ± 0.11	**-88x**
	$Asp^{674}Glu$	0.022 ± 0.002	**-2x**	15.8 ± 0.61	**-7x**
ADP	WT[#]	1.56 ± 0.15		138 ± 1	
	$Asp^{674}Ala$	1.42 ± 0.11	**-1.1x**	2.86 ± 0.15	**-48x**
	$Asp^{674}Asn$	0.43 ± 0.01	**-3.6x**	1.20 ± 0.11	**-115x**
	$Asp^{674}Glu$	1.44 ± 0.08	**-1.1x**	25.0 ± 2.4	**-5.5x**
P_i	WT[#]	1.77 ± 0.18		115 ± 8	
	$Asp^{674}Ala$	0.39 ± 0.03	**-4.5x**	2.64 ± 0.17	**-44x**
	$Asp^{674}Asn$	0.57 ± 0.05	**-3.1x**	0.93 ± 0.04	**-124x**
	$Asp^{674}Glu$	2.84 ± 0.88	**+1.6x**	24.5 ± 5.0	**-4.7x**

[#] as reported in (11)

V. DISCUSSION

The catalytic Hisα is a defining feature of ACD enzymes

NDP-forming acyl-CoA synthetases participate in phosphoryl transfer through a catalytic His residue. This phosphorylation was first observed in the structure of *E. coli* SCS (27) and mutagenesis of this phosphorylated His residue in multiple forms of ATP citrate lyase abolished enzymatic activity (28,29). Likewise, alteration of this His residue in *Eh*ACD (His252) renders the enzyme completely inactive and incapable of phosphorylation.

This catalytic Hisα residue is a defining feature of ACD enzymes and can be useful in classifying putative enzymes from other organisms. This is especially important in distinguishing between ACD and acetyltransferases such as PatZ from *E. coli*. These acetyltransferases share homology with ACD (1) and have the same arrangement of domains as ACD even though domain shuffling is uniquely common within this superfamily of enzymes (1). However, acetyltransferases lack the critical catalytic Hisα residue enabling them to be easily distinguished from acyl-CoA synthetases.

Role of Glu213 in phosphorylation of Hisα

E. coli SCS has two critical glutamate residues that play a role in phosphorylation of the catalytic Hisα (16). Glu208α of SCS is conserved in ACDs and was shown to interact directly with Hisα by accepting a hydrogen bond with N1 of the imidazole ring in order to leave N3 unprotonated and thus stabilize the phosphohistidine (16). This interaction was again confirmed with *ckc*ACDI (21). Alteration of the homologous *Eh*ACD residue Glu213 to Ala resulted in complete loss of activity. Even conservative

replacement with Asp still resulted in barely detectible activity, which is consistent with the highly reduced activity of Glu218Asp from *P. furiosus* ACD (20). It appears that ACD has very little flexibility at this position. Isotopic labeling of the Glu213Ala variant are intriguing because phosphorylation is eliminated when the enzyme is incubated with acetyl-CoA and $^{32}P_i$, but not when incubated with [γ-^{32}P]ATP, showing Glu213 is essential for phosphorylation of Hisα in Site I but not for phosphorylation by ATP. This suggests that phosphorylated Hisα is stuck in its Site II position and is unable to "swing" back into the Site I position when Glu213 is absent. Alternatively, the Glu213Ala enzyme may be phosphorylated on a residue other than Hisα and this would be unaffected by Glu213.

Role of Asp674 in stabilization of phosphorylated Hisα

Glu197β in *E. coli* SCS was proposed to participate in stabilization of the phosphorylated Hisα when positioned at Site II (19). The equivalent residue in *Eh*ACD is Asp674 located in the ATP grasp domain. Alteration of this residue to Ala or Asn resulted in a drastic loss of activity; however, replacement by Glu maintained partial activity. This suggests that the carboxyl group of this Asp residue is important for catalysis, which is consistent with the previously observed function of this residue. In the *ckc*ACDI structure, the equivalent Asp209β hydrogen bonds with the side chain of Thr255α and the backbone nitrogen of His254α when the phosphohistidine segment is pointing toward Site II (21). Consistent with this, the lack of a functional side chain in the Asp674Ala variant reduced but did not eliminate the ability of ACD to be phosphorylated in both directions of the reaction. Thr255α is conserved within all ACDs but is replaced

by Ala in SCS (FIG 3.1B). Thus, if this Asp in ACD functions similarly to the equivalent Glu in SCS, the hydrogen bonding pattern must differ.

The necessity of Hisβ phosphorylation remains undetermined

The reduced activity of the His533 variants undoubtedly establishes that this residue is important for optimal catalysis in *Eh*ACD. However, the exact role it plays in the catalytic mechanism remains unclear. Replacement of His68β in *ckc*ACDI reduced activity to ~ 1% that of the wild type enzyme when changed to Asn and 0.3% activity when changed to Ala (21). These results are consistent with the effects of alterations at His533 of *Eh*ACD, which resulted in highly reduced activity with the exception of His533Arg. Multiple sequence alignment of members of the NDP-forming acyl-CoA synthetase family demonstrated that this position is either occupied by a His as in ACD, or by an Arg residue as in SCS, ACL, and MCS (1). Therefore, it was not entirely surprising that the His533 variant with the highest activity was His533Arg. The partial recovery of activity of the His533Arg variant versus the other variants suggests that these two residues may have overlapping functions. The four-step mechanism in which Hisβ is directly phosphorylated would oppose that possibility, since Arg would not typically be capable of phosphorylation. Alternatively, if ACD-Hisβ is directly phosphorylated, this step may potentially be bypassed when that His is replaced.

Isotopic labeling by [γ-^{32}P]ATP and by $^{32}P_i$ and acetyl-CoA suggests the His533Ala variant is phosphorylated in both directions of the reaction, just as for the wild-type enzyme. This result is inconsistent with the proposed four-step mechanism as phosphorylation by [γ-^{32}P]ATP would be expected to be absent or highly reduced when the functional side chain of His533 was eliminated. This result warrants further analysis

in order to determine whether the mechanism indeed proceeds through a second phosphoenzyme intermediate.

The *ckc*ACDI structure co-crystallized with the non-hydrolyzable ATP analog AMPPCP has the catalytic Hisα residue oriented toward the beta subunit (21). Weiße *et al.* (21) indicate that this structure supports the four-step reaction mechanism proposed by Brasen *et al.* (20) because the distance is too great for direct transfer of the phosphate group between Hisα and ATP. The distances they use to draw this conclusion are between AMPCP, an ADP analog, and the two His residues. They are reported as 8.7 Å between AMPCP and His254α, 6.7 Å between AMPCP and His68β, and 7.1 Å between His254α and His68β.

However, these do not accurately represent the distance for phosphate transfer. Instead, we measured the distance between the terminal phosphate of AMPPCP, an ATP analog, and the N3 position of the imidazole ring of His254α and found it to be just 5.7 Å, shorter than the distances for phosphoryl transfer from ATP to Hisβ (7.9 Å) and then to His254α (9.0 Å) (FIG 3.4). Distances were also calculated for the alternative N1 position of His68β and these too were greater than the direct distance between AMPPCP and His254α (8.5 Å to His254α and 6.2 Å to the terminal phosphate group of AMPPCP). Thus, direct phosphorylation of His254α by ATP is more likely than phosphorylation of His68β followed by transfer to His254α, consistent with a three-step mechanism as for SCS rather than a four-step mechanism.

An interesting phenomenon in ACL may explain the additional phosphorylation observed in *Pf*ACD (20). Isotopic labeling revealed that low levels of phosphorylation occur in *Chlorobium limicola* ACL after long periods of time when the catalytic Hisα was

altered. This group suggested that a second unproductive phosphorylation site may be present within the active site. This phenomenon may hold true for at least some ACDs as well.

Conclusion

We have demonstrated the importance of four residues involved in catalysis of *E. histolytica* ACD and their contributions to phosphorylation of the enzyme. We propose that *Eh*ACD follows a three-step mechanism analogous to that of SCS rather than the four-step mechanism involving two phosphoenzyme intermediates as proposed by Brasen *et al.* (20); however, more direct evidence related to the mechanism is needed. The dimeric *Eh*ACD has fused alpha and beta domains, resulting in a different subunit structure than *Pf*ACD and *ckc*ACDI, both of which are heterotetramers with separate alpha and beta subunits. As a result, ACDs may fall into two classes based on subunit structure, one of which can directly transfer the phosphate group between Hisα and ATP and the other of which relies on a two-step transfer to bridge that distance.

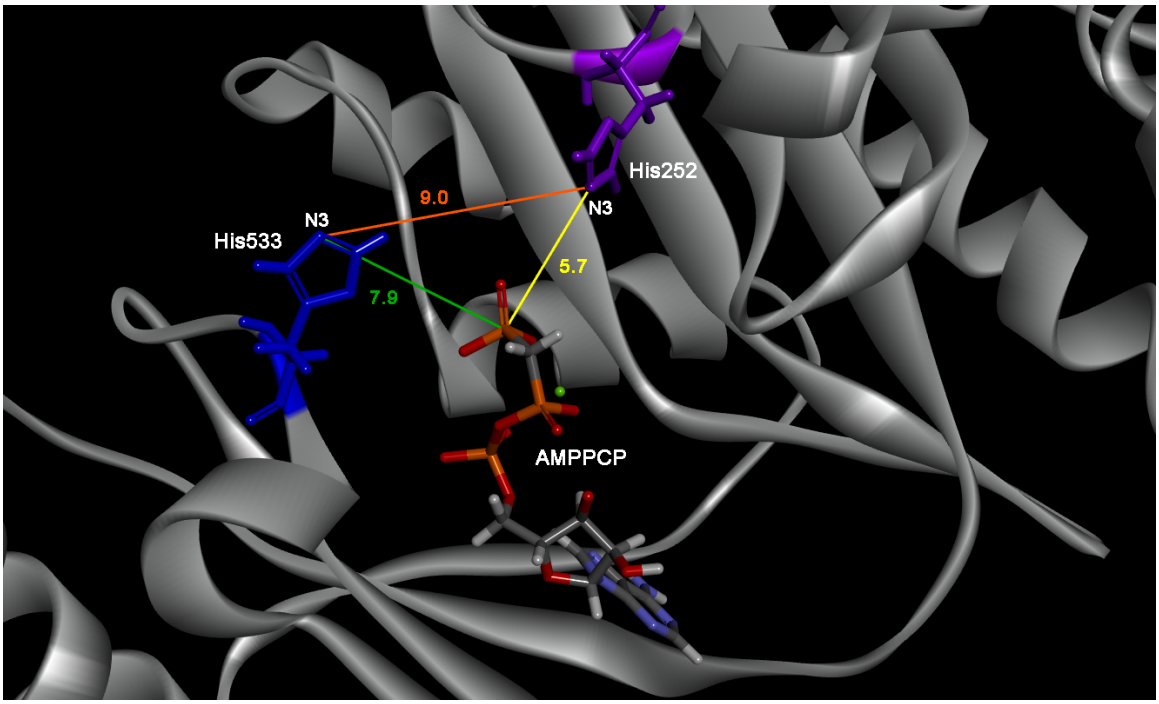

FIG 3.4 Distance measurements in Site II of *ckc*ACDI. The *ckc*ACDI structure crystallized with CoA and MgAMPPCP with Hisα in Site II of the active site was obtained from PDB (accession #4XZ3). His254α is shown in purple and His68β is shown in blue. MgAMPPCP is colored by element: C (gray), P (orange), O (red), N (purple), H (light gray), and Mg (green). The distance between N3 of Hisα and P of AMPPCP (yellow line) is 5.7 Å. The distances between Hisα and Hisβ (orange line) and between Hisβ and P of AMPPCP (green line) are 9 Å and 7.9 Å, respectively.

VI. ACKNOWLEDGEMENTS

We thank Kerry Smith (Clemson University) for beneficial discussions regarding this work. Funding for this research was provided by National Science Foundation Award #0920274 (Kerry Smith, PI, and C.I.-S., co-PI), a National Science Foundation Graduate Research Fellowship award to C. J., and Clemson University.

VII. REFERENCES

1. Sanchez, L. B., Galperin, M. Y., and Muller, M. (2000) Acetyl-CoA synthetase from the amitochondriate eukaryote Giardia lamblia belongs to the newly recognized superfamily of acyl-CoA synthetases (Nucleoside diphosphate-forming). *J Biol Chem* **275**, 5794-5803

2. Brasen, C., and Schonheit, P. (2004) Unusual ADP-forming acetyl-coenzyme A synthetases from the mesophilic halophilic euryarchaeon Haloarcula marismortui and from the hyperthermophilic crenarchaeon Pyrobaculum aerophilum. *Arch Microbiol* **182**, 277-287

3. Sanchez, L. B., and Muller, M. (1996) Purification and characterization of the acetate forming enzyme, acetyl-CoA synthetase (ADP-forming) from the amitochondriate protist, Giardia lamblia. *FEBS Lett* **378**, 240-244

4. Schmidt, M., and Schonheit, P. (2013) Acetate formation in the photoheterotrophic bacterium Chloroflexus aurantiacus involves an archaeal type ADP-forming acetyl-CoA synthetase isoenzyme I. *FEMS Microbiol Lett* **349**, 171-179

5. Glasemacher, J., Bock, A. K., Schmid, R., and Schonheit, P. (1997) Purification and properties of acetyl-CoA synthetase (ADP-forming), an archaeal enzyme of acetate formation and ATP synthesis, from the hyperthermophile Pyrococcus furiosus. *Eur J Biochem* **244**, 561-567

6. Mai, X., and Adams, M. W. (1996) Purification and characterization of two reversible and ADP-dependent acetyl coenzyme A synthetases from the hyperthermophilic archaeon Pyrococcus furiosus. *J Bacteriol* **178**, 5897-5903

7. Schäfer, T., and Schönheit, P. (1991) Pyruvate metabolism of the hyperthermophilic archaebacterium Pyrococcus furiosus. *Arch. Microbiol.* **155**, 366-377

8. Schäfer, T., Selig, M., and Schönheit, P. (1993) Acetyl-CoA synthetase (ADP forming) in archaea, a novel enzyme involved in acetate formation and ATP synthesis. *Arch. Microbiol.* **159**, 72-83

9. Reeves, R. E., Warren, L. G., Susskind, B., and Lo, H. S. (1977) An energy-conserving pyruvate-to-acetate pathway in Entamoeba histolytica. Pyruvate synthase and a new acetate thiokinase. *J Biol Chem* **252**, 726-731

10. Lindmark, D. G. (1980) Energy metabolism of the anaerobic protozoon Giardia lamblia. *Mol Biochem Parasitol* **1**, 1-12

11. Jones, C. P., and Ingram-Smith, C. (2014) Biochemical and kinetic characterization of the recombinant ADP-forming acetyl coenzyme A synthetase from the amitochondriate protozoan Entamoeba histolytica. *Eukaryot Cell* **13**, 1530-1537

12. Pineda, E., Vazquez, C., Encalada, R., Nozaki, T., Sato, E., Hanadate, Y., Nequiz, M., Olivos-Garcia, A., Moreno-Sanchez, R., and Saavedra, E. (2016) Roles of acetyl-CoA synthetase (ADP-forming) and acetate kinase (PPi-forming) in ATP and PPi supply in Entamoeba histolytica. *Biochim Biophys Acta* **1860**, 1163-1172

13. Bailey, D. L., Fraser, M. E., Bridger, W. A., James, M. N., and Wolodko, W. T. (1999) A dimeric form of Escherichia coli succinyl-CoA synthetase produced by site-directed mutagenesis. *J Mol Biol* **285**, 1655-1666

14. Musfeldt, M., and Schonheit, P. (2002) Novel type of ADP-forming acetyl coenzyme A synthetase in hyperthermophilic archaea: heterologous expression and characterization of isoenzymes from the sulfate reducer Archaeoglobus fulgidus and the methanogen Methanococcus jannaschii. *J Bacteriol* **184**, 636-644

15. Fraser, M. E., James, M. N., Bridger, W. A., and Wolodko, W. T. (1999) A detailed structural description of Escherichia coli succinyl-CoA synthetase. *J Mol Biol* **285**, 1633-1653

16. Fraser, M. E., James, M. N., Bridger, W. A., and Wolodko, W. T. (2000) Phosphorylated and dephosphorylated structures of pig heart, GTP-specific succinyl-CoA synthetase. *J Mol Biol* **299**, 1325-1339

17. Joyce, M. A., Brownie, E. R., Hayakawa, K., and Fraser, M. E. (2007) Cloning, expression, purification, crystallization and preliminary X-ray analysis of Thermus aquaticus succinyl-CoA synthetase. *Acta Crystallogr Sect F Struct Biol Cryst Commun* **63**, 399-402

18. Joyce, M. A., Hayakawa, K., Wolodko, W. T., and Fraser, M. E. (2012) Biochemical and structural characterization of the GTP-preferring succinyl-CoA synthetase from Thermus aquaticus. *Acta Crystallogr D Biol Crystallogr* **68**, 751-762

19. Fraser, M. E., Joyce, M. A., Ryan, D. G., and Wolodko, W. T. (2002) Two glutamate residues, Glu 208 alpha and Glu 197 beta, are crucial for phosphorylation and dephosphorylation of the active-site histidine residue in succinyl-CoA synthetase. *Biochemistry* **41**, 537-546

20. Brasen, C., Schmidt, M., Grotzinger, J., and Schonheit, P. (2008) Reaction mechanism and structural model of ADP-forming Acetyl-CoA synthetase from the hyperthermophilic archaeon Pyrococcus furiosus: evidence for a second active site histidine residue. *J Biol Chem* **283**, 15409-15418

21. Weisse, R. H., Faust, A., Schmidt, M., Schonheit, P., and Scheidig, A. J. (2016) Structure of NDP-forming Acetyl-CoA synthetase ACD1 reveals a large rearrangement for phosphoryl transfer. *Proc Natl Acad Sci U S A* **113**, E519-528

22. Altschul, S. F., Madden, T. L., Schaffer, A. A., Zhang, J., Zhang, Z., Miller, W., and Lipman, D. J. (1997) Gapped BLAST and PSI-BLAST: a new generation of protein database search programs. *Nucleic Acids Res* **25**, 3389-3402

23. Sievers, F., Wilm, A., Dineen, D., Gibson, T. J., Karplus, K., Li, W., Lopez, R., McWilliam, H., Remmert, M., Soding, J., Thompson, J. D., and Higgins, D. G. (2011) Fast, scalable generation of high-quality protein multiple sequence alignments using Clustal Omega. *Mol Syst Biol* **7**, 539

24. Srere, P. A. (1963) Citryl-Coa. An Substrate for the Citrate-Cleavage Enzyme. *Biochim Biophys Acta* **73**, 523-525

25. Lipmann, F. T., C. T. . (1945) A specific micromethod for the determination of acyl phosphates. *J Biol Chem* **159**, 21-28

26. Jones, M. E. L., F. (1955) Aceto-CoA-kinase. *Methods in Enzymology* **I**, 585-595

27. Wolodko, W. T., Fraser, M. E., James, M. N., and Bridger, W. A. (1994) The crystal structure of succinyl-CoA synthetase from Escherichia coli at 2.5-A resolution. *J Biol Chem* **269**, 10883-10890

28. Kanao, T., Fukui, T., Atomi, H., and Imanaka, T. (2002) Kinetic and biochemical analyses on the reaction mechanism of a bacterial ATP-citrate lyase. *Eur J Biochem* **269**, 3409-3416

29. Fan, F., Williams, H. J., Boyer, J. G., Graham, T. L., Zhao, H., Lehr, R., Qi, H., Schwartz, B., Raushel, F. M., and Meek, T. D. (2012) On the catalytic mechanism of human ATP citrate lyase. *Biochemistry* **51**, 5198-5211

CHAPTER 4

PROBING THE FUNCTION OF ADDITIONAL RESIDUES WITHIN ADP-FORMING ACETYL-COA SYNTHETASE OF *ENTAMOEBA HISTOLYTICA* USING COMPUTATIONAL MODELING AND SITE-DIRECTED MUTAGENESIS

Cheryl Jones, Noah Smith, and Cheryl Ingram-Smith

I. ABSTRACT

The ADP-forming acetyl-CoA synthetase (ACD) from *Entamoeba histolytica* belongs to the NDP-forming acyl-CoA synthetase superfamily. Interest in this family of enzymes has increased due to their role in the central carbon metabolism of almost all organisms. The most well-studied enzyme of this family is succinyl-CoA synthetase from *Escherichia coli*. However, structural characterization of ACD from *Candidatus Korarchaeum cryptofilum* has added great insight into ACD function. In order to probe the functional role of proposed active site residues of the *E. histolytica* ACD, site-altered variants were produced for Gln159, Lys534, and Asp314. Characterization, along with computational modeling of these residues, gives evidence regarding their potential significance.

II. INTRODUCTION

ADP-forming acetyl-CoA synthetase (ACD; EC 6.2.1.13) is an acetate thiokinase that catalyzes the reversible conversion of acetate to acetyl-CoA. ACD was first identified in *Entamoeba histolytica* extracts in 1977 (1) and was later recombinantly produced, purified, and characterized (2). Investigation into the catalytic mechanism of *E. histolytica* ACD has confirmed the importance of the primary catalytic Hisα residue (C. Jones, K. Khan, and C. Ingram Smith, in preparation). Crystal structures of the separate alpha and beta subunits from *Pyrococcus horikoshii* (accession numbers 1WR2 and 2CSU) were solved in 2005 but gave incomplete information regarding the quaternary structure of ACD. Recent structural characterization of ACDI from *Candidatus Korarchaeum cryptofilum* revealed insight into the tertiary and quaternary structure (3). ACD contains two distinct locations of the active site, designated Site I and Site II (3). Acetyl-CoA and P_i bind to the enzyme in Site I, forming a transient acetyl-phosphate bound intermediate, and releasing CoA. The phosphoryl moiety is then transferred to N3 of the imidazole ring on the catalytic His residue located on the phosphohistidine loop of Site I. It was previously postulated that this loop then swings to site II to transfer this phosphoryl group to ADP to form ATP. Analysis of the *Ca. K. cryptofilum* structure revealed that an α-helix of the phosphohistidine loop partially unravels in order to "swing" to Site II (3). The NDP substrate bound within Site II is then phosphorylated, returning the enzyme to its normal state.

Some NDP-forming acyl-CoA synthetases directly phosphorylate the NDP substrate. However, Brasen *et al.* (4) proposed that ACD requires an additional

phosphoryl transfer step involving a second His residue, utilizing the following four-step mechanism:

Step 1: $E + \text{acetyl-CoA} + P_i \leftrightarrow E\sim\text{acetyl-P} + \text{CoA}$

Step 2: $E\sim\text{acetyl-P} \leftrightarrow E\sim\text{His}\alpha\text{-P}$

Step 3: $E\sim\text{His}\alpha\text{-P} \leftrightarrow E\sim\text{His}\beta\text{-P}$

Step 4: $E\sim\text{His}\beta\text{-P} + \text{ADP} \leftrightarrow E + \text{ATP}$

Crystal structures of *Ca. K. cryptofilum* solved in the presence of various ligands demonstrated the Hisα residue phosphorylated in both Site I and Site II; however, a structure in which the Hisβ residue was phosphorylated was not obtained (3). Characterization of Hisβ variants has shown this residue to be important for catalysis (4), but our results suggest that it is not essential (C. Jones, K. Khan, and C. Ingram-Smith, in preparation).

Other enzymes within the NDP-forming acyl-CoA synthetase superfamily have been structurally characterized, including human ATP-citrate lyase (ACL) (5,6), and succinyl-CoA synthetase (SCS) from *Escherichia coli* (7-11), pig heart (12-14), and *Thermus aquaticus* (15,16). The significant shuffling of domains within this family poses a challenge in comparing structural data from one enzyme to another. Yet, the increasing number of structures available signifies that we are working toward a deeper understanding of the common and defining features between enzymes in this family.

Here we continue to investigate the role of additional residues in *E. histolytica* ACD (*Eh*ACD) and construct a homology model based on the recently solved *Ca. K. cryptofilum* ACD (*ckc*ACD) structure.

III. MATERIALS AND METHODS

Materials

Chemicals were purchased from Sigma Aldrich, Gold Biotechnology, Fisher Scientific, or VWR. Oligonucleotide primers were purchased from Integrated DNA Technologies, Inc.

Sequence Alignment

Amino acid sequences annotated as ADP-forming acetyl-CoA synthetases were acquired from NCBI and additional sequences were identified using PSI-BLAST (http://blast.ncbi.nlm.nih.gov/Blast.cgi?PAGE=Proteins) (17) with the *E. histolytica* ACD sequence (GI: 67481881) as the query. The multiple sequence alignment was constructed using ClustalOmega (http://www.ebi.ac.uk/Tools/msa/clustalo/) (18).

Site-directed mutagenesis

The codon-optimized *E. histolytica acd* gene, cloned into pET21b which provides for an addition of a C-terminal 6xHis tag, was subjected to site-directed mutagenesis using the QuikChange II kit (Agilent Technologies, Inc.). Mutagenesis primers used are as follows: Gln159Asp, (F) GTGGCCTTCATCTCTGACAGTGGCGCACTGTGT and (R) ACACAGTGCGCCACTGTCAGAGATGAAGGCCAC; Asp314Ala, (F) CCGGGTGTGATTAGTACGGCTCGCCTGGTTAGCGTTCATG and (R) CATGAACGCTAACCAGGCGAGCCGTACTAATCACACCCGG; Lys534Arg, (F) GAGTCCGGATATTATGCATCGAACCGATGTTGGCGG and (R) CCGCCAACATCGGTTCGATGCATAATATCCGGACTC. The His533Ala Lys534Arg variant was constructed using the mutagenized *Eh*ACD His533Ala pET21b plasmid and

the following primers: (F) GAGTCCGGATATTATTGGCTCGAACCGATGTTGGCGG and (R) CCGCCAACATCGGTTCGAGCCATAATATCCGGACTC. Mutagenesis was confirmed via DNA sequencing (Clemson University Genomics Institute).

Production of *Eh*ACD variants

E. coli Rosetta2 (DE3) pLysS cells (EMD) carrying pET21b containing the mutated *acd* gene were grown in LB medium to an optical density of 0.6 at 600 nm. ACD protein production was induced by adding IPTG to a final concentration of 1 mM, and cells were grown overnight shaking at 200 rpm at room temperature. Cells were harvested by centrifugation and *Eh*ACD was purified by nickel affinity chromatography as described previously (2).

Enzyme assays

*Eh*ACD activity was determined in the acetyl-CoA forming direction using the hydroxamate assay (2,19). Initial activity assays were conducted at 37°C using the saturating substrate concentrations determined for the wild-type enzyme (2): 50 mM Tris-HCl pH 7.3, 300 mM hydroxylamine pH 7.0, 20 mM $MgCl_2$-ATP, 1 mM CoA, and 100 mM sodium acetate. The reaction volume was 150 μl and reactions were terminated by the addition of an equal volume of a solution containing 2.5% $FeCl_3$ and 10% trichloroacetic acid in 2N HCl. Saturating substrate concentrations for Gln159Glu were 450 mM sodium acetate, 1 mM CoA, 40 mM $MgCl_2$, and 15 mM ATP. Assays for kinetic characterization of Gln159Glu were carried out for 30 minutes at 37°C. Kinetic parameters were determined as previously described (2), using non-linear regression (Kaleidagraph, Synergy software).

Generation of homology models

The *Ca. K. cryptofilum* ACDI is a heterotetramer of two alpha and two beta chains (3). Since *Eh*ACD is a dimer in which the subunits represent a fusion of the alpha and beta domains, two chains were used to align the sequences and generate homology models based on the *Ca. K. cryptofilum* template structures using Accelrys Discovery Studio 3.5 software. Three models were generated based on different conformations of the catalytic residues. For each, the model with the lowest DOPE (discreet optimized protein energy) score was selected for further analysis. Model 1, based on *Ca. K. cryptofilum* 4YBZ, shows ACD complexed with ADP and the catalytic Hisα at Site 1. Model 2, based on *Ca. K. cryptofilum* 4YYM, shows ACD in complex with coenzyme A, Ca-AMPCP (ADP analog) and $HgCl^{+}$, and the Hisα is positioned near Site I. Model 3 is based on *Ca. K. cryptofilum* 4XZ3 and shows ACD in complex with CoA and Mg-AMPPCP (ATP analog) and the phosphorylated Hisα in Site II. *In silico* analysis of Asp314Ala and Asp314Glu alterations was performed by altering the residue within the sequence of both chains and subsequently building a homology model based on 4XYM.

IV. RESULTS

Gln159, conserved in ACD sequences (FIG 4.1A) but replaced by Arg in other family members such as SCS, ACL, and malyl-CoA synthetase (MCS) (20), is predicted to interact with the phosphohistidine loop based on the function of the Arg residue in *E. coli* SCS (11). Altering this Gln to a Glu substantially decreased activity to approximately 8% that of the wild-type enzyme (FIG 4.1B). Kinetic characterization of the Gln159Glu variant revealed a 13-fold decrease in k_{cat} (TABLE 4.1). The K_m values for CoA and ATP showed only minor changes compared to wild-type, but the K_m for acetate increased 6-fold.

The catalytically important His533 and the adjacent Lys534 are conserved in ACD, pimeloyl-CoA synthetase, acetyltransferases, and several predicted acyl-CoA synthetases (20). However His533 is homologous to an Arg and Lys534 is homologous to a Gly residue in SCS, MCS, and ACL. A Lys534Arg variant and a His533Ala Lys534Arg double variant were generated and analyzed. The double variant had little to no activity (<0.5%), however the Lys534Arg variant retained ~12% activity (FIG 4.2).

Homology models of *E. histolytica* ACD were generated based on structures from *Ca. K. cryptofilum* (FIG 4.3). *Eh*ACD, which is a homodimer (2), shares 37% identity with *ckc*ACD, a heterotetramer (3). There are two active sites within ACD; the phosphohistidine loop containing His252α is capable of changing conformation to occupy either Site I (FIG 4.4 and 4.5) or Site II (FIG 4.6A). Site II is the location of the ADP/ATP binding site and His533β (FIG 4.6B). As seen in Figure 4.6C, Lys534 is oriented on the opposite side of His533.

Asp314, conserved among all known NDP-forming acyl-CoA synthetases (20), is predicted to interact with the phosphohistidine loop (7), but was also demonstrated to play a role in oligomer formation in *E. coli* SCS (21). Attempts to produce the Asp314Ala variant were unsuccessful. Therefore, *in silico* analysis was used to attempt to understand whether Asp314 contributes to the structural integrity of the enzyme. Asp314 is located within an α-helix near the catalytic His residue (FIG 4.7A), and participates in hydrogen bonds between the two chains (example shown in FIG 4.7B). Hydrogen bonding occurred at the interface of the two monomers between Asp314 on one chain and residues 240-242 on the opposite chain. In all models generated, Asp314 was responsible for three out of ten total intermolecular hydrogen bonds between the monomers. Asp314Ala and Asp314Glu alterations were generated *in silico* and revealed that Asp314Glu was capable of hydrogen bonding in a similar fashion (FIG 4.7D), while Asp314Ala lost the ability (FIG 4.7C). Loss of this bonding may prevent oligomerization, which subsequently affects stability.

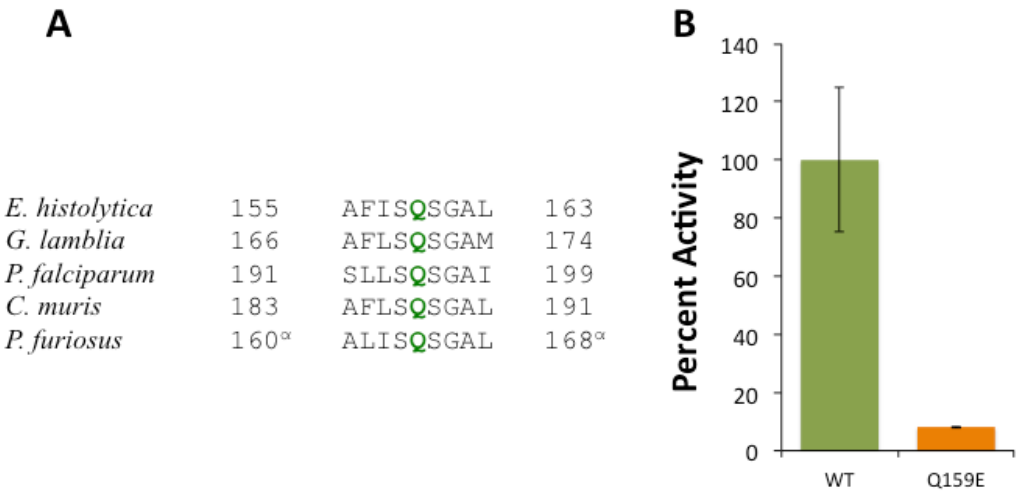

FIG 4.1 *Eh*ACD Gln159. (A) Sequence alignment of Gln159 in ACDs. (B) Activity of Gln159Asp variant compared to wild-type in the acetyl-CoA forming direction.

TABLE 4.1 Kinetic parameters for the Gln159Glu variant in the acetyl-CoA forming direction.

Substrate	Enz	K_m (mM)	Fold change	k_{cat} (sec^{-1})	Fold change
Acetate	WT	14 ± 0.6	**+6.4x**	233 ± 2.7	**-13x**
	Q159E	89 ± 9		18 ± 0.5	
CoA	WT	0.20 ± 0.01	**-1.3x**	328 ± 5	**-14x**
	Q159E	0.16 ± 0.01		24 ± 0.3	
ATP	WT	12 ± 0.4	**-2.9x**	320 ± 4	**-15x**
	Q159E	4.1 ± 0.2		22 ± 0.01	

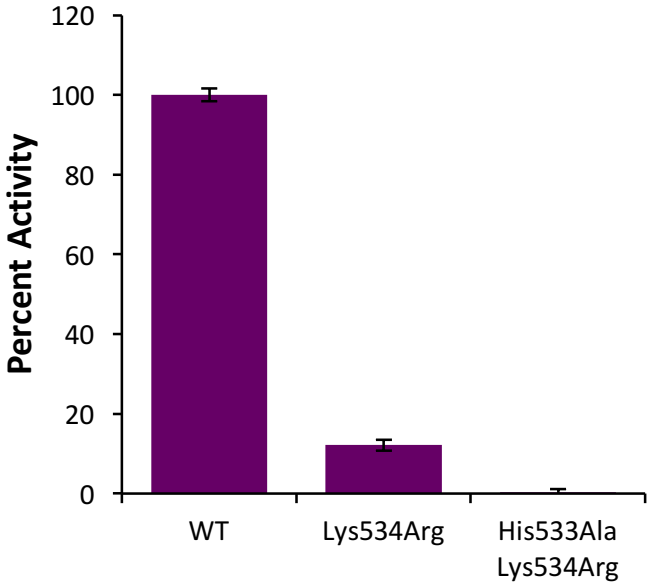

FIG 4.2 Activity of Lys534 variants in the acetyl-CoA forming direction.

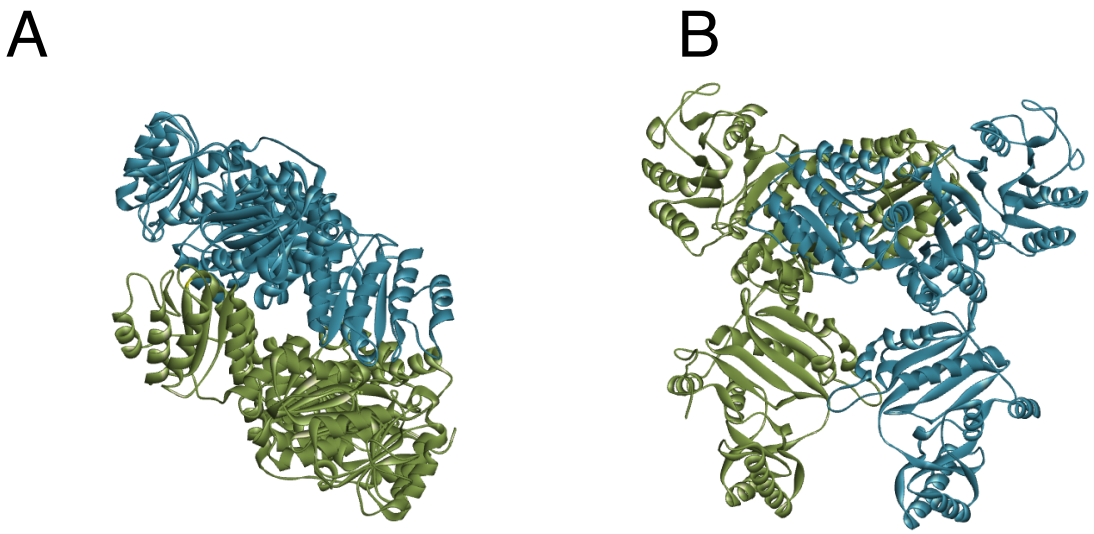

FIG 4.3 Ribbon diagram of *Eh*ACD homology model based on 4YBZ. (A) Top view (B) Front view. Chain A is shown in green and Chain B in blue.

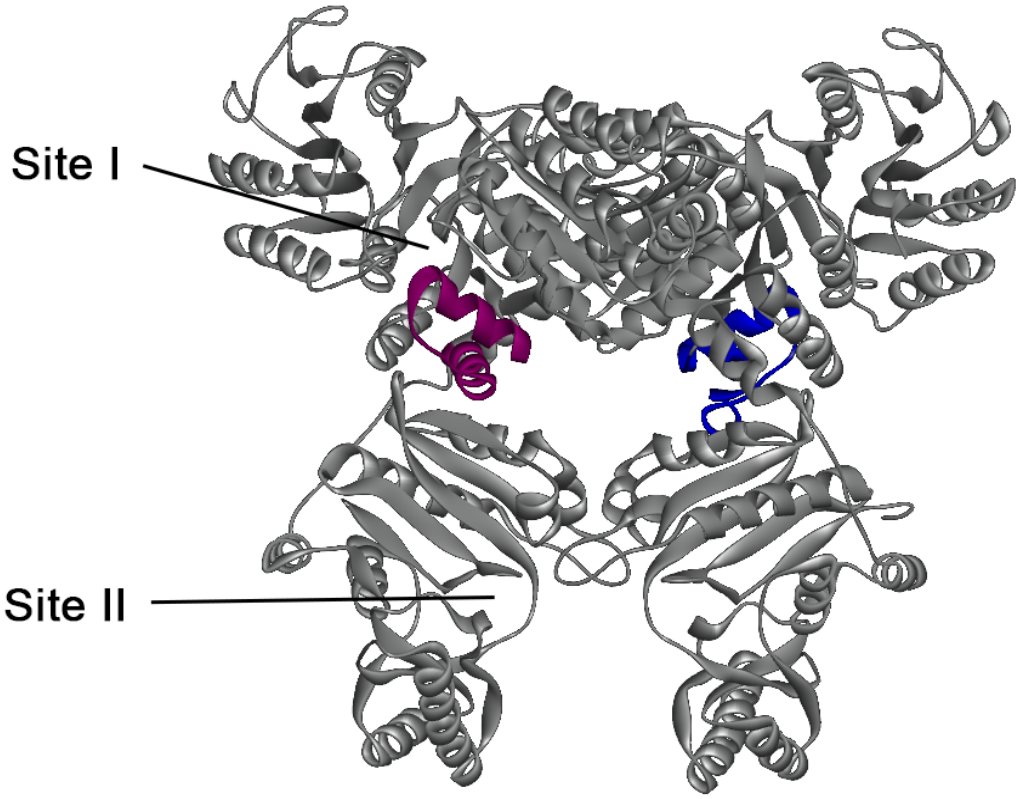

FIG 4.4 Active sites of *Eh*ACD with the phosphohistidine loop pointed toward Site I. Homology model of *Eh*ACD based on 4XYM. The phosphohistidine loop of Chain A is colored in pink and the phosphohistidine loop of Chain B is colored in blue. The position of the two active sites of Chain A are as designated.

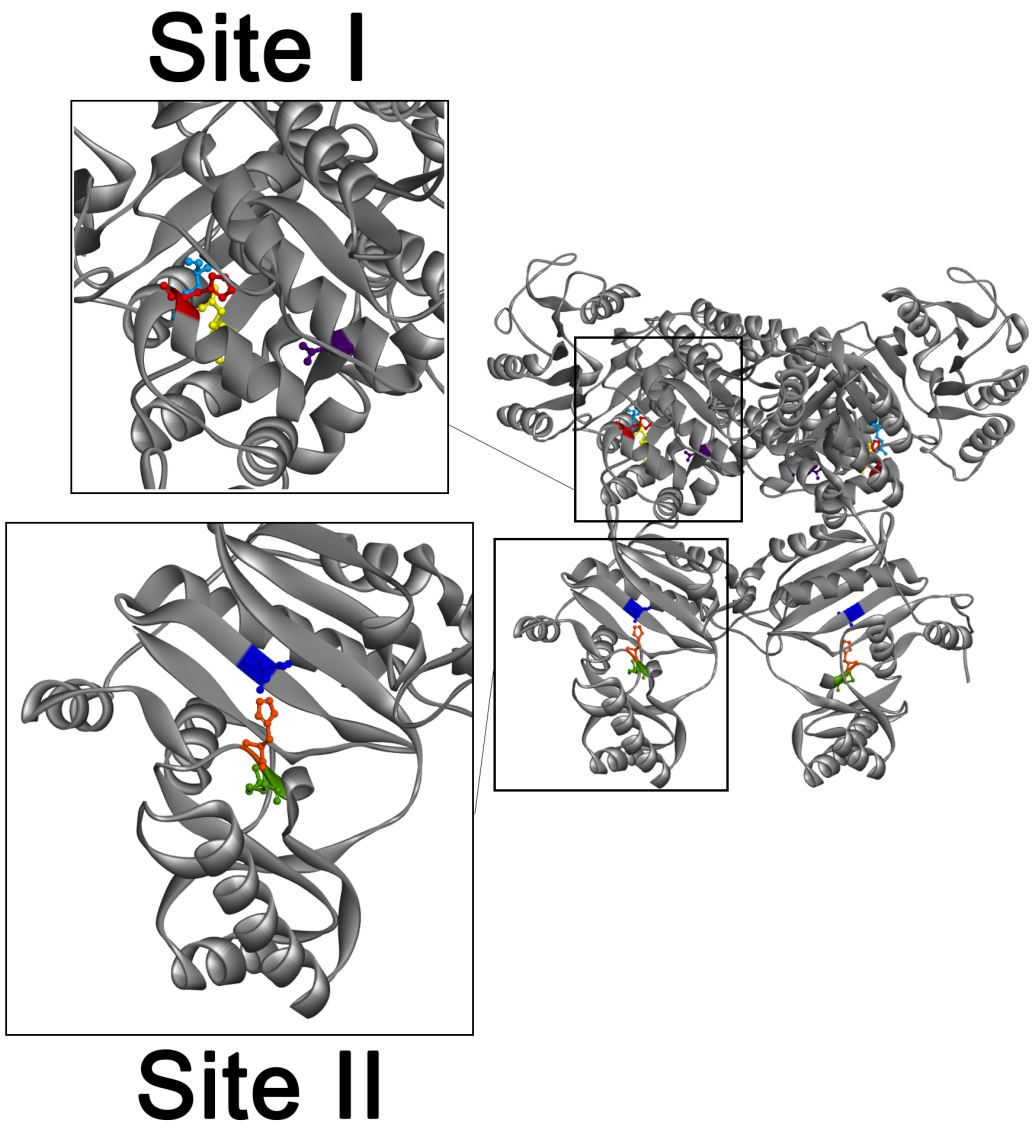

FIG 4.5 Targets of site-directed mutagenesis. Within Site I: Gln159 (light blue), Glu213 (yellow), His252 (red), Asp314 (purple). Within Site II: His533 (orange), Lys534 (green), Asp674 (dark blue).

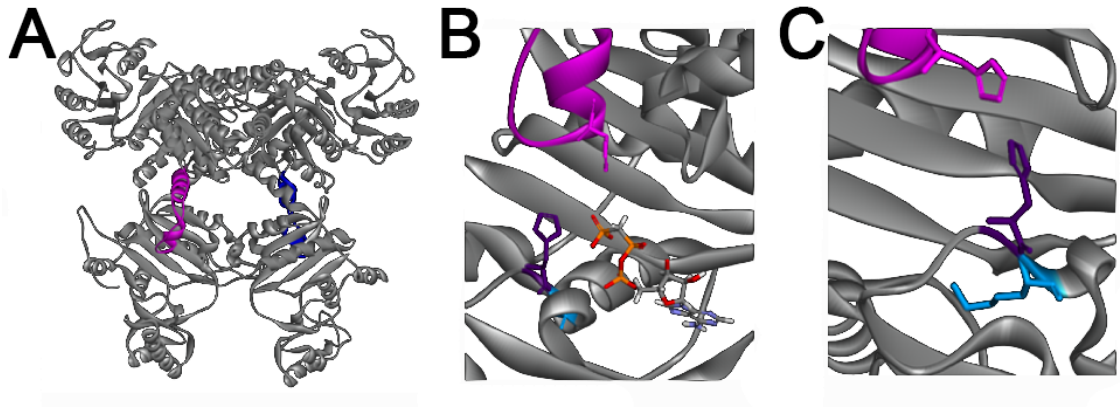

FIG 4.6 Homology model of *Eh*ACD with the phosphohistidine loop pointed toward Site II. This structure was modeled based on 4XZ3, which includes CoA and AMPPCP as ligands. (A) Ribbon diagram of the dimer with the phosphohistidine loops shown in pink (chain A) and blue (chain B). (B) Proximity of His252α (pink) and His533β (purple) to the AMPPCP ligand. (C) Lys534 (blue) has an orientation opposite of His533β (purple).

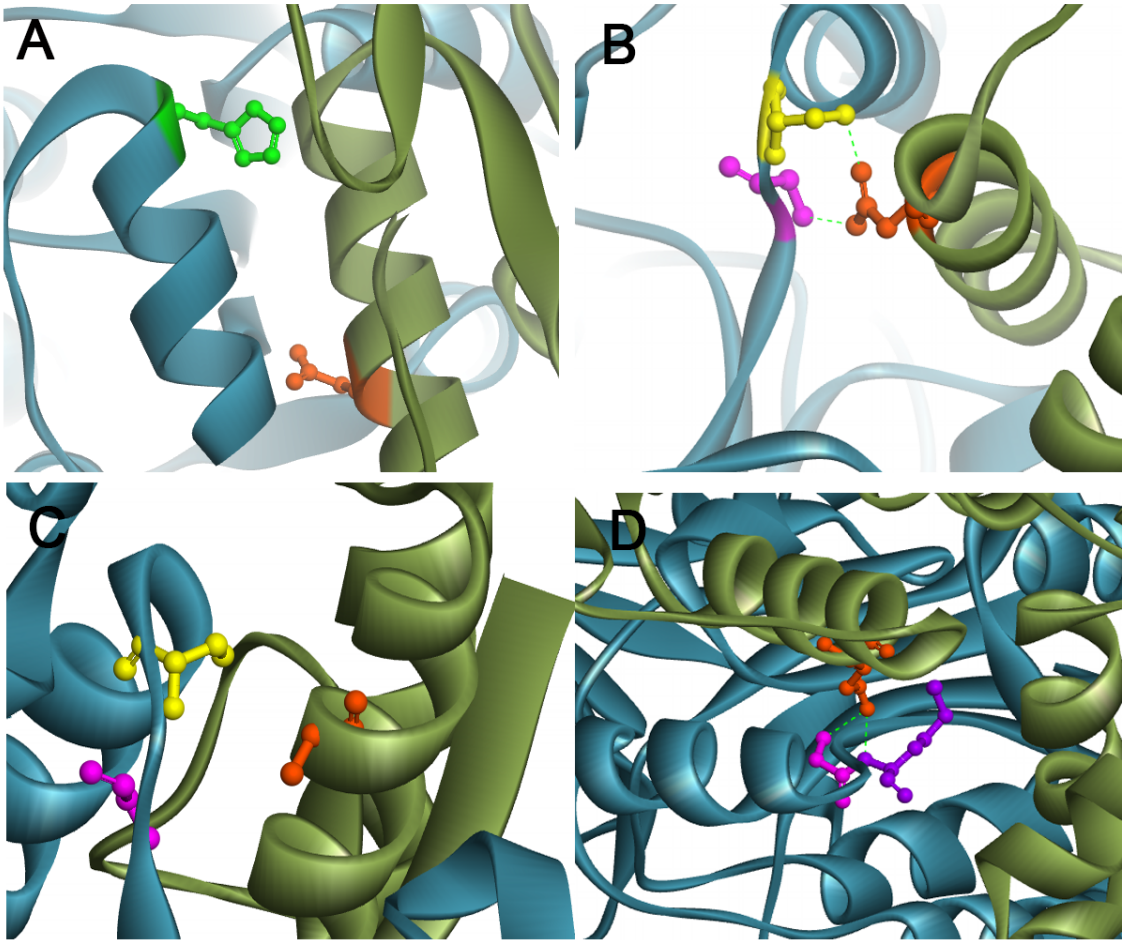

FIG 4.7 *In silico* analysis of Asp314. Chain A is shown in green and Chain B is shown in blue. (A) Asp314 of Chain B is part of an α-helix located parallel to an α-helix of the phosphohistidine loop of Chain A. His252 (green) and Asp314 (orange) are shown in ball and stick model. (B) Asp314 (orange) is predicted to hydrogen bond with a side chain O of Ser242 (yellow) and a main chain N of Gly240 (pink) on the opposite chain. Hydrogen bonds are indicated by dotted green lines. (C) *In silico* analysis of alteration of Asp314 to Ala shows a loss of intermolecular hydrogen bonding, whereas (D) Asp314Glu is predicted to hydrogen bond with Gly240 (pink) and Lys241 (purple).

V. DISCUSSION

Gln159 is located within a set of conserved residues [Ser-Gln-Ser-Gly-Ala] that reside in Site I. These residues are near the acetyl-CoA/acetate binding pocket and are part of an α-helix. This helix is one of two helices designated by Fraser *et al.* (8) as power helix 1 and power helix 2 due to their role in the coordination of the phosphorylated histidine. The Gly-Ala residues of this motif in power helix 1 are thought to interact with the acetyl moiety of acetyl-CoA (3). Given the proximity of Gln159 to the acetate binding pocket as well as the increased K_m for acetate, we hypothesize that alteration of Gln159 disrupts acetate binding or coordination. However, replacing Gln with the negatively charged Glu may also disrupt power helix 1, causing inefficient catalysis. Further characterization with additional variants such as Gln159Ala and Gln159Asn could provide additional insight regarding the function of this residue.

Although *E. histolytica* ACD consists of fused alpha and beta subunits, the hinge region connecting the subunits is very short. Consequently, homology modeling based on the heterotetrameric structure resulted in significant overlap with very few diverging residues. In contrast to SCS, a single active site of ACD consists of residues from both chains, demonstrating the necessity for dimer formation. However, it remains unclear if the active sites can function simultaneously or have any affect on one another.

Before structural information was available, we hypothesized that alteration of Lys534 could potentially compensate for the reduced activity observed in His533 variants (C. Jones, K. Khan, C. Ingram-Smith, in preparation). These adjacent residues share the same pattern of conservation within the enzyme superfamily. The Arg-Gly

residues in SCS and the corresponding His-Lys residues of ACD could potentially result in a positively charged environment. The reduced activity of the Lys534Arg variant indicates that this residue is necessary for maximal catalysis but that the positive charge alone is not sufficient, and that appropriate side chain length is also important. Homology modeling revealed that the side chain of Lys534 has an orientation opposite that of His533. This suggests that Lys534 is unable to compensate for the lack of His533 in providing the positive charge environment needed. However, the corresponding Lys69β residue in *ckc*ACDI was shown to interact with the ADP substrate by both the side-chain amine and the backbone nitrogen. Kinetic analysis should be performed in order to determine if the absence of Lys534 affects the K_m of ADP as a substrate.

Asp314 is located at the interface of the two monomers of ACD and participates in hydrogen bonding with residues on the opposite chain. After repeated failed attempts at production and purification, we hypothesized that alterations of this residue may result in an unstable protein product. Structural modeling supports this theory, as *in silico* alteration of Asp314 to Ala resulted in disruption of intermolecular hydrogen bonding, potentially preventing proper oligomerization.

In summary, the new structural information available for ACD provides a basis for understanding the function and mechanism of this enzyme. Multiple residues were identified to influence activity or structure, including Gln159 and Asp314 of the alpha subunit and Lys534 of the beta subunit. However, a crystal structure of the fused alpha-beta enzyme of *E. histolytica* would be useful in the future.

VI. ACKNOWLEDGEMENTS

We thank Dr. Kerry Smith (Clemson University) for helpful insight on this project. This work was supported by NSF award 0920274, an NSF Graduate Research Fellowship to CJ, Clemson University Creative Inquiry, and Clemson University.

VII. REFERENCES

1. Reeves, R. E., Warren, L. G., Susskind, B., and Lo, H. S. (1977) An energy-conserving pyruvate-to-acetate pathway in *Entamoeba histolytica*. Pyruvate synthase and a new acetate thiokinase. *J Biol Chem* **252**, 726-731

2. Jones, C. P., and Ingram-Smith, C. (2014) Biochemical and kinetic characterization of the recombinant ADP-forming acetyl coenzyme A synthetase from the amitochondriate protozoan *Entamoeba histolytica. Eukaryot Cell* **13**, 1530-1537

3. Weiße, R. H., Faust, A., Schmidt, M., Schonheit, P., and Scheidig, A. J. (2016) Structure of NDP-forming Acetyl-CoA synthetase ACD1 reveals a large rearrangement for phosphoryl transfer. *Proc Natl Acad Sci U S A* **113**, E519-528

4. Brasen, C., Schmidt, M., Grotzinger, J., and Schonheit, P. (2008) Reaction mechanism and structural model of ADP-forming Acetyl-CoA synthetase from the hyperthermophilic archaeon *Pyrococcus furiosus*: evidence for a second active site histidine residue. *J Biol Chem* **283**, 15409-15418

5. Sun, T., Hayakawa, K., Bateman, K. S., and Fraser, M. E. (2010) Identification of the citrate-binding site of human ATP-citrate lyase using X-ray crystallography. *J Biol Chem* **285**, 27418-27428

6. Sun, T., Hayakawa, K., and Fraser, M. E. (2011) ADP-Mg^{2+} bound to the ATP-grasp domain of ATP-citrate lyase. *Acta Crystallogr Sect F Struct Biol Cryst Commun* **67**, 1168-1172

7. Fraser, M. E., James, M. N., Bridger, W. A., and Wolodko, W. T. (1999) A detailed structural description of *Escherichia coli* succinyl-CoA synthetase. *J Mol Biol* **285**, 1633-1653

8. Fraser, M. E., Joyce, M. A., Ryan, D. G., and Wolodko, W. T. (2002) Two glutamate residues, Glu 208 alpha and Glu 197 beta, are crucial for phosphorylation and dephosphorylation of the active-site histidine residue in succinyl-CoA synthetase. *Biochemistry* **41**, 537-546

9. Joyce, M. A., Fraser, M. E., Brownie, E. R., James, M. N., Bridger, W. A., and Wolodko, W. T. (1999) Probing the nucleotide-binding site of *Escherichia coli* succinyl-CoA synthetase. *Biochemistry* **38**, 7273-7283

10. Joyce, M. A., Fraser, M. E., James, M. N., Bridger, W. A., and Wolodko, W. T. (2000) ADP-binding site of *Escherichia coli* succinyl-CoA synthetase revealed by x-ray crystallography. *Biochemistry* **39**, 17-25

11. Wolodko, W. T., Fraser, M. E., James, M. N., and Bridger, W. A. (1994) The crystal structure of succinyl-CoA synthetase from *Escherichia coli* at 2.5-A resolution. *J Biol Chem* **269**, 10883-10890

12. Fraser, M. E., Hayakawa, K., Hume, M. S., Ryan, D. G., and Brownie, E. R. (2006) Interactions of GTP with the ATP-grasp domain of GTP-specific succinyl-CoA synthetase. *J Biol Chem* **281**, 11058-11065

13. Fraser, M. E., James, M. N., Bridger, W. A., and Wolodko, W. T. (2000) Phosphorylated and dephosphorylated structures of pig heart, GTP-specific succinyl-CoA synthetase. *J Mol Biol* **299**, 1325-1339

14. Huang, J., Malhi, M., Deneke, J., and Fraser, M. E. (2015) Structure of GTP-specific succinyl-CoA synthetase in complex with CoA. *Acta Crystallogr F Struct Biol Commun* **71**, 1067-1071

15. Joyce, M. A., Brownie, E. R., Hayakawa, K., and Fraser, M. E. (2007) Cloning, expression, purification, crystallization and preliminary X-ray analysis of *Thermus aquaticus* succinyl-CoA synthetase. *Acta Crystallogr Sect F Struct Biol Cryst Commun* **63**, 399-402

16. Joyce, M. A., Hayakawa, K., Wolodko, W. T., and Fraser, M. E. (2012) Biochemical and structural characterization of the GTP-preferring succinyl-CoA synthetase from *Thermus aquaticus*. *Acta Crystallogr D Biol Crystallogr* **68**, 751-762

17. Altschul, S. F., Madden, T. L., Schaffer, A. A., Zhang, J., Zhang, Z., Miller, W., and Lipman, D. J. (1997) Gapped BLAST and PSI-BLAST: a new generation of protein database search programs. *Nucleic Acids Res* **25**, 3389-3402

18. Sievers, F., Wilm, A., Dineen, D., Gibson, T. J., Karplus, K., Li, W., Lopez, R., McWilliam, H., Remmert, M., Soding, J., Thompson, J. D., and Higgins, D. G. (2011) Fast, scalable generation of high-quality protein multiple sequence alignments using Clustal Omega. *Mol Syst Biol* **7**, 539

19. Lipmann, F. T., C. T. . (1945) A specific micromethod for the determination of acyl phosphates. *J Biol Chem* **159**, 21-28

20. Sanchez, L. B., Galperin, M. Y., and Muller, M. (2000) Acetyl-CoA synthetase from the amitochondriate eukaryote *Giardia lamblia* belongs to the newly recognized superfamily of acyl-CoA synthetases (Nucleoside diphosphate-forming). *J Biol Chem* **275**, 5794-5803

21. Binieda, A., Fuhrmann, M., Lehner, B., Rey-Berthod, C., Frutiger-Hughes, S., Hughes, G., and Shaw, N. M. (1999) Purification, characterization, DNA sequence and cloning of a pimeloyl-CoA synthetase from *Pseudomonas mendocina* 35. *Biochem J* **340 (Pt 3)**, 793-801

CHAPTER 5

CONCLUSIONS AND FUTURE WORKS

ACD's role in cellular metabolism

ADP-forming acetyl-CoA synthetase is responsible for the interconversion of acetyl-CoA and acetate coupled to the formation of ATP. This is an energy conserving reaction that exchanges one high-energy bond for another. The amitochondriate parasite *Entamoeba histolytica* lacks many typical eukaryotic metabolic pathways, making the conservation of energy especially important. Thus, we believe that ACD could be important for maintaining energy homeostasis in *E. histolytica* under the varying conditions it encounters.

Pineda *et al.* (1) demonstrated that ACD is responsible for acetate production by *E. histolytic*a during growth on glucose *in vitro* and theorized that it functions to recycle CoA. Although they found that ACD's contribution to the ATP pool was not significant during *in vitro* growth, the nutrient environment surrounding the cell differs greatly when inside the host compared to the controlled environment in culture. Thus, these *in vitro* results may not be truly representative of ACD's role in ATP production.

As our results have shown that ACD is subject to inhibition by ATP in the acetate-forming direction of the reaction (2), ACD function in the cell is likely regulated by the AMP:ATP ratio. If ATP levels drop and AMP levels rise, ACD is capable of producing additional ATP for the cell and concomitantly producing acetate (FIG 5.1A). In addition, if acetyl-CoA levels are in excess, they can be shuttled through ACD as a type

of overflow metabolism in order to recycle CoA and conserve energy through ATP production (FIG 5.1B). When ATP is plentiful, excess ATP could then be redirected towards activation of acetate in order to utilize this potential carbon source (FIG 5.1C). This would be particularly useful within the acidic microenvironment of the colon where the concentration of short-chain fatty acids such as acetate and propionate are high, and these compounds can diffuse through the membrane. When acetic acid enters the cell in its protonated form, it quickly dissociates into acetate and a proton at the neutral intracellular pH. As this could be toxic to the cell, activation by ACD would serve as a method of detoxifying acetate and maintaining intracellular pH (FIG 5.1D).

ACD may also function in activating acetate that is produced from endogenous sources. Cysteine has been determined to be essential for its redox capacity in *E. histolytica* (3) and consequently, the cysteine synthesis pathway has been maintained. Cysteine synthesis occurs through acetylation of serine and release of acetate when the sulfide group is added. ACD could theoretically function in a loop to recycle the acetate into another acetyl-CoA molecule to refuel cysteine synthesis (FIG 5.1E).

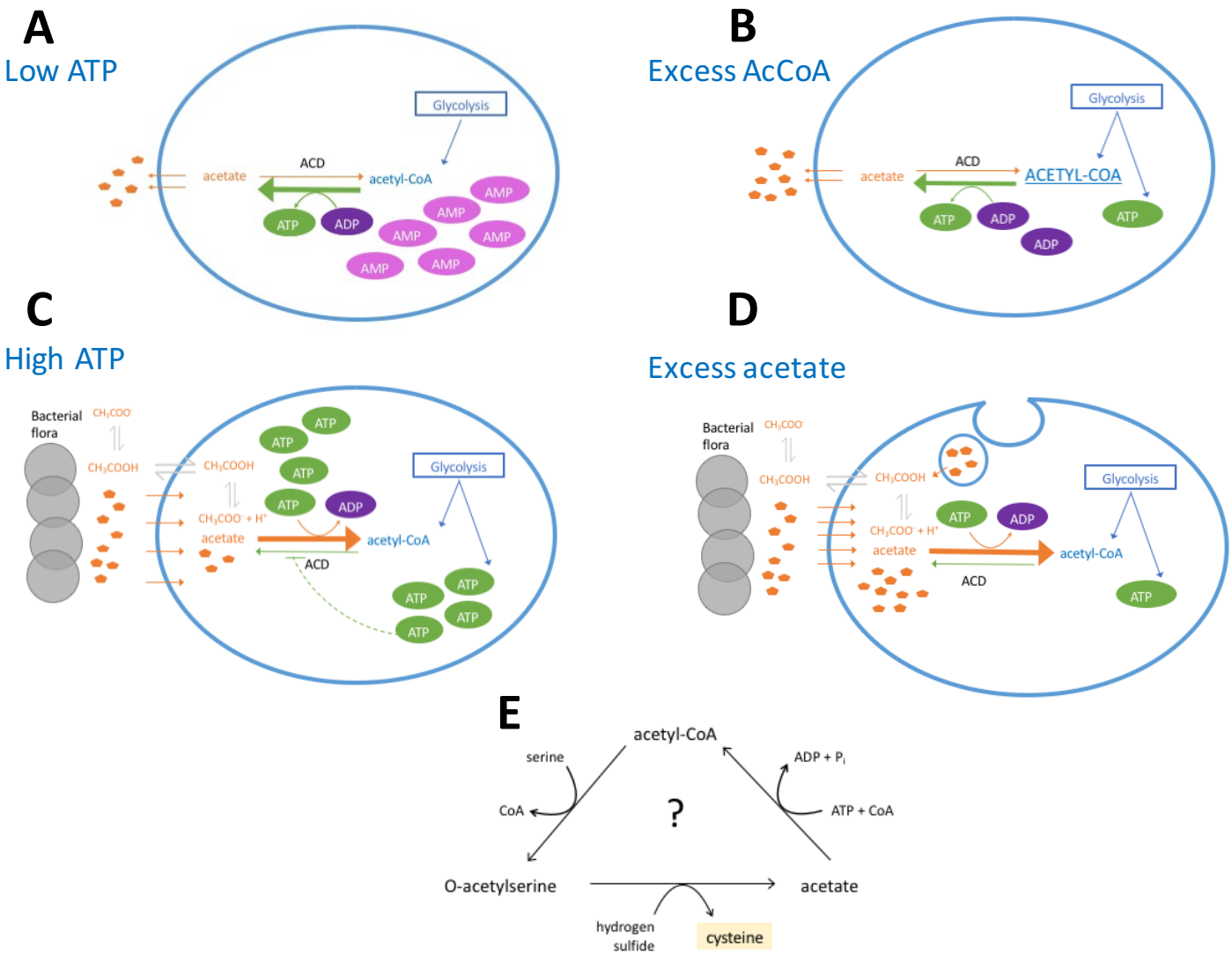
A
Low ATP
Glycolysis
acetate
ACD
acetyl-CoA
ATP
ADP
AMP
B
Excess AcCoA
ACETYL-COA
C
High ATP
Bacterial flora
CH3COO-
CH3COOH
CH3COO- + H+
D
Excess acetate
E
acetyl-CoA
serine
CoA
?
ADP + Pi
ATP + CoA
O-acetylserine
acetate
hydrogen sulfide
cysteine

FIG 5.1 *Eh*ACD may function as a reversible enzyme in response to the cell's needs. Acetate is represented by orange pentagons, ATP by green ovals, ADP by purple ovals, and AMP by pink ovals. (A) Under low ATP concentrations, ACD can function in the acetate-forming direction and supplement ATP levels. (B) When acetyl-CoA is in excess, ACD could function in the acetate-forming direction as a type of overflow metabolism. (C) When ATP concentrations are high, ACD is inhibited in the acetate-forming direction and would instead use the excess ATP to activate acetate to acetyl-CoA. (D) Exogenous acetate may diffuse into the cell or be taken in by fluid-phase endocytosis. When acetate is in excess, ACD can negate its potentially toxic effects by converting it to acetyl-CoA. (E) ACD could also function by using endogenous sources of acetate, such as from cysteine synthesis.

These assumptions are based on characterization of the recombinant enzyme (2) and therefore further experimental evidence is needed to fully explore the role of ACD within *E. histolytica*. These possible scenarios can be investigated by changing culture media conditions (pH, acetate concentrations, etc.) and comparing wild-type and ACD knockdown cell lines.

Enzymatic mechanism

Based on the characterization of site-altered variants and isotopic labeling by phosphorylation, we hypothesize that ACD proceeds through a three-step mechanism similar to that for succinyl-CoA synthetase (FIG 5.2). Acetyl-CoA and P_i bind within Site I and form a transient acetyl phosphate intermediate. This intermediate phosphorylates the Hisα residue within Site I. Crystal structures of ACD were obtained with Hisα phosphorylated in Site I (4), suggesting a binding event or release of CoA may be required for the conformational change of the phosphohistidine loop to occur. One possibility is that upon ADP binding, the phosphorylated Hisα moves into position within Site II and phosphorylates ADP to form ATP. The opposite reaction also takes place. ATP binds within Site II and causes Hisα to move into Site II where it becomes phosphorylated. Then Hisα-P moves back to Site I where it can transfer the phosphoryl group to acetate. Acetyl phosphate then acetylates CoA and releases phosphate.

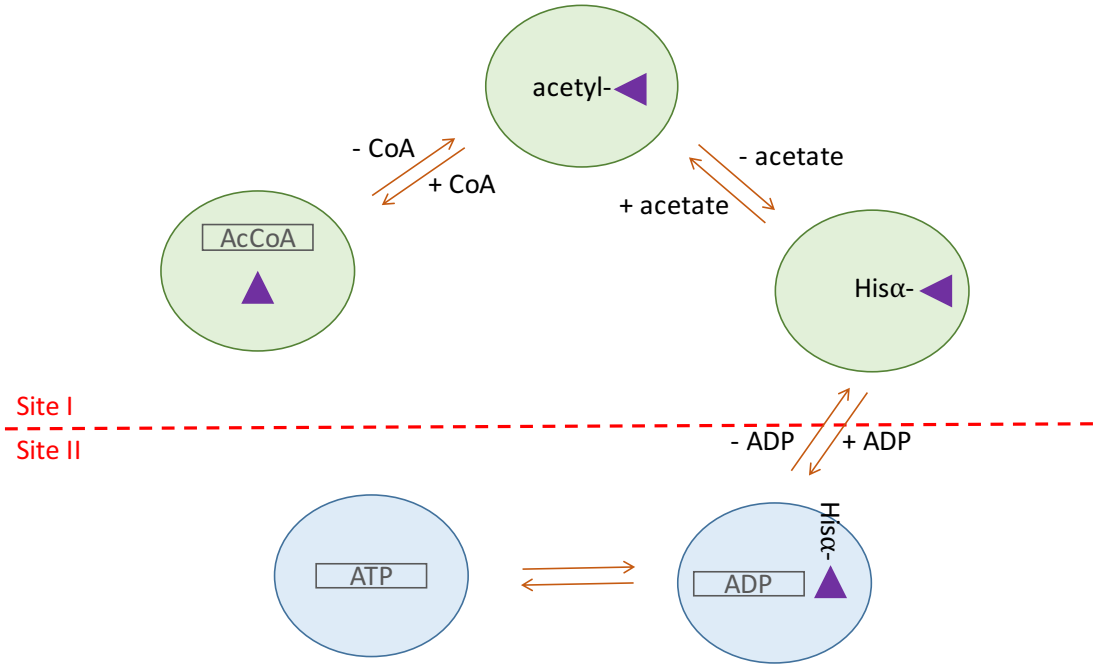

FIG 5.2 Schematic of the proposed three-step ACD mechanism. Green ovals represent Site I and blue ovals represent Site II. The transferred phosphate group is shown as a purple triangle.

Glu213 is required for stable phosphorylation of Hisα by the acetyl phosphate intermediate within Site I to occur. However, isotopic labeling revealed His252 may be phosphorylated within Site II when Glu213 is absent, so it is not necessary for ATP phosphorylation of Hisα. This variant could be a useful tool for determining the crystal structure of ACD with a phosphorylated Hisα in Site II. The absence of His533 does not prevent phosphorylation from occurring in either direction, challenging the four-step reaction proposed by Brasen et al. (5) in which His533 is directly phosphorylated during the catalysis.

Asp674 is important for optimal phosphorylation to occur, and based on the homologous residue within *ckc*ACDI (4), is thought to help stabilize Hisα when located in Site II. Asp314 located within power helix 1, is likely important for the structural integrity of the enzyme. Lys534 alteration resulted in reduced activity, and this residue is postulated to bind the ADP/ATP substrate. Kinetic characterization of Gln159Glu suggests a role for this residue in acetate binding or coordination. Future structural analysis using the recently generated model combined with kinetic characterization will enhance our understanding of the function and mechanism of this enzyme. In addition, an *Eh*ACD crystal structure is in the final stages of refinement (S. Swaminathan, personal communication) and will allow direct analysis of the active sites of the homodimeric *Eh*ACD and comparison to the heterotetrameric archaeal ACDs.

REFERENCES

1. Pineda, E., Vazquez, C., Encalada, R., Nozaki, T., Sato, E., Hanadate, Y., Nequiz, M., Olivos-Garcia, A., Moreno-Sanchez, R., and Saavedra, E. (2016) Roles of acetyl-CoA synthetase (ADP-forming) and acetate kinase (PPi-forming) in ATP and PPi supply in *Entamoeba histolytica*. *Biochim Biophys Acta* **1860**, 1163-1172

2. Jones, C. P., and Ingram-Smith, C. (2014) Biochemical and kinetic characterization of the recombinant ADP-forming acetyl coenzyme A synthetase from the amitochondriate protozoan *Entamoeba histolytica*. *Eukaryot Cell* **13**, 1530-1537

3. Agarwal, S. M., Jain, R., Bhattacharya, A., and Azam, A. (2008) Inhibitors of Escherichia coli serine acetyltransferase block proliferation of *Entamoeba histolytica* trophozoites. *Int J Parasitol* **38**, 137-141

4. Weiße, R. H., Faust, A., Schmidt, M., Schonheit, P., and Scheidig, A. J. (2016) Structure of NDP-forming Acetyl-CoA synthetase ACD1 reveals a large rearrangement for phosphoryl transfer. *Proc Natl Acad Sci U S A* **113**, E519-528

5. Brasen, C., Schmidt, M., Grotzinger, J., and Schonheit, P. (2008) Reaction mechanism and structural model of ADP-forming Acetyl-CoA synthetase from the hyperthermophilic archaeon *Pyrococcus furiosus*: evidence for a second active site histidine residue. *J Biol Chem* **283**, 15409-15418